Characterization of position 64 in *Saccharomyces cerevisiae* tRNA nucleotidyltransferase: Exploring the mechanism of suppression

Zahra Aryanpour

A Thesis

in

The Department

of

Biology

Presented in Partial Fulfillment of the Requirements for

The Degree of Master of Science (Biology) at

Concordia University

Montreal, Quebec, Canada

September 2020

CONCORDIA UNIVERSITY

School of Graduate Studies

This is to certify that the thesis prepared

By: Zahra Aryanpour

Entitled: Characterization of position 64 in *Saccharomyces cerevisiae* tRNA nucleotidyltransferase: Exploring the mechanism of suppression

Submitted in partial fulfillment of the requirements for the degree of

Master of Science (Biology)

Complies with the regulations of the University and meets the accepted standards with respect to originality and quality.

Signed by the final Examining Committee:

Dr. David Kwan	_____	Examiner and Chair
Dr. Malcolm Whiteway	_____	Examiner
Dr. Patrick Gulick	_____	External Examiner
Dr. Paul Joyce	_____	Supervisor

Approved by Dr. Robert Weladji _____ Graduate Program Director

Dr. Pascale Sicotte _____ Dean of Faculty

Date: September 10th, 2020

ABSTRACT

Characterization of position 64 in *Saccharomyces cerevisiae* tRNA nucleotidyltransferase: Exploring the mechanism of suppression

Zahra Aryanpour

The enzyme ATP(CTP): tRNA-specific tRNA nucleotidyltransferase catalyzes the addition of cytidine, cytidine, adenosine (CCA) to the 3' end of transfer RNAs (tRNAs) during their synthesis and repair. This CCA sequence is required for aminoacylation and protein synthesis. The *Saccharomyces cerevisiae* enzyme is defined as a Class II tRNA nucleotidyltransferase through five motifs (A to E) conserved in the amino-terminal half of the protein. Functions have been assigned to each of these motifs. Our previous studies have shown that enzyme activity is reduced by mutations in motif C leading to a temperature-sensitive (*ts*) phenotype. Further, we also have shown that these *ts* mutations can be suppressed by a second-site mutation in motif A suggesting an interaction between motifs A and C. Here we use site-directed mutagenesis to make specific changes in residues in these motifs to explore these interactions.

Specifically, arginine 64 found in motif A was changed to phenylalanine, proline or alanine and the effects of these substitutions on wild-type and mutant backgrounds was determined. Changing arginine 64 to proline (R64P) resulted in a lethal phenotype in any background tested. Converting arginine to phenylalanine (R64F) resulted in no measurable changes in growth in a wild-type background in our *in vivo* assay and also suppressed the *ts* phenotype resulting from the conversion of glutamate 189 to phenylalanine (E189F) or lysine (as had been seen previously for an arginine 64 to tryptophan substitution). In contrast, the R64F substitution could not rescue the lethal phenotype resulting from conversion of aspartate 190 to phenylalanine (D190F). Changing arginine 64 to alanine (R64A) resulted in reduced growth at the restrictive temperature in a wild-type background and did not suppress the E189F, E189K, or D190A *ts* phenotypes. Moreover, the R64A change in the D190A background enhanced the growth defect at the permissive temperature. Taken together, these data support our hypothesis of a direct interaction between elements of motifs A and C. Computational modelling is used to explore how the phenotypes observed are linked to changes in the structure of the protein.

ACKNOWLEDGMENTS

I would like to appreciatively acknowledge various people who have been journeyed with me during the time I was working in the Joyce lab.

Of course, without my supervisor's wise guidance and endless support this research and thesis would not have been completed. I would like to express my deepest appreciation to Dr. Paul Joyce for supporting me during the time I was working in his lab. Working in the Joyce lab was the best academic experience I have ever had. I also would like to extend my gratitude to Dr. Pamela Hanic-Joyce for providing indispensable advice, information, and support on difficult aspects of this project. I know that no word can do justice to thank this supportive and kindhearted couple. Thank you for trusting me.

I am grateful to my committee members, Dr. Malcolm Whiteway and Dr. David Kwan, whom for their continuous supports, being in my committee, taking time to answer uncountable questions and discuss with me regarding the progress of my research on many occasions. Your support and help were very valuable in this research.

Although COVID-19 lockdown halted some exciting parts of this research, I would like to thank Drs. Peter Pawelek and Yves Gélinas for generously providing me with their lab equipment to perform Crystallography and preparing the samples for FTIR spectroscopy. Unfortunately, this work is excluded these experiments.

I would like to specially thank my friends, Nathalie, Shayesteh, and Maria for making these years at Concordia University a delight. You are all special to me.

This acknowledgement would not be complete without conveying my special thanks to my mom, dad, and my brother, to whom I am very much indebted for their support and love during my study.

Any omission in this brief acknowledgment does not mean lack of gratitude.

TABLE OF CONTENTS

LIST OF FIGURES

LIST OF TABLES

LIST OF ABBREVIATIONS

Amp	Ampicillin
AMP	Adenosine monophosphate
APS	Ammonium persulfate
ATP	Adenosine triphosphate
BSA	Bovine serum albumin
CCA	Cytidine-cytidine-adenosine
CD	Circular dichroism
CMP	Cytidine monophosphate
CTP	Cytidine triphosphate
DNA	Deoxyribonucleic acid
dNTP	Deoxynucleoside triphosphate
dH_2O	Distilled water
EDTA	Ethylenediaminetetraacetic acid
FOA	5-fluoroorotic acid
GST	Glutathione S-transferase
H-bond	Hydrogen bond
IPTG	Isopropyl-β-D-thiogalactopyranoside
NTP	Nucleoside triphosphate
OD	Optical density
PAGE	Polyacrylamide gel electrophoresis
PBS	Phosphate-buffered saline
PDB	Protein Data Bank
SC-HIS-URA	Synthetic complete medium lacking histidine and uracil
SDS	Sodium dodecyl sulfate
TBE	Tris/Borate/EDTA
TEMED	Tetraethylmethlenediamine
tRNA	Transfer ribonucleic acid
tRNA-NT	tRNA nucleotidyltransferase

ts	Temperature-sensitive
UV-vis	UV-visible
YPD	Yeast extract, Peptone, Dextrose
YT	Yeast extract, Tryptone
xg	Times gravity

1.0 INTRODUCTION

1.1 tRNA nucleotidyltransferase

ATP(CTP):tRNA-specific tRNA nucleotidyltransferase (tRNA-NT) is responsible for the incorporation of CMP and AMP residues into tRNAs that lack a 3'-terminal cytidine-cytidine-adenosine (CCA) sequence (Deutscher, 1982). As a complete 3'-CCA sequence is required for the addition of an amino acid to a tRNA (Sprinzl and Cramer, 1979) and subsequent functioning of the tRNA in protein synthesis (Green and Noller, 1997), this enzyme is essential in organisms with tRNA genes that lack the CCA sequence (Aebi *et al.,* 1990). Moreover, this enzyme plays a role in the repair of tRNAs damaged at their 3'ends (Rosset and Monier, 1965, Deutscher, Foulds, McClain 1974) and in tRNA quality control (Wilusz *et al.,* 2011, Wellner *et al*., 2018). The importance of tRNA-NT activity is apparent in organisms as diverse as *Escherichia coli*, *Saccharomyces cerevisiae*, and humans where reduced tRNA-NT activity resulted in a reduced growth rate (Zhu and Deutscher, 1987), a temperature-sensitive phenotype (Aebi *et al*., 1990, Shan *et al*., 2008), and multiple human disease phenotypes (reviewed in Slade *et al*., 2020), respectively.

All eukaryotic and eubacterial tRNA-NTs are members of Class II (Yue *et al.,* 1996) of the polymerase β nucleotidyltransferase superfamily (Holm and Sander, 1996, Aravind and Koonin, 1999). Class II tRNA nucleotidyltransferases show a conserved seahorse-shaped crystal structure (Li *et al.,* 2002; Augustin *et al.,* 2003; Tomita *et al.,* 2004; Tomita *et al.,* 2006; Toh *et al.,* 2009; Toh *et al.,* 2011) with defined head, neck, body and tail domains (Fig. 1.1). All Class II tRNA-NTs show five conserved motifs (A, B, C, D and E) in the amino-terminal head and neck regions of the protein (Fig. 1.1) (Li *et al*., 2002), but little primary sequence similarity in the C-terminal body and tail domains.

Biochemical and crystallographic experiments have revealed that the body and tail domains of tRNA-NTs are involved in tRNA recognition and binding (Li *et al*., 2002, Tomita *et al*., 2004, Xiong *et al*., 2003, Xiong *et al*., 2004, Betat *et al*., 2004, Leibovitch *et al*., 2013,Yamashita *et al*., 2015,Yamashita and Tomita, 2016, Leibovitch *et al*., 2019). These experiments also indicated that the head and neck domains (which contain motifs A to E) contain the active site of the enzyme and that conserved residues in sequence motifs A to E are important for catalysis. In fact, specific

functions have been assigned to each of these motifs (reviewed in Betat *et al*, 2010, Vörtler and Mörl, 2010).

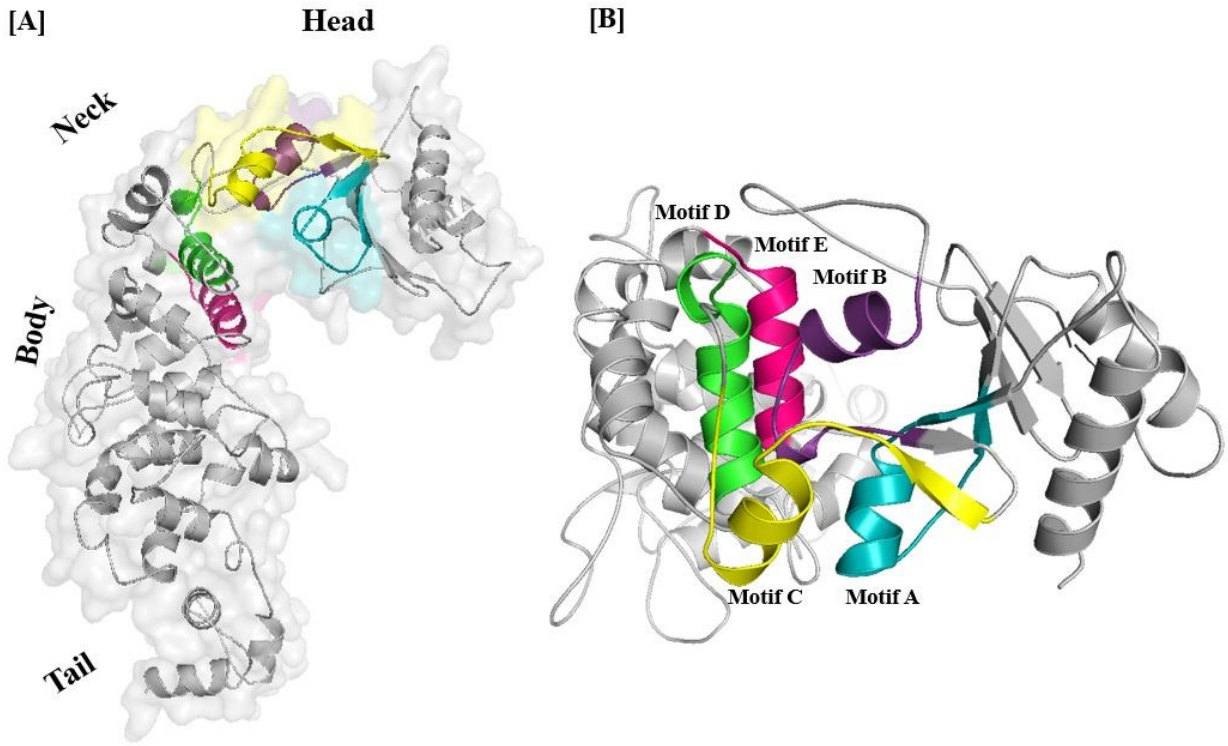

Figure 1.1 Model structure of the *Saccharomyces cerevisiae* tRNA-NT based on the solved crystal structure of the *Thermotoga maritima* tRNA-NT (PDB ID: 3h38, Toh *et al*., 2009). A: Model of the whole protein indicating the positions of head, neck, body, and tail domains and the positions of conserved motifs A (teal), B (purple), C (yellow), D (green), and E (magenta). B: A close up of the head and neck domains showing the five conserved motifs (colours as in A). The model was produced by aligning the primary and secondary structures of the *S. cerevisiae* enzyme with those of *Thermotoga maritima* tRNA-NT and by generating a homology model with SWISS-MODEL (Biasini *et al*., 2014). The homology model with the lowest energy level was viewed using PyMol (Version 2.4.0 Schrödinger).

1.2 The functions of the conserved motifs

The available crystal structures of tRNA-NTs (Augustin *et al*., 2003; Kuhn *et al*., 2015, Li *et al.,* 2002; Xiong *et al.,* 2003; Tomita *et al.,* 2004; Xiong and Steitz 2004; Yamashita and Tomita 2016) show a single 5-8 strand antiparallel β-sheet in the head domain of the protein. This β-sheet is a distinguishing feature of the polymerase β nucleotidyltransferase superfamily (Holm and Sander, 1996) with the minimal nucleotidyltransferase (MNT) structure defined by a four-stranded

β-sheet (Aravind and Koonin, 1999). The model structure of the yeast tRNA-NT (Fig. 1.1) shows a predicted 7-stranded antiparallel β-sheet in the head domain.

1.2.1 Motif A

This is the most amino-terminal motif and is found only four residues from the amino terminus of the *E. coli* enzyme (Li *et al*., 2002). This motif (Figure 1.2) is defined by a highly conserved GGxVRD sequence separated by approximately 10 residues from a conserved DxD sequence (where D represents an aspartic acid residue and x is any residue). This DxD sequence is found in all nucleotidyltransfrases (Holm and Sander, 1995) and is involved in catalysis and the binding of incoming nucleotide triphosphates through coordinating two magnesium ions that facilitate the triphosphate binding and a two-metal ion polymerization reaction similar to that used

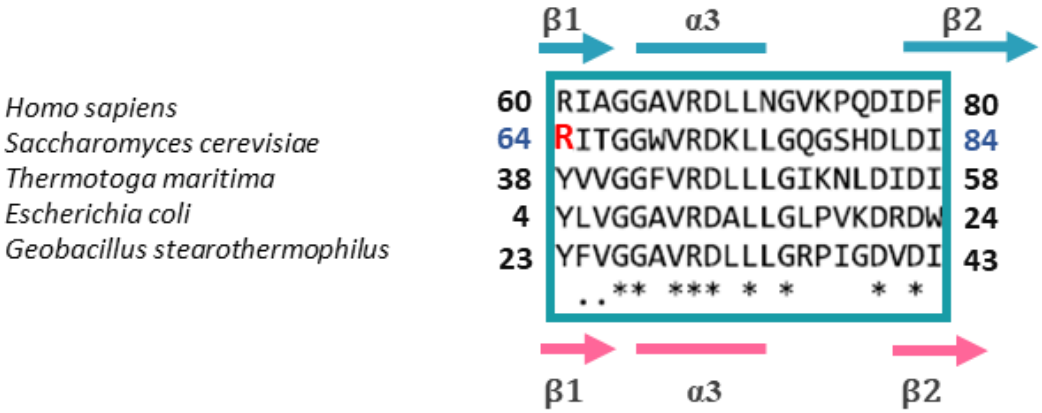

Figure 1.2 Alignment of motif A in the head domain of five class II tRNA nucleotidyltransferases. The alignment was performed using ClustalW2 software (Martin *et al.,* 2007). Numbers represent residue positions in the protein, letters stand for one letter code for the amino acids. Strongly conserved (*), highly similar amino acids (:) and slightly conserved (.) amino acids are indicated below the sequence. Arginine at position 64 in the yeast enzyme, discussed in this study, is in red. The regions identified as either β-strands (β) or α-helices (α) in the crystal structure of the human enzyme (Augustin *et al*., 2003) (blue) and the model structure of the yeast enzyme (pink) are shown above and below the alignment, respectively.

by other polynucleotide polymerases (Steitz, 1998; Li *et al.,* 2002; Betat *et al.,* 2010). The DxD sequence of motif A is typically found on the open face of the β-sheet and contributes to the active site geometry of the enzyme (Sawaya *et al*., 1994). Based on our model of the *S. cerevisiae* enzyme

residue D83 is found in strand β2 of the β-sheet and D81 is found contiguous to this strand (Fig. 1.3).

Crystal structures of DNA polymerase-βs (Sawaya *et al*.,1994, Davies *et al*., 1994, Pelletier *et al*., 1994) and human tRNA-NT (Augustin *et al*., 2003) with metal ions and/or nucleotide triphosphates bound revealed a third carboxylate required to coordinate the two metal ions. This third carboxylate was found in a subsequent β-strand of the β-sheet (Sawaya *et al*., 1994, Augustin *et al*., 2003). This also is predicted to be the case in the *S. cerevisiae* enzyme (section 1.2.2).

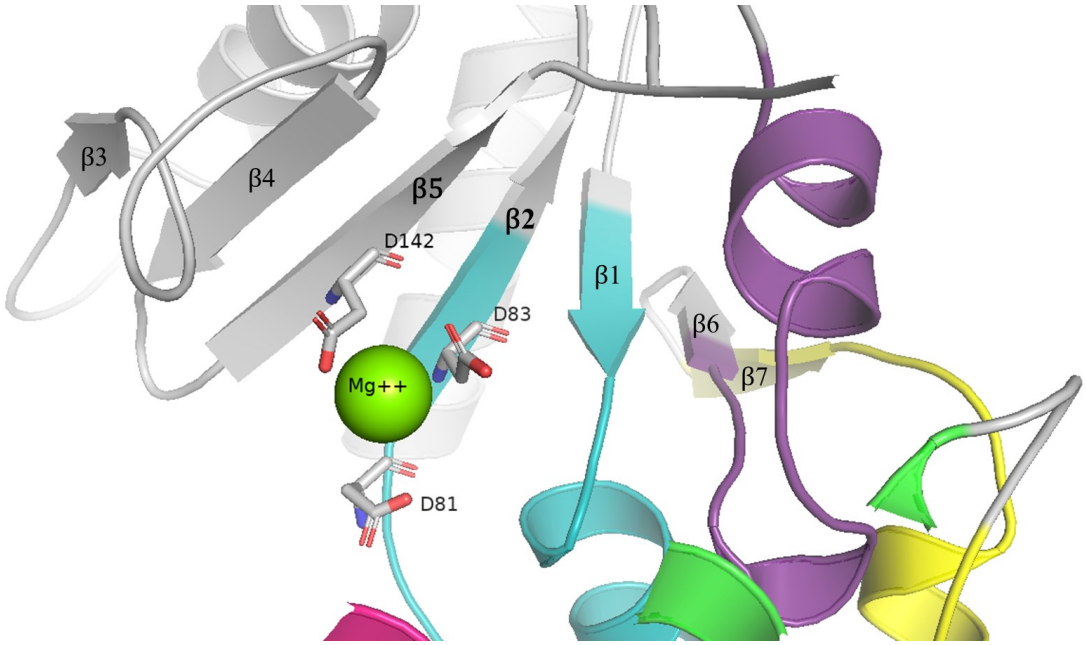

Figure 1.3 The model structure of *S. cerevisiae* tRNA-NT showing the single β-sheet characteristic of tRNA-NTs. The positions of motifs contained in this region are shown (colours as in Fig. 1.1). The R groups of aspartic acids 81 and 83 (in or near β2 of the β-sheet) and 142 (in β5 of the β-sheet) are shown. A magnesium ion required for catalysis is shown in green.

1.2.2 B/A loop

This region of the protein, which lacks primary sequence conservation among different tRNA-NTs, is found between motifs A and B (Fig. 1.4). This loop is named for the B/A element that it contains (where B is a basic residue and A is an acidic residue). The presence of this loop and the B/A element is a defining feature of CCA and A-adding tRNA-NTs (Just *et al*., 2008, Tretbar *et*

al., 2011). This loop contains a flexible region that is thought to change conformation as the CCA-adding enzyme converts from CMP incorporation to AMP incorporation, *i.e*., the nucleotide triphosphate binding pocket must change shape during catalysis to accept the larger purine base as opposed to the smaller pyrimidine base (McGann and Deutscher 1980; Zhu *et al*. 1986; Li *et al.*, 2002; Augustin *et al*., 2003; Tomita *et al*., 2004; Neuenfeldt *et al*., 2008; Just *et al*., 2008; Toh *et al.*, 2009; Hoffmeier *et al*., 2010). Therefore, tRNA-NTs that add a complete CCA sequence contain a large loop between motifs A and B while tRNA-NTs that lack this flexible loop are confined to CMP incorporation (Neuenfeldt *et al*., 2008). This region of the protein also is thought to play a role in proof-reading the 3' ends of tRNAs to ensure that AMP and not CMP is inserted at the final position (Just *et al*., 2008; Neuenfeldt *et al.,* 2008). The conserved B/A element found near the beginning of motif B (green arrows in Fig. 1.4) is thought to position the tRNA-NCC (through hydrogen bonding between the basic residue and C75 of the elongating tRNA) for terminal A addition in CCA-adding enzymes (Tomita *et al*., 2004, Neuenfeldt *et al*., 2008, Toh *et al*., 2009). This region also functions as a quality control step during CCA addition as the inability to form this bond will result in incomplete CCA addition.

This region of the protein also contains the third acidic residue involved in metal ion binding and catalysis (Fig. 1.3) (red arrow in Fig. 1.4).

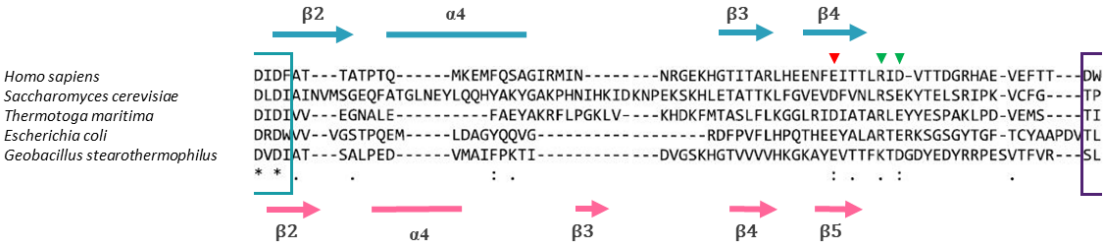

Figure 1.4 Alignment of the B/A loop in the head domain of five class II tRNA nucleotidyltransferases. The alignment was performed using ClustalW2 software (Martin *et al*., 2007) and optimized by eye. Letters are one letter code for the amino acids. Strongly conserved (*), highly similar amino acids (:) and slightly conserved (.) amino acids are indicated below the sequence. The blue line marks the end of motif A and the red line indicates the beginning of motif B. The third carboxylate required to coordinate the two metal ions (Sawaya *et al*., 1994, Augustin *et al.,* 2003) is shown in red and bolded. The B/A element is indicated by green arrows. The regions identified as either β-strands (β) or α-helices (α) in the crystal structure of the human enzyme (Augustin *et al*., 2003) (blue) and the model structure of the yeast enzyme (pink) are shown above and below the alignment, respectively.

1.2.3 Motif B

Motif B (Figure 1.5) plays a role in ribose recognition via the conserved RRD sequence (Li *et al.*, 2002). This sequence recognizes the 2'-hydroxyl group of the ribose of the incoming nucleotide triphosphate (Li *et al.*, 2002) through forming H-bonds between the guanidinium group of the central arginine and the 2'-OH group of the incoming nucleotide triphosphate. As deoxyribonucleotides lack this 2'-OH group, no H-bond can be formed and deoxyribonucleotides are bound less efficiently. When site-directed mutagenesis was used to convert this arginine to isoleucine (replacing the hydrogen bonding potential of the guanidinium group with the more hydrophobic isoleucine R group) the efficiency for binding deoxyribonucleotides was increased such that addition of dCdCdA to the 3' end of tRNAs occurred (Cho *et al*., 2007). These authors also found that this same Arg to Ile substitution resulted in a 100-fold reduction in the use of ATP suggesting that this arginine residue also is involved in positioning ATP (but not CTP) for binding and catalysis (Cho *et al*., 2007). Naturally occurring mutations in the TRNT1 gene encoding human tRNA-NT also have suggested the importance of motif B in tRNA-NT activity. The conversion of alanine 148 to valine (Sasarman *et al.*, 2015), or threonine 154 to isoleucine (Chakraborty *et al.*, 2014), or methionine 158 to valine (Chakraborty *et al.*, 2014) were found in patients suffering from congenital sideroblastic anemia with B-cell immunodeficiency, periodic fevers and developmental delay (SIFD) (numbering based on the TRNT1 mitochondrial isoform, containing the 29 residues leader sequence, NP_886552.2). Interestingly, both the T154I and M158V substitutions result in decreased binding of CTP but not ATP (Leibovitch *et al*., 2018).

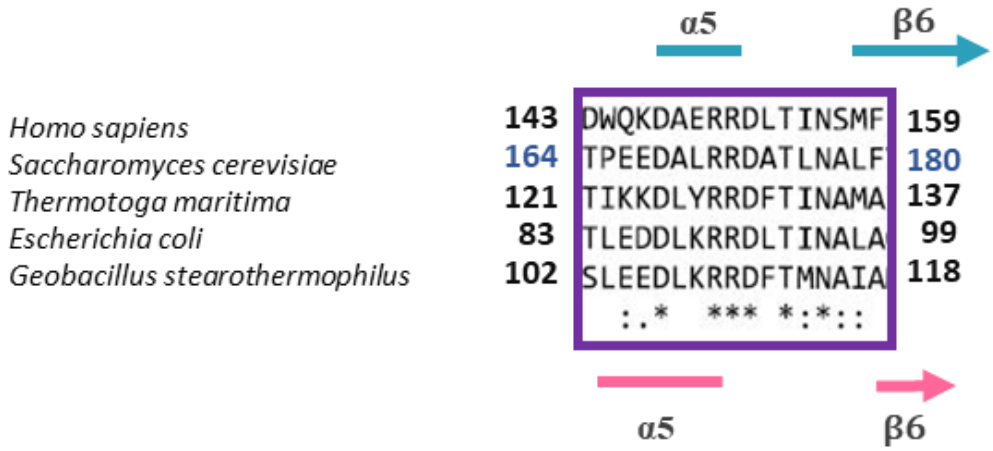

Figure 1.5 Alignment of motif B in the head domain of five class II tRNA nucleotidyltransferases. The alignment was performed using ClustalW2 software (Martin *et al.,* 2007). Numbers represent residue positions in the protein, letters stand for one letter code for the amino acids. Strongly conserved (*), highly similar amino acids (:) and slightly conserved (.) amino acids are indicated below the sequence. The regions identified as either β-strands (β) or α-helices (α) in the crystal structure of the human enzyme (Augustin *et al*., 2003) (blue) and the model structure of the yeast enzyme (pink) are shown above and below the alignment, respectively.

1.2.4 Motif C

Motif C (Fig. 1.6) is the least well conserved of the five defined motifs in the head and neck region of the protein and initially was thought (Li *et al.,* 2002; Cho *et al.,* 2007) simply to serve as a connector between the head and neck domains (Fig. 1.7). However, crystallographic studies (Yamashita and Tomita, 2016) and domain swapping experiments (Toh *et al*., 2009) led to this motif being defined as a "springy hinge" that serves to regulate the processivity and specificity of nucleotide incorporation (Tomita and Yamashita, 2014). Motif C would allow for reorganization of the head and neck domains relative to each other to define first CMP incorporation and then AMP incorporation as required. More recently, these observations were supported by EPR spectroscopy with the human tRNA-NT (Ernst *et al.,* 2015). These authors placed spin labels on the head and body domains of the enzyme and measured changes in their location in space through Double Electron-Electron Resonance (DEER) experiments. Their proposed mechanism requires that motif C play a role in adjusting the catalytic core of the enzyme and the tRNA binding site for the binding and addition of each NTP. They propose that motif C expands upon tRNA binding and remains in this expanded conformation to allow for the incorporation of two CMP and one AMP to the 3'-end of the tRNA. Once ATP binds at the active site of the enzyme there is a slight

contraction of motif C that limits the number of added nucleotides and/or rearranges the active site to allow ATP (rather than CMP) incorporation into the terminal position of the tRNA. So, motif C serves as an essential element required for the proper orientation of the two reactants within the catalytic core.

These authors also used site-directed mutagenesis to convert the aspartic acid at position 168 of the human enzyme (corresponding to D190 in the yeast enzyme, Fig. 1.6) to alanine and showed that in the D168A variant the spring element had lost some of its functionality such that tRNA binding does not result in an expanded enzyme. However, even without this expansion upon tRNA binding there remains space at the active site for CTP binding and CMP incorporation. When ATP binds at the active site, the enzyme does expand but the orientation and/or distance of the tRNA-CC and bound ATP does not allow for an efficient nucleophilic attack of the tRNA's 3′-OH group on the bound ATP. In this D168A variant the kinetics of tRNA-CC and ATP binding remain unaffected, but the enzyme shows a strongly reduced A-adding activity. Ernst *et al*. (2015) conclude by suggesting that in the human enzyme this flexible spring element in motif C does not act alone but instead acts in concert with the region of two neighboring α-helices (α8, α11) to form a second spring stabilized by hydrogen bonds that also helps to define the number of nucleotides added to the tRNA.

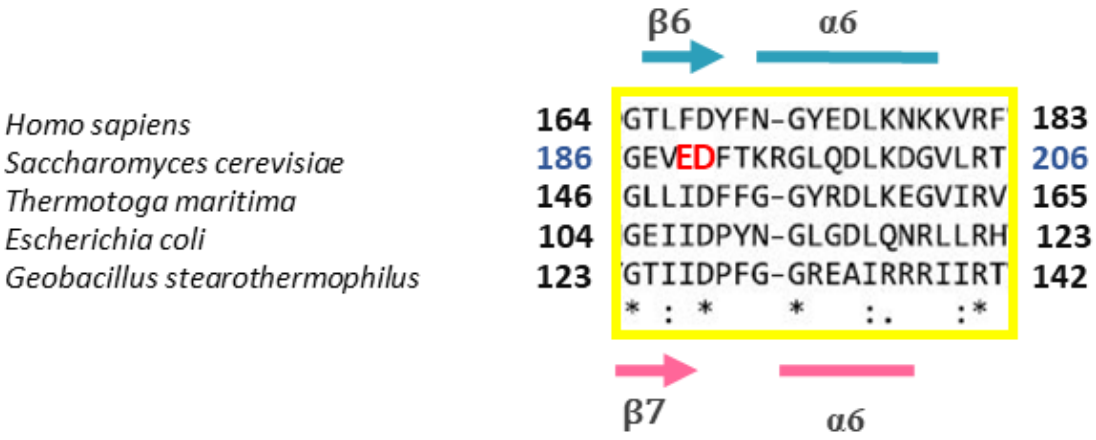

Figure 1.6 Alignment of motif C in the head domain of five class II tRNA nucleotidyltransferases. The alignment was performed using ClustalW2 software (Martin *et al.,* 2007). Numbers represent residue positions in the protein, letters stand for one letter code for the amino acids. Strongly conserved (*) and highly similar amino acids (:) amino acids are indicated below the sequence. E189 and D190 in the yeast enzyme are indicated in red as they are discussed in the current project. The regions identified as either β-strands (β) or α-helices (α) in the crystal structure of the human enzyme (Augustin *et al*., 2003) (blue) and the model structure of the yeast enzyme (pink) are shown above and below the alignment, respectively.

Extensive studies on the role of motif C in *Saccharomyces cerevisiae* tRNA-NT structure and function have been carried out using a combination of genetic, biochemical, and biophysical approaches in the Joyce lab and will be discussed in section 1.3.

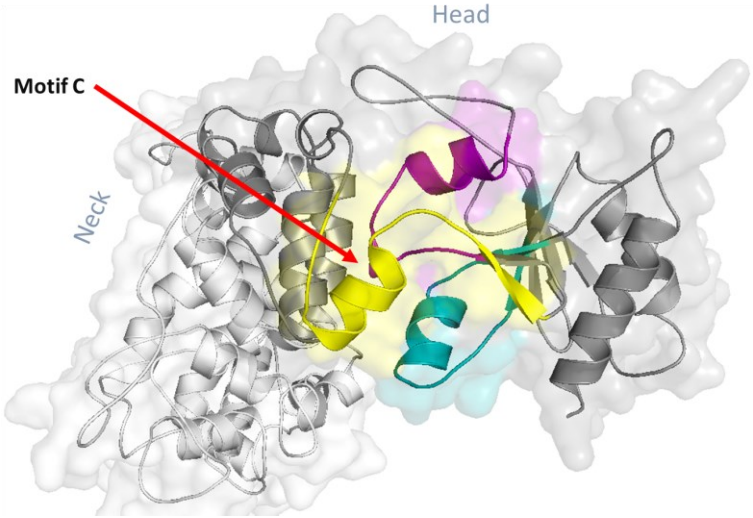

Figure 1.7 The model structure of head and neck domains showing the location of motifs in the head domain. Motif A (teal), motif B (purple), and motif C (yellow) which is highlighted by a red arrow.

1.2.5 Motif D

Motif D, found in the neck domain of tRNA-NT (Fig. 1.1), plays a role in nucleotide recognition (Li *et al*., 2002, Cho *et al*., 2007). This region contains a conserved EDxxR sequence (Fig. 1.8) such that Watson-Crick-like H-bonds are formed between the arginine residue and the corresponding edge of the incoming base and the aspartic acid residue and the same edge of the incoming base (Li *et al*., 2002). The glutamic acid in this motif plays a role in altering the orientation of the guanidinium group of the arginine residue to change the hydrogen bonding potential such that it first recognizes cytosine and then after reorganizing, adenine. By converting this EDxxR motif to NNxxE, base specificity was changed from adenine to guanine by altering the H-bonding potential (Cho *et al*., 2007). Similarly, when this sequence was converted to SNxxE the enzyme incorporated UMP instead of CMP showing the importance of this sequence in base recognition (Cho *et al*. 2007). Moreover, our studies on *Candida glabrata* tRNA-NT (Colasurdo, 2011) showed that converting the conserved arginine to alanine, glutamate, or glutamine resulted in decreased nucleotide incorporation efficiency for CMP, CMP and AMP incorporation, decreased specificity at the penultimate position, and an increase in specificity for AMP incorporation (compared to the native enzyme). This suggests that this conserved arginine residue plays roles not only in orienting residues in the binding pocket but also in altering the size of the binding pocket to aid in discrimination between nucleotides at the different positions. This supports observations that amino acid substitutions in this region of the protein can alter a complex network of hydrogen bonds that are involved in organizing the correct orientation of the protein, the incoming nucleotides, and 3′ end of the tRNA (Cho *et al*., 2007).

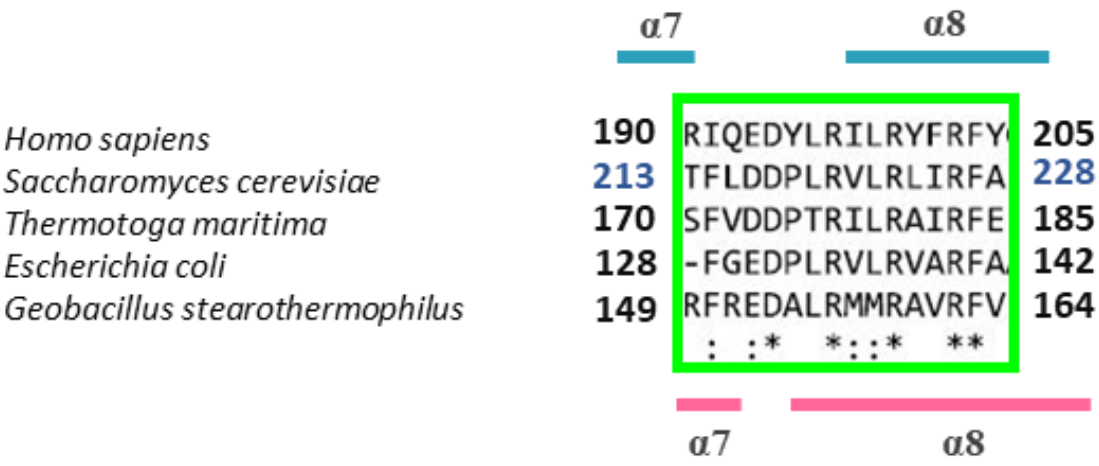

Figure 1.8 Alignment of motif D in the head domain of five class II tRNA nucleotidyltransferases. The alignment was performed using ClustalW2 software (Martin *et al.,* 2007). Numbers represent residue positions in the protein, letters stand for one letter code for the amino acids. Strongly conserved (*), highly similar amino acids (:) and slightly conserved (.) amino acids are indicated below the sequence. The regions identified as either β-strands (β) or α-helices (α) in the crystal structure of the human enzyme (Augustin *et al*., 2003) (blue) and the model structure of the yeast enzyme (pink) are shown above and below the alignment, respectively.

1.2.6 Motif E

Motif E (Fig. 1.1) in the neck domain of the enzyme plays a role in the termination of nucleotide addition and in stabilizing interactions between the tRNA and the protein (Li *et al.,* 2002). This motif is defined by a conserved RxxxExxKxL sequence (Fig. 1.9). Conversion of the first five residues of this motif (RxxME) to AxxAA in the *Geobacillus stearothermophilus* enzyme converted the enzyme to a poly (C, A) polymerase enzyme by removing the restraints on the growing tRNA 3' terminus (Cho *et al*., 2007). Our studies on the *Candida glabrata* tRNA-NT showed that replacement of the first arginine in this motif with alanine, lysine or methionine did not allow for extension of the 3'-end of the tRNA beyond three nucleotides but did lead to a loss of nucleotide addition at position 74, a reduction of nucleotide specificity at position 75, and an increase in nucleotide specificity at position 76 as compared to the native enzyme (Arthur, 2009). These results suggest that this arginine residue plays a role not only in binding and orienting the substrates (nucleotide triphosphates and tRNA) for catalysis, but also in excluding ATP from the active site prior to nucleotide addition to positions 74 and 75.

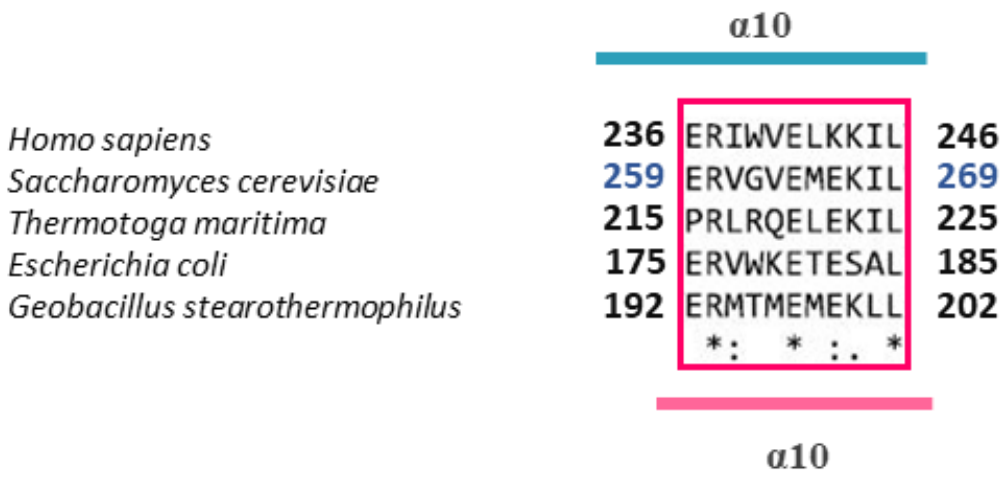

Figure 1.9 Alignment of motif E in the head domain of five class II tRNA nucleotidyltransferases. The alignment was performed using ClustalW2 software (Martin *et al.,* 2007). Numbers represent residue positions in the protein, letters stand for one letter code for the amino acids. Strongly conserved (*) and highly similar amino acids (:) amino acids are indicated below the sequence. The regions identified as either β-strands (β) or α-helices (α) in the crystal structure of the human enzyme (Augustin *et al*., 2003) (blue) and the model structure of the yeast enzyme (pink) are shown above and below the alignment, respectively.

In summary, it is apparent that residues involved in catalysis and in defining the structure of the active site of tRNA-NTs are far apart in the primary structure of the protein but must be brought together in the native enzyme to allow for catalysis and the alteration in the structure of the active site as different substrates (CTP or ATP, tRNA-N, tRNA-NC, or tRNA-NCC) are recognized. The role of motif C has become more evident in these reactions, but its exact function still remains to be explored.

1.3 *Saccharomyces cerevisiae* tRNA nucleotidyltransferase

1.3.1 Identifying the *ts* mutation

The *Saccharomyces cerevisiae CCA1* gene represented the first gene encoding a tRNA-NT to be isolated from any eukaryote (Aebi *et al.*, 1990). This gene was identified by complementation of the temperature-sensitive (*ts*) yeast strain ts352. After a shift to the restrictive temperature the *ts* strain quickly accumulated tRNAs lacking a complete CCA sequence (Aebi *et al.* 1990). When this *ts* strain was transformed with a plasmid bearing the *CCA1* gene, the tRNA population showed complete CCA extension, consistent with the loss of the *ts* phenotype (Chen *et al*., 1990).

Subsequently, the ts352 allele was sequenced and shown to possess a single guanine to adenine transition that resulted in the substitution of a lysine for a glutamate at position 189 in the yeast tRNA-NT (Shan *et al*., 2008). The same study also showed that converting residue 189 to histidine or phenylalanine also generated a *ts* phenotype (Shan *et al*., 2008). The *ts* phenotype in the E189K, E189F or E189H variants was linked to reduced enzyme activity and/or reduced thermal stability (Shan *et al*., 2008). When the predicted structure of the yeast enzyme showing the location of E189 in a β-turn connecting β-strand 7 and α-helix 6 was compared to the existing tRNA-NT crystal structures, it was proposed that the increase in the size of the R group at position 189 in the E189K, E189F and E189H variants resulted in a change in the organization of this turn such that the β-strand and α-helix altered their positioning relative to one another changing the organization of (at least) this region of the protein (Shan *et al*., 2008). When residue 189 was converted to alanine, the *ts* phenotype also was seen and these E189A variants also showed reduced activity (Rahman, 2017). This suggested that not only an increase in the size of the residue at position 189 but also a decrease in the size of this residue could change the organization of the protein to lead to the reduced activity seen *in vitro* and the *ts* phenotype seen *in vivo*.

1.3.2 Identifying a suppressor

To develop a better understanding of the role of E189 (and by extension motif C) in enzyme activity and to explore more deeply the cause of the *ts* phenotype, suppressor analysis was utilized (Goring *et al*., 2013). Cells expressing the E189F variant were irradiated with UV light and then tested for their ability to grow at the restrictive temperature. Of the 0.0003% of the cells that grew at the restrictive temperature, approximately 25% of those screened showed a single C to T transition resulting in an arginine (CGG) to tryptophan (TGG) substitution at residue 64 in the gene product. In a few cases a single G to A transition resulting in an arginine (CGG) to glutamine (CAG) substitution at residue 64 in the gene product was seen (Gea-Mallorqui, 2011). This analysis revealed the importance of residue 64 in suppressing the *ts* phenotype but provided no information as to how this was accomplished.

1.3.3 The role of residue 64

Naively, one could imagine at least two ways that an intragenic suppressor could eliminate a *ts* phenotype. In one case, the first mutation disrupts a defined interaction between specific amino acids that alters the structure, function or stability of the enzyme leading to the *ts* phenotype. So, in this case perhaps E189 interacts specifically with R64. Given the relative charges on these two residues and their positions in the protein (Fig. 1.10) one could imagine electrostatic or hydrogen bonding interactions between these two residues involved in defining the structure of the protein. This interaction would be lost when E189 was converted to alanine, lysine, phenylalanine or histidine leading to an altered organization of the protein and the *ts* phenotype observed.

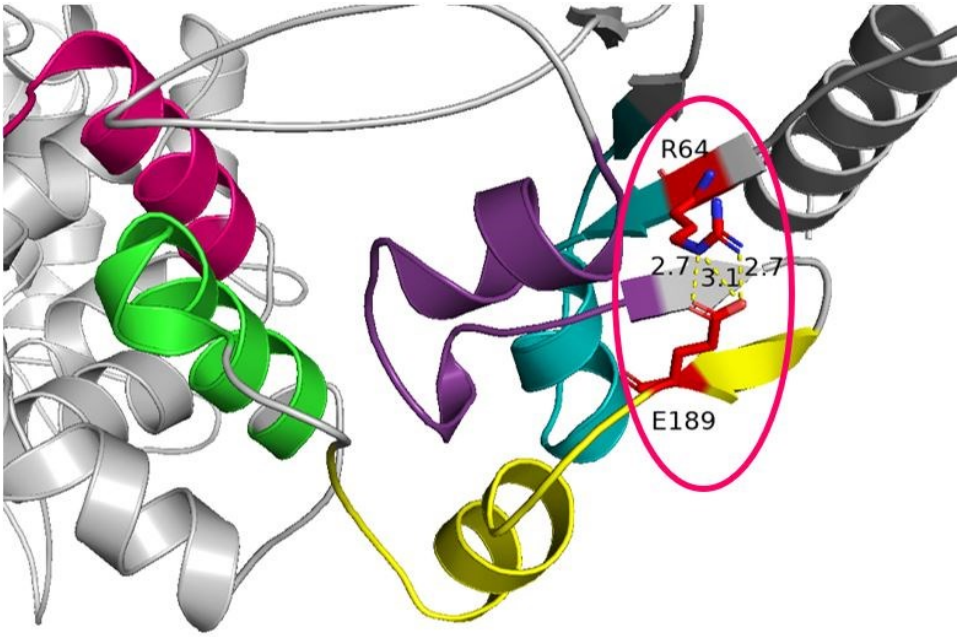

Figure 1.10 The relative positions of R64 and E189 in a model structure of the yeast tRNA-NT. Arginine at position 64 and glutamic acid at position 189 are shown in red in the pink circle. The distances between the oxygens and nitrogens of the R groups of E189 and R64, respectively, are shown in Å. The positions of motifs contained in this region of the protein are shown (colours as in Fig. 1.1).

As the R64W substitution on its own (which would disrupt any predicted electrostatic interaction and reduce the H-bonding potential) does not generate a *ts* phenotype and does not

dramatically affect enzyme activity or thermal stability (Goring *et al*., 2013), this simple explanation is likely not valid. The loss of the E189-R64 interactions in the variant containing the R64W substitution would likely not be compensated for by the little hydrogen bonding or hydrophobic interaction potential between E189 and W64 (Fig. 1.11). Additionally, the R64W substitution allows for growth of cells expressing the E189A (Rahman, 2017) and E189K (Goring *et al*., 2013) variants at the restrictive temperature. Again, in these examples it is difficult to imagine any potential direct molecular interactions (*e.g*., electrostatic, H-bonding, hydrophobic, or VanderWaals) between W64 and A189 or K189 (Fig. 1.12) that could replace the possible electrostatic interactions between R64 and E189.

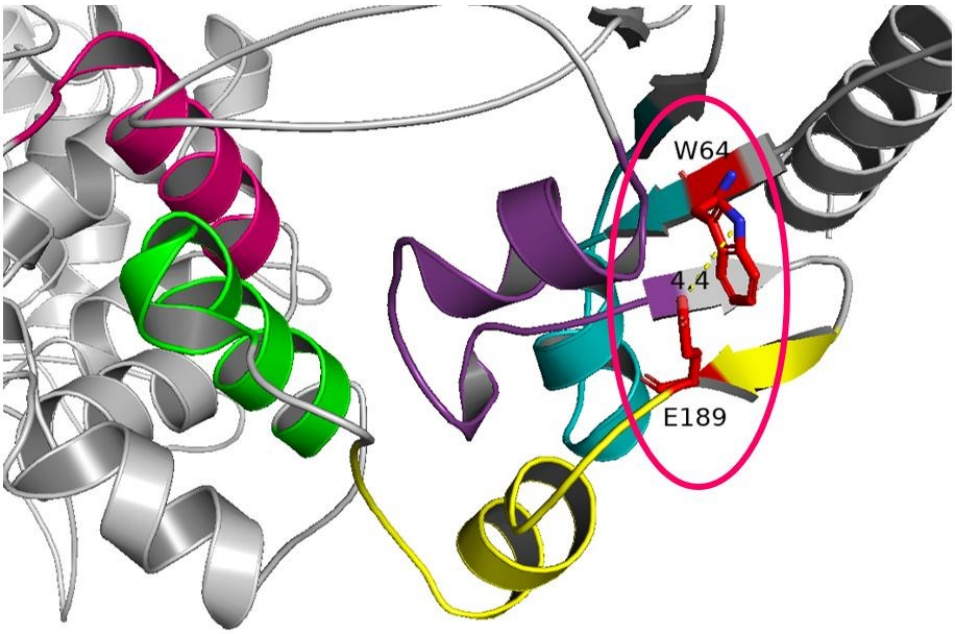

Figure 1.11 Relative positions of W64 and E189 in a model structure of the yeast tRNA-NT. Arginine at position 64 and glutamic acid at position 189 are shown in red in the pink circle. The distance between an oxygen and a nitrogen of the R groups of E189 and W64, respectively, are shown in Å. The positions of motifs contained in this region are shown (colours as in Fig. 1.1).

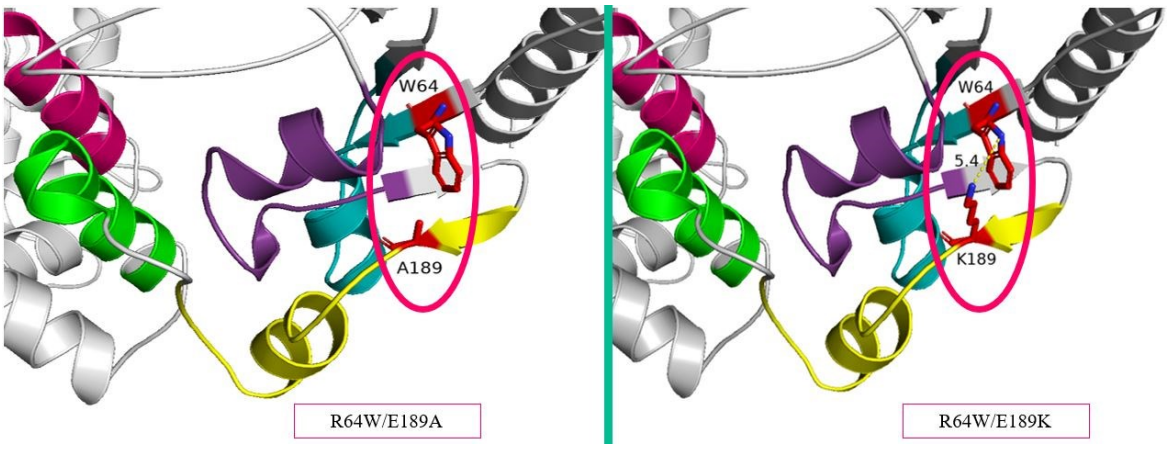

Figure 1.12 Model structure of the yeast tRNA-NT indicating positions 64 and 189 in R64W/E189A and R64W/E189K variants. The tryptophan at position 64 and the alanine (left) or lysine (right) at position 189 are shown in red in the pink circle. The distance between nitrogens of the R groups of K189 and W64 are shown in Å. The positions of motifs contained in this region of the protein are shown (colours as in Fig. 1.1).

Finally, yeast expressing the R64E/E189R variant (Fig. 1.13) where the R groups are switched between residues 64 and 189 remains *ts* indicating that whatever interactions are required to suppress the *ts* phenotype are directional (Goring *et al*., 2013). Moreover, the R64E substitution cannot suppress the *ts* phenotype in cells carrying the E189F or E189K substitutions (Goring *et al*., 2013). Taken together these data do not support a model where the R groups of E189 and R64 interact directly.

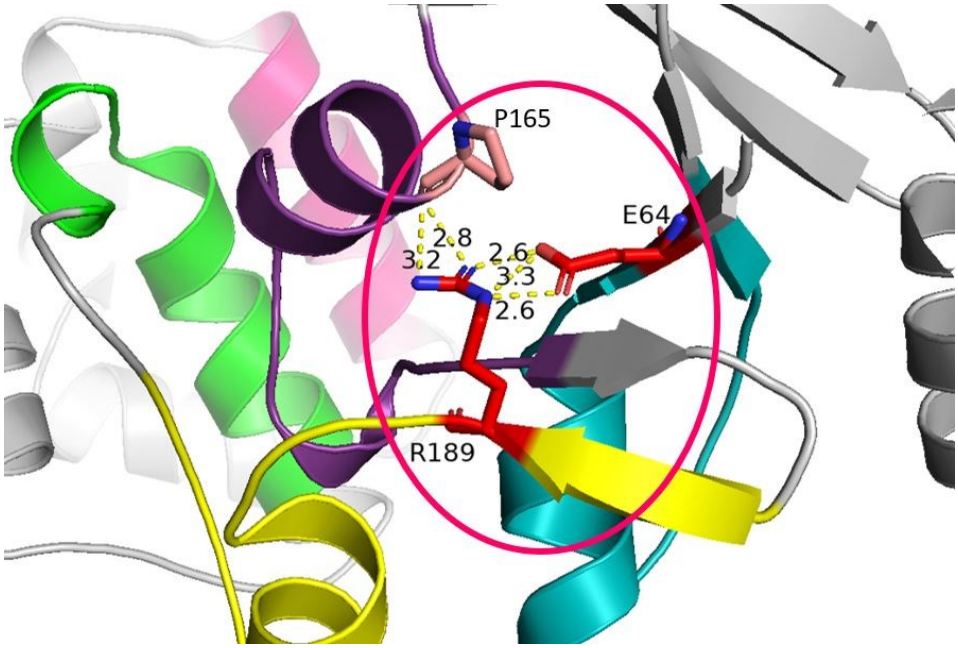

Figure 1.13 Relative positions of E64 and R189 in a model structure of the yeast tRNA-NT. Glutamic acid at position 64 and arginine at position 189 are shown in red in the pink circle. The distances in Å between the R group nitrogens of R189 and the R group oxygens of E64 are shown as are the distances between the R group nitrogens of R189 and the main chain oxygen of P165. The positions of motifs contained in this region are shown (colours as in Fig. 1.1).

These models suggest that it is not simply the loss of a direct interaction between E189 and R64 that is leading to the *ts* phenotype. Therefore, one must imagine a second possible explanation for intragenic suppression. If the first mutation results in a change in the protein such that its structure, activity or stability is altered so that it cannot function well enough to meet the needs of the cell at the restrictive temperature, then the second mutation may alter the protein somewhere else in a manner that makes up for the first deleterious change. If this is the case, then either substitution alone may be unfavorable but the two changes together will compensate for these defects. As an example of this, when residue 189 is converted to alanine, the specificity constant for tRNA for the enzyme (reflecting changes in K_M and k_{cat}) drops by approximately 800 fold as compared to the native enzyme (Rahman, 2017). When residue 64 alone is changed to tryptophan the specificity constant drops to 50% of that of the native enzyme, but this second substitution in the E189A variant results in a specificity constant that is increased by approximately 600 fold to ~70% that of the native enzyme (Rahman, 2017). Somehow a change in the enzyme mediated by

the R64W substitutions counteracts the dramatic drop in the specificity constant seen in the E189A variant.

In almost all of these cases (with the exception of the E189A substitution) changes at residues 189 and 64 result in limited changes in protein structure as measured by circular dichroism and fluorescence spectroscopy (Shan *et al*., 2008, Goring *et al*., 2013, Rahman, 2017) and it appears that the *ts* phenotype results from a decrease in enzyme activity and not a change in thermal stability because, in almost all cases, the R64W substitution suppresses the *ts* phenotype by restoring enzyme activity and not by increasing thermal stability (Goring *et al*., 2013, Rahman, 2017).

1.3.4 The role of residue 190

In our initial study of motif C, we proposed that residue E189 in the yeast tRNA-NT corresponded to D168 in the human homologue (Shan *et al*., 2008). More recent work with the human enzyme suggests that D168 (residue D139 in the numbering system of Ernst *et al*., 2015) in the human tRNA-NT is the equivalent of D190 in the yeast enzyme (Ernst *et al*., 2015). Given the strength of their arguments (sequence alignments, structural overlays, role of D168 in helix capping) we have adjusted our alignments accordingly (Fig. 1.6). Taking this into consideration, it became important to assess the role of D190 in motif C in the yeast enzyme. Ernst *et al*. (2015) showed that in the human enzyme converting D168 to alanine resulted in an 18-fold reduction in specificity constant for ATP, but showed no major changes in tRNA binding. We, therefore, set out to explore what effect changing residue 190 in the yeast enzyme would have on the structure, stability and activity of the yeast tRNA-NT. To address this question, we initially converted the corresponding aspartate residue in the yeast enzyme to alanine or phenylalanine as examples of smaller and larger amino acids at this position. In good agreement with what had been shown in the human enzyme we saw an approximately 8-fold reduction in specificity constant for ATP in the D190A variant as compared to the native enzyme and an even greater decrease (75 fold) for the D190F variant as compared to the native enzyme (Rahman, 2017).

In viability assays in yeast, the D190F variant showed no growth even at the permissive temperature while the D190A variant showed a *ts* phenotype (Rahman, 2017). This is in good

agreement with what was seen in the kinetics assays. When the R64W substitution was introduced into these backgrounds, both strains grew at the permissive and restrictive temperatures and the specificity constants for ATP showed approximately 1.4 (R64WD190A) and 39-fold (R64WD190F) increases as compared to the D190A and D190F variants, respectively. These increases in activity *in vitro* correlate well with the *in vivo* viability assays.

None of these variants showed any major changes in structure or thermostability (Rahman, 2017). So, it appears that the R64W substitution also can compensate for changes at position 190 in the yeast tRNA-NT. Given that our models predict that D190 and R64 do not interact (Fig. 1.14) this further supports the hypothesis that it is not a direct interaction between these amino acids, but a more general alteration in protein structure that leads first to the reduced growth phenotype and then to the R64W-induced suppression of this phenotype.

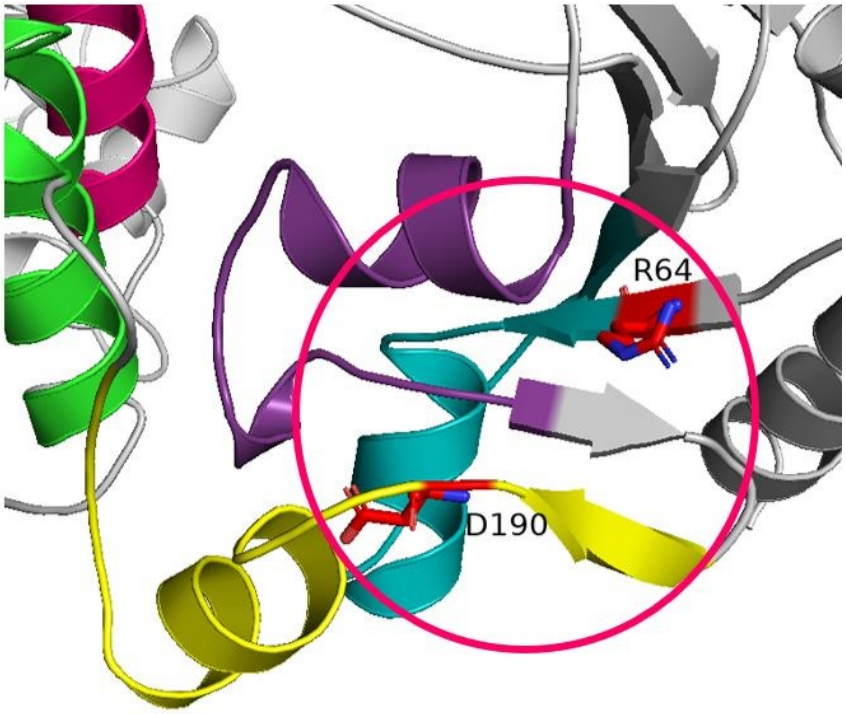

Figure 1.14 Predicted structure of a region of yeast tRNA-NT showing the relative positions of residues R64 and D190 (shown in red). Conserved motifs are colored as in Figure 1.1.

1.4 Project objectives

As discussed above, we have generated multiple variant enzymes to study the role of motif C in yeast tRNA-NT structure, function and stability. These studies have shown that amino acid substitutions at residues 189 and 190 in motif C may reduce enzyme activity and lead to a *ts* (or in one instance a non-viable) phenotype. We also have shown that the conversion of residue 64 in motif A from arginine to tryptophan can, in almost every instance, increase enzyme activity in the initial variants and eliminate the *ts* or inviable phenotype. These data suggest that it is not simply a change in a direct interaction between the residues at positions 64 and 189 or 190 that leads to these phenotypes. More likely the generation of these phenotypes (by alterations at residues 189 and 190) and the subsequent suppression of these phenotypes (in the R64W background) reflects small changes in the organization of the active site such that the R64W substitution compensates for deleterious changes in the 189 and 190 variants. Given that residues 189 and 190 are linked to motif C and that motif C is thought to be involved in the reorganization of the active site during catalysis while R64 is at the edge of the catalytically essential motif A, this structural compensation hypothesis makes sense.

Here, I focus on exploring in more detail the role of residue 64 in *Saccharomyces cerevisiae* tRNA-NT with the intention of more clearly defining the coordination of motifs A and C. We already have seen the effects of multiple amino acid substitutions at positions 189 and 190, but only in the context of the native enzyme and the R64W variant. To supplement these data, I will generate a number of yeast tRNA-NT variants with new substitutions at residue 64. Specifically, I will replace the arginine at position 64 with phenylalanine (large and hydrophobic like tryptophan, but lacking hydrogen bonding potential), alanine (much smaller than arginine or tryptophan) or proline (which should disrupt the β-sheet) to see what effect these changes have on the structure or function of the native enzyme and the existing E189 and D190 variants.

Given that arginine is seen at the corresponding position to R64 in motif A in the human enzyme, but that tyrosine is found in the corresponding position in the bacterial enzymes (Fig. 1.2) we anticipate that a phenylalanine at this position would be an extremely conservative substitution. The phenylalanine would be a large residue like arginine or tyrosine and would differ only slightly from these residues in that it would have no hydrogen bonding potential. If our model is correct,

we would expect no major differences when the R64F variant is compared to the R64W variant. If hydrogen bonding potential, but not size is important at position 64 we should see some differences between the R64 and F64 variants.

In the case of the arginine to alanine substitution at position 64 we may expect a more dramatic change in the protein as we are replacing the residue at this position with one that is much smaller and which has no H-bonding potential. The glutamate to alanine substitution at position 189 in the native enzyme resulted in atypical results in thermostability and CD and fluorescence spectroscopy. While most variants showed emission spectra with intensities within 30% of that of the native enzyme, the E189A variant had an emission profile with an intensity less than one half that of the native enzyme (Rahman, 2017). This protein also was the only variant tested that gave a much-reduced CD signal as compared to the native enzyme and was one of two (with E189Q) that showed an increased denaturing temperature as compared to the native enzyme (Rahman, 2017). If size is the primary variable which controls the organization of this portion of yeast tRNA-NT then we should expect the R64A substitution to show changes in structure, stability and activity.

Finally, we anticipate that conversion of the arginine residue at position 64 to proline should cause a major disruption in the structure, stability and activity of yeast tRNA-NT. Proline residues are not tolerated well in β-strands and residue 64 is found in motif A in β-strand 1 in the single β-sheet that defines a polymerase β-family nucleotidyltransferase.

Here, I will use a combination of genetic, biochemical and biophysical assays to begin to explore the effects of changes at position 64 on the structure, activity and stability of yeast tRNA-NT to provide insight into the role of this residue in enzyme function and suppression of growth phenotypes.

2.0 MATERIALS AND METHODS

2.1 Strains and Plasmids

The strains and plasmids used in this study are shown in Tables 2.1 and 2.2, respectively.

Table 2.1 *Escherichia coli (E. coli)* and *Saccharomyces cerevisiae (S. cerevisiae)* strains used in this study.

Strain	Use	Supplier	Genetic Background
BL21 (DE3) (*E. coli*)	Heterologous protein expression	Stratagene	*E. coli* str. B F– ompT gal dcm lon hsdSB(rB–mB–) λ(DE3 [lacI lacUV5-T7p07 ind1 sam7 nin5]) [malB+]K-12(λS)
XL2-Blue (*E. coli*)	DNA manipulations	Stratagene	end A1 supE44 thi-1 hsdR17recA1 gyrA96 relA1 lac [F´proAB lacIqZΔM15 Tn10 (Tet^r) Amy Cam^r]
SCDT8 (*S. cerevisiae)*	Viability assays	Leibovitch *et al.* (2013)	*MATα leu2-3,112 trp1-1 can1-100 ura3-1 ade2-1 his3-11,15 cca1::TRP1* bearing a derivative of pRS316 containing the wild-type *CCA1* gene of *S. cerevisiae*

Table 2.2 *E. coli* and *S. cerevisiae* plasmids used in this study

Plasmid	Reference
pGEX-2T–CCA1	Open reading frame of *S. cerevisiae CCA1* gene in pGEX-2T (GE Healthcare) (Goring *et al*., 2013)
pSCH12-1	Open reading frame of *S. cerevisiae CCA1* gene with *CCA1* promoter in pG131-2T (kindly provided by Dr. PJ Hanic-Joyce)
pGEX-2T-CCA1-E189F	Open reading frame of *S. cerevisiae* mutant *cca1* gene expressing E189F substitution in pGEX-2T (Shan *et al*. 2008)
pGEX-2T-CCA1-E189K	Open reading frame of *S. cerevisiae* mutant *cca1* gene expressing E189K substitution in pGEX-2 (Shan *et al*., 2008)
pGED190A13	Open reading frame of *S. cerevisiae* mutant *cca1* gene expressing D190A substitution in pGEX-2T (Rahman, 2017) (kindly provided by Dr. PJ Hanic-Joyce)
pGED190F16-2	Open reading frame of *S. cerevisiae* mutant *cca1* gene expressing E189F substitution in pGEX-2T (Rahman, 2017) (kindly provided by Dr. PJ Hanic-Joyce)
pGEX-2T-CCA1-R64A	Open reading frame of *S. cerevisiae* mutant *cca1* gene expressing R64A substitution in pGEX-2T (Generated by Sabine El-Khoury)
pGEX-2T-CCA1-R64F	Open reading frame of *S. cerevisiae* mutant *cca1* gene expressing R64F substitution in pGEX-2T (Generated by Sabine El-Khoury)
pGEX-2T-CCA1-R64P	Open reading frame of *S. cerevisiae* mutant *cca1* gene expressing R64P substitution in pGEX-2T (Generated by Camille Gervais)
pSCH12-1-R64A	Open reading frame of *S. cerevisiae* mutant *cca1* gene expressing R64A substitution in pSCH12-1 (Generated by Sabine El-Khoury)

pSCH12-1-R64F	Open reading frame of *S. cerevisiae* mutant *cca1* gene expressing R64F substitution in pSCH12-1 (Generated by Sabine El-Khoury)
pGEX-2T-RAEF	Open reading frame of *S. cerevisiae* mutant *cca1* gene expressing R64A/E189F substitutions in pGEX-2T (This work)
pGEX-2T-RFEF	Open reading frame of *S. cerevisiae* mutant *cca1* gene expressing R64F/E189F substitutions in pGEX-2T (This work)
pGEX-2T-RPEF	Open reading frame of *S. cerevisiae* mutant *cca1* gene expressing R64P/E189F substitutions in pGEX-2T (This work)
pGEX-2T-RAEK	Open reading frame of *S. cerevisiae mutant cca1* gene expressing R64A/E189K substitutions in pGEX-2T (This work)
pGEX-2T-RFEK	Open reading frame of *S. cerevisiae mutant cca1* gene expressing R64F/E189K substitutions in pGEX-2T (This work)
pGEX-2T-RADA	Open reading frame of *S. cerevisiae mutant cca1* gene expressing R64A/D190A substitutions in pGEX-2T (This work)
pGEX-2T-RFDA	Open reading frame of *S. cerevisiae mutant cca1* gene expressing R64F/D190A substitutions in pGEX-2T (This work)
pGEX-2T-RADF	Open reading frame of *S. cerevisiae mutant cca1* gene expressing R64FA/D190F substitutions in pGEX-2T (This work)
pGEX-2T-RFDF	Open reading frame of *S. cerevisiae mutant cca1* gene expressing R64F/D190F substitutions in pGEX-2T (This work)
pSCH12-1-R64P	Open reading frame of *S. cerevisiae mutant cca1* gene expressing R64P substitution in pSCH12-1 (This work)
pSCH12-1-RAEF	Open reading frame of *S. cerevisiae mutant cca1* gene expressing R64A/E189F substitutions in pSCH12-1(This work)
pSCH12-1-RFEF	Open reading frame of *S. cerevisiae mutant cca1* gene expressing R64F/E189F substitutions in pSCH12-1 (This work)
pSCH12-1-RPEF	Open reading frame of *S. cerevisiae mutant cca1* gene expressing R64P/E189F substitutions in pSCH12-1 (This work)
pSCH12-1-RAEK	Open reading frame of *S. cerevisiae mutant cca1* gene expressing R64A/E189K substitutions in pSCH12-1 (This work)
pSCH12-1-RFEK	Open reading frame of *S. cerevisiae mutant cca1* gene expressing R64F/E189K substitutions in pSCH12-1 (This work)
pSCH12-1-RADA	Open reading frame of *S. cerevisiae mutant cca1* gene expressing R64A/D190A substitutions in pSCH12-1 (This work)
pSCH12-1-RFDA	Open reading frame of *S. cerevisiae mutant cca1* gene expressing R64F/D190A substitutions in pSCH12-1 (This work)
pSCH12-1-RADF	Open reading frame of *S. cerevisiae mutant cca1* gene expressing R64A/D190F substitutions in pSCH12-1 (This work)
pSCH12-1-RFDF	Open reading frame of *S. cerevisiae mutant cca1* gene expressing R64F/D190F substitutions in pSCH12-1 (This work)

2.2 Solutions and Growth Media

The solutions and growth media used in this study are listed in Table 2.3.

Table 2.3 Solutions and growth media used in this study.

	Solutions / Growth Media	Ingredients
Buffers	1X PBS (Sambrook *et al.*, 1989)	137 mM NaCl, 1.8 mM KH_2PO_4, 10 mM Na_2HPO_4, 2.7 mM KCl (pH 7.5)
	Lysis buffer in GST-tag protein purification (Modified from Shan *et al.,* 2008)	1X PBS containing 1 mM EDTA
	GST-tag Elution buffer (Modified from Lin, 2008)	50 mM Tris-HCl, 10 mM reduced glutathione, 20 mM dithiothreitol (pH 8)
	5X TBE (Modified from Sambrook *et al.*, 1989)	250 mM Tris-HCl, 25 mM Boric acid, 0.5 M EDTA (pH 8)
SDS-PAGE Solutions	5X SDS running buffer (Modified from Sambrooke *et al.,* 1989)	1M Glycine, 1M Tris-HCl, 17 mM SDS
	30% Acrylamide Solution (29:1) (Sambrook *et al.,* 1989)	29 g Acrylamide, 1 g bis-acrylamide in 100 ml dH_2O
	SDS (5X) Loading Dye (Modified from Walker, 2002)	Tris-HCl (45 mM) (pH 6.8), 10% SDS (w/v), 50% glycerol (v/v), 25% β-mercaptoethanol (v/v), 0.25% bromophenol blue (w/v)
	Solution A (Staining) (Wong *et al.,* 2000)	0.05% Coomassie brilliant blue, 25% Isopropanol, 10% Acetic acid
	Solution B (Destaining) (Wong *et al.,* 2000)	0.005% Coomassie brilliant blue, 10% Isopropanol,10% Acetic acid
	Solution D (Destaining) (Wong *et al.,* 2000)	10 % Isopropanol, 10% Acetic acid
	SDS-PAGE resolving gel 13% (10 ml) (Modified from Sambrook *et al.,* 1989)	30% acrylamide - 4.3 ml, Tris (1.5 M, pH 8.8) - 2.5 ml, dH_2O - 3.0 ml, APS (10%) - 100 µl, SDS (10%) - 100 µl, TEMED - 10 µl
	SDS-PAGE 10% stacking gel (10 ml) (Modified from Sambrook *et al.,* 1989)	30% acrylamide - 1.4 ml, Tris (0.5 M, pH 6.8) - 2.5 ml, dH_2O - 6.0 ml, APS (10%) - 100 µl, SDS (10%) - 100 µl, TEMED - 10 µl
Media	100X T-mix (Guthrie and Fink, 1991)	0.3% tyrosine, 0.2% tryptophan, 2% threonine, adjusted to pH 10 with NaOH, filter sterilized
	YT (Guthrie and Fink, 1991)	0.8 % Tryptone, 0.5%, NaCl, 0.5% Yeast extract
	YPD (Sambrook *et al.,* 1989)	0.2% Peptone, 2% Glucose, 1% Yeast extract (Plates contain 1.5% agar)
	SC-HIS-URA (Guthrie and Fink, 1991)	0.67% Yeast nitrogen base (minus amino acids), 2% Glucose, 20 mg/l each of adenine, L-arginine-HCl, L-methionine, 30mg/l each of L-leucine, L-isoleucine, L-lysine-HCl, 50 mg/l phenylalanine, after autoclaving add 100X T-mix (10 ml/l) and agar to 1.5% (for plates)
	5-fluoroorotic acid (5-FOA) (adapted from Cold Spring Harbor Protocols, 2016)	Filter sterilize 1.68 g yeast nitrogen base (without amino acids), 5g glucose, 5 mg each of Adenine, Histidine, and Tryptophan, 12.5 mg Uracil, and 125 mg FOA in a final volume of 125 ml Autoclave 5g agar in 125 ml dH_2O and add to filter sterilized solution.

2.3 QuikChange™ site-directed mutagenesis (Agilent)

Site-directed mutagenesis reactions were brought to a final volume of 100 µl with dH_2O and contained 10-30 ng of the appropriate plasmid (Table 2.2), 10 pmol of the appropriate forward and reverse primers (Table 2.4), 1X Hf buffer (NEB), 0.2 mM dNTPs (Biobasic Inc), and 0.8 units Phusion™ high fidelity DNA polymerase (NEB). All primers were purchased from Integrated DNA Technologies (IDT). Control reactions included template without primers. The reactions were performed in a BIO-RADT100™ Thermal Cycler under specific conditions (Table 2.5). To complete the QuikChange protocol, 5 units (0.5 µl) of *Dpn*I were added to each sample with incubation at 37°C for 1 h prior to transformation into *E. coli*.

Table 2.4 Primers used in site-directed mutagenesis.

Variant	Oligonucleotides
R46A	F: GTACCACAATAAGCCTGAACCATTGACTCTTGCTATCACGGGCGGATGG
	R: CCATCCGCCCGTGATAGCAAGAGTCAATGGTTCAGGCTTATTGTGGTAC
R64F	F: GTACCACAATAAGCCTGAACCATTGACTCTTTTTATCACGGGCGGATGG
	R: CCATCCGCCCGTGATAAAAAGAGTCAATGGTTCAGGCTTATTGTGGTAC
R46P	F: GTACCACAATAAGCCTGAACCATTGACTCTTCCAATCACGGGCGGATGG
	R: CCATCCGCCCGTGATTGGAAGAGTCAATGGTTCAGGCTTATTGTGGTAC
E189K	F: CATTCATAAAGGTGAAGTTAAAGATTTCACTAAGAGAGGTCTGCAAG
	R: CTTGCAGACCTCTCTTAGTGAAATCTTTAACTTCACCTTTATGAATG
D190A	F: GGTGAAGTGGAAGCTTTCACCAAGAGAGG
	R: CCTCTCTTGGTGAAAGCTTCCACTTCACC
D190F	F: GGTGAAGTGGAATTCTTCACCAAGAGAGG
	R: CCTCTCTTGGTGAAGAATTCCACTTCACC

The nucleotides of the codon modified are indicated in pink and bold. A single G to A silent nucleotide substitution that removes a *Dde*I restriction site (CTNAG) is shown in blue and bold. A single C to T silent nucleotide substitution that adds a *Dde*I restriction site is shown in green and bold.

Table 2.5 QuikChange™ reaction conditions

Step	Function	Temperature (°C)	Time (s)
1	Initial Denaturation	98	30
2	Denaturation	98	10
3	Annealing	40	30
4	Extension	72	300
5	Amplification	18 cycles of steps 2 to 4	
6	Final Extension	72	600
7	Hold	12	Overnight

2.4 *E. coli* transformation (Ausubel *et al.*, 1989)

Competent (Capage and Hill, 1979) *E. coli* cells BL21 (New England BioLabs) or XL2 (Stratagene) were kindly provided by Nathalie Reid. Frozen competent cells from -80°C were thawed on ice and 50 µl aliquots distributed to prechilled Eppendorf tubes on ice. Typically, 10 to 50 ng of DNA (in a maximum volume of 5 µl) was added with stirring with the pipette tip and the samples were left on ice for 20-60 min. The samples then were heat shocked in a 42°C water bath for 45 sec and returned to the ice for a minimum of 1 min. Subsequently, 500 µl of YT medium was added with stirring with the pipette tip and the samples were placed at 37°C for 1 h. After this incubation, the microfuge tube containing the sample was centrifuged at 12 000 xg for 1 min at room temperature to pellet the cells. Prior to resuspending the cells, 400 µl of the supernatant was discarded and the cells pellet resuspended in the remaining YT using the pipette tip. The cells suspension was then spread on YT plus 100 µg/µl ampicillin plates and incubated overnight at 37°C.

2.5 Restriction digestions

Diagnostic restriction digestions were typically carried out in a final volume of 15 µl (adjusted with dH_2O) while linearization of plasmid DNA prior to ligation reactions was performed in a final volume of 25 µl. In either case the reaction contained 1-10 µg of DNA, 1X CutSmart buffer (NEB) and 5 units of the appropriate restriction enzyme(s), *Dpn*I, *Dde*I, *Hin*dIII, *Bbs*I, or *Sal*I and *Sac*I, or *Eco*RI (NEB). Typically, digestions were performed at 37°C for 1 h. In order to dephosphorylate

linearized vectors, 5 units (0.5 µl) of calf intestinal phosphatase (NEB) was added and the sample returned to the water bath for an additional 30 min.

2.6 Agarose gel electrophoresis and visualization

Agarose gels (0.8% or 2%) were prepared in 50 ml 1X TBE (Table 2.3) and electrophoresis was carried out for 1 h at 100 mV. Typically, 3 µl of 6X Purple Gel Loading Dye (NEB) was added to a 15 µl sample, or to sample plus dH_2O. The Foto/Prep®I transilluminator was used to visualize the DNA.

2.7 Gel extraction and isolation of DNA fragments (Bewsey *et al.*, 1991)

Fragments to be isolated were visualized on preparative mode on the Foto/Prep®I transilluminator and excised as quickly as possible by using a metal spatula. The gel slice was transferred to an Eppendorf tube and ground using the same tool. An equal volume of Tris-saturated phenol (typically ~300 µl) was added with vortexing at room temperature for 10 min. The Eppendorff tube was subsequently placed at -80°C for a minimum of 30 min. The sample then was placed in a 37°C water bath for a minimum of 30 min, another 300 µl phenol was added and the freeze-thaw cycle was repeated. After finishing the second freeze-thaw cycle, 150 µl dH_2O and 40 µl of 3 M sodium acetate (pH 5.2) were added, the sample was vortexed for 10 min and then centrifuged at 12 000 xg for 15 min at 4°C. The aqueous phase was collected in an Eppendorff centrifuge, and an equal volume of phenol was added with vortexing for 3 min and centrifugation at 12 000 xg and 4°C for 3 min. The aqueous phase was collected, and the phenol extraction repeated as above. Again, the aqueous phase was collected, and an equal volume of water-saturated ether was added with vortexing for 1 min and centrifugation at 12 000 xg and 4°C for 3 min to separate the phases. The aqueous phase was collected, and the ether extraction was repeated as described above. The final aqueous phase was then concentrated by ethanol precipitation.

2.8 Ethanol precipitation (modified from Sambrook *et al.*, 1989)

In order to concentrate the DNA, the samples first were taken to 0.3 M sodium acetate (by adding one tenth volume 3 M sodium acetate if necessary) and then 2-2.5 volumes of 99% cold

ethanol were added with vigorous vortexing. The samples then were placed at -80°C for a minimum of 30 min (or at -20°C overnight). At the end of this time, the samples were centrifuged for 20-30 min at 12 000 xg and 4°C, the ethanol was discarded, 500 µl of cold 80% ethanol was added to wash the pellet, and the sample was centrifuged for 5 min at 12 000 xg and 4°C. The ethanol was discarded, and the DNA pellets were dried under vacuum for at least 20 min at room temperature. Finally, the dried DNA was resuspended by vortexing in sterile dH_2O to an appropriate volume (usually 10 µl).

2.9 Ligation reactions

Ligations were carried out in a final volume of 20 µl (adjusted with dH_2O) and contained 150 ng of appropriate insert DNA, 50 ng of vector DNA, 160 units of T4 DNA ligase (NEB) and 1X ligase buffer (NEB). Typically, ligations were performed for 16 h at 4°C. In cases where QuikChange mutagenesis was unsuccessful, DNA fragments carrying the required mutations were excised by restriction digestion from DNA containing the mutation and ligated into an acceptor plasmid that had been digested with the same restriction enzymes. Diagnostic restriction digestions then were used to show whether the DNA fragment containing the desired mutation(s) had replaced the original DNA fragment to generate the new plasmid.

All E189F and E189K variants were digested with *Dde*I. Plasmids (pGEX-2T derivatives) carrying the D190F variants (RADF and RFDF) were digested with *Eco*RI. Since a new *Eco*RI was added to the open reading frame in designing the D190F variant (Table 2.3), two fragments (1081 bp *Eco*RI-*Sal*I and 508 bp *Eco*RI/*Eco*RI) resulted from an *Eco*RI/*Sal*I double digestion of the insert. Subsequently, the 1081 bp *Eco*RI/*Sal*I fragment was ligated into pSCH12-1 digested with the same two enzymes. After isolating these new chimeric plasmids, they were linearized with *Eco*RI and the *Eco*RI/*Eco*RI fragment was inserted by ligation. The correct orientation of the *Eco*RI/*Eco*RI fragment was confirmed by restriction digestion using an internal *Bbs*I site.

2.10 *S. cerevisiae* transformation (Akada *et al.*, 2000)

Yeast strain SCDT8 (Leibovitch *et al*., 2013) was made competent by the procedure of Akada *et al*. (2000) by Dr Pamela Hanic-Joyce and stored at -80°C. For transformations, the competent

cells were thawed on ice and 75 µl aliquots were dispensed into prechilled microfuge tubes on ice. Then, ~10 µg of the appropriate plasmid DNA was added to the cells, mixed vigorously for 10 s and incubated at 42°C for 2 h at which point the cells were spread directly onto the appropriate selection plates and incubated at 30°C. For long-term storage, a colony from the selection plate was picked and added to 700 µl of selection medium with vortexing. Subsequently, 300 µl of 50% glycerol was added, the sample vortexed, and stored at -80°C.

2.11 Viability assay (Leibovitch *et al*., 2019).

In brief, three colonies from a successful transformation were patched onto selection medium (SC-HIS-URA in these examples, Table 2.3) and incubated at room temperature for 48 h. The resulting patches were replica-plated to YPD plates and incubated at room temperature for 24 h to allow for possible plasmid loss. The patches on each plate were replica-plated sequentially first to plates containing (+FOA) or lacking (-FOA) 5-fluoroorotic acid and then to SC-HIS-URA plates (Table 2.3). These plates then were incubated at room temperature or at 37°C for two to three days. Each experiment was performed three times with each variant. Cells retaining pRS316 bearing the URA3 gene will die in the presence of FOA due to the production of a toxic metabolite by the URA3 gene product.

2.12 Protein expression and purification (Modified from Shan *et al*., 2008)

BL21 (DE3) cells carrying plasmids of interest were grown in 10 ml YT+Amp (Table 2.3) in 50 ml screw cap tubes for 16 to 20 h at 37°C with shaking (225 rpm). This overnight culture was transferred to a Fernbach flask containing 1 l of YT+Amp medium and the flask was placed in a New Brunswick Scientific Innova^{TM} 4330 Refrigerated Incubator Shaker at 37°C and 225 rpm for ~2 h to reach an OD_{600} of ~0.6. At this point, 0.5 ml of 1 mM IPTG was added and the flask was placed on the shaker at 18°C and 225 rpm for 24 h to induce the expression of the protein. The sample then was divided between three 500 ml tared centrifuge bottles and centrifuged at 4°C for 15 min at 4 000 xg (Lynx Centrifuge) to pellet the cells. After decanting the liquid, the centrifuge bottles were stored at -80°C for a minimum of 2 h until needed.

2.12.1 Cell lysis (Modified from Shan *et al.*, 2008)

The cells pellets were resuspended in 2 ml/g cell pellet of Lysis Buffer (Table 2.3) containing 40 µl/ml cOmplete, EDTA free, protease inhibitor cocktail (MilliporeSigma) by vortexing at 4°C for 45 min. The contents of the bottles then were transferred to 50 ml plastic beakers for cell lysis via Sonication. Sonication consisted of 20 cycles with the power set at 50 and the pulse at 15 sec using an Ultrasonic Homogenizer (BioLogics, Inc Model 300 V/T) with the sample cooled on ice for 2 minutes between cycles. A small amount (~10 µl) of the crude extract was collected and the remaining sample was transferred to a 50 ml centrifuge bottle for centrifugation at 14 000 xg for 30 minutes at 4°C. The supernatant then was transferred to a new centrifuge bottle and the centrifugation repeated. The supernatant was collected as the cleared lysate for further characterization.

2.12.2 Protein purification (Modified from Shan *et al.*, 2008)

A 10 cm × 1.5 cm column (Bio-Rad), containing 2 ml Glutathione Agarose Resin (BIOGOLD) was equilibrated by passing 150 ml 1X PBS (pH 4.5). The whole-cell lysate (section 2.12.1) was then added to the column and incubated with the resin at 4°C for 24 h with occasional gentle mixing. Subsequently, the column was drained by gravity and ~ 10 µl of the flow through was saved. Then, 400 ml of cold and sterile 1X PBS was loaded onto the column to remove proteins that were bound non-specifically to the resin. The fractions were eluted by gravity and the first ml of wash buffer off the column and the last ml of wash buffer off the column were kept for further analysis. After this initial washing step, elution buffer (Table 2.3) was added to release the proteins of interest from the resin. Initially, the resin was incubated with 10 ml of elution buffer overnight at 4 °C with gentle shaking. The elution buffer then was collected by gravity in 1 ml fractions and an additional 10 ml of elution buffer was added to the resin with incubation at 4°C for 2 h before 1 ml fractions of this elution were collected by gravity. SDS-PAGE (section 2.12.4) was used to show what proteins were contained in each fraction and to determine which fractions should be characterized further.

Between protein purifications the resin was regenerated by washing first with 6 M Guanidine-HCl (10 ml) and then with 50 ml dH_2O and 50 ml 70% ethanol. The regenerated resin was stored in 5 ml 20% ethanol at 4°C until used again.

2.12.3 Removal of the GST tag

Fractions showing the protein of interest (typically 5 ml in total) were transferred to Spectra/PorR 7 Dialysis Membrane Tubing (MWCO 50 kDa) and 25 µl of thrombin (1 unit/µl, GE Healthcare) was added to the sample. To remove cleaved GST tag from the protein sample, dialysis was carried out first for 3 h at 4°C against 1 liter of 1X PBS (Table 2.3) and then against 2 liters of fresh 1X PBS at 4°C overnight.

The following day the dialyzed sample (< 10 ml) which should contain a mixture of the mature protein, any cleaved tag that was not lost during dialysis and any uncut fusion protein was returned to the column containing the Glutathione Agarose resin. Any free GST tags and any uncut GST-tagged-protein should bind to the resin while the mature tRNA nucleotidyltransferase should be collected in the flow through. The flow-through was collected by gravity and passaged through the column two additional times to ensure that the greatest amount of GST tag and any uncut fusion protein were eliminated.

The pure protein of interest was stored at -80°C in 10% (v/v) glycerol in the dialysis buffer. The concentration of the pure protein was determined using the Bradford Assay (Bradford, 1976) with BSA (Sigma-Aldrich) as the protein standard. The Bradford reagent and protocol were provided by Bio-Rad.

2.12.4 SDS-PAGE (Modified from Sambrook *et al.*, 1989)

To analyze samples collected during protein purification, SDS-PAGE through a 4% stacking gel and a 13% resolving gel was performed at room temperature for 1 hour at 80 mV on 10 cm x 4 cm gels with 0.75 mm spacers. To visualize the proteins the procedure of Wong *et al*. (2000) was used. After distaining in dH_2O the gel was scanned on a SNAPSCAN 1212 scanner (AGFA).

2.13 Biophysical Characterization

2.13.1 UV-visible spectroscopy

Before biophysical characterization, the pure proteins were treated with a final concentration of 30 ng/ml RNaseA (Bioshop) to remove any co-purified tRNAs or other nucleic acids. RNAseA

treatment was carried out in a dialysis bag overnight against 1 l of 1X PBS (pH 7.5) at 4℃ to remove the resulting small nucleic acid fragments and nucleotide monophosphates generated. The following day, the concentration of each sample was determined by Bradford Assay (Bradford, 1976). The UV absorbance of 1 ml of each sample before and after RNaseA treatment was measured at 260 nm and 280 nm (Shimadzu UV-260 UV-Visible) to show the loss of the nucleic acid (which absorbs more strongly at 260 nm than does the protein).

2.13.2 Circular Dichroism Spectroscopy (Modified from Leibovitch *et al.*, 2013)

To determine the secondary structure of the protein variants, CD spectroscopy was used. After RNaseA treatment and dialysis, 1 ml of each sample was centrifuged at 4℃ and 14 000 xg for 5 min and the resulting supernatant liquid collected for Bradford assay. All of the samples were diluted with 1X PBS (pH 7.5) to a concentration of 0.1 mg/ml. Subsequently, 0.4 ml of each sample was transferred to 0.1 cm cuvette for CD analysis using the Jasco-815 CD machine. The Spectrum measurement program was selected, and the scan range was set from 200 nm to 260 nm. For this experiment, five times data accumulation at 20℃ was performed, and prior to plotting the data, the data for the blank were subtracted and the curves smoothed using the Jasco smoothing software.

2.14 Activity assay

Aliquots (8 µl) of reaction solution: 1 mM ATP, 0.4 mM CTP, 10 mM $MgCl_2$, 10 ng of the appropriate [α-^{32}P]GTP transcribed tRNA (kindly provided by Nathalie Reid) and 100 mM glycine buffer (pH 9), were prewarmed at 37℃ for 2 min in Eppendorf tubes. The reaction was then initiated by the addition of 2 µl of enzyme solution (containing the appropriate number of ng of protein and/or dH_2O). After an appropriate duration (typically 2 min), the reaction was terminated by the addition of an equal volume of Peattie's loading buffer (Peattie, 1979). The samples were stored at -20℃ until used for denaturing gel electrophoresis. (Nathalie Reid performed the electrophoresis).

2.15 Computational analysis and visualization of the protein variants

The *S. cerevisiae* tRNA-NT primary sequence (for the native or variant enzymes) was used as the input sequence and was aligned with all available crystal structures solved to date (Li *et al.,* 2002; Augustin *et al.,* 2003; Tomita *et al.,* 2004; Toh *et al.,* 2009; Toh *et al.,* 2011; Yamashita *et al*., 2014; Kuhn *et al*., 2015). Based on this alignment, the *Thermotoga maritima* (Toh *et al.,* 2009) tRNA-NT crystal structure (PDB ID: 3h38) was top-ranked with the highest GMQE and the lowest QMEAN4. SWISS-MODEL (Biasini *et al.,* 2014) was used to generate the *S. cerevisiae* tRNA-NT model structure. To show the active site and catalytic region involved with magnesium ion binding, the *S. cerevisiae* head domain was modelled based on the structure of the *Thermotoga maritima* tRNA-NT crystalized with tRNA bound (PDB ID: 5ch9) (Yamashita and Tomita, 2016). All structures were viewed using PyMol (Schrödinger).

3.0 RESULTS

3.1 Confirmation of site-directed mutagenesis

QuikChange™ site-directed mutagenesis was performed to replace arginine at residue 64 with alanine, phenylalanine or proline using the templates pGEX2T-E189F, pGEX2T-E189K, pGED190A13, pGED190F16-2 and pSCH12-1 (Table 2.2). After *Dpn*I digestion, agarose gel electrophoresis of an aliquot of each QuikChange reaction was used to confirm that the DNA template had been amplified *in vitro* (Fig. 3.1). Successful amplification generates a DNA product that lacks methylation and therefore is resistant to digestion by *Dpn*I. In each case shown (Fig. 3.1), there is a *Dpn*I-resistant product that is not seen in the control reactions which lacked the mutagenic primers.

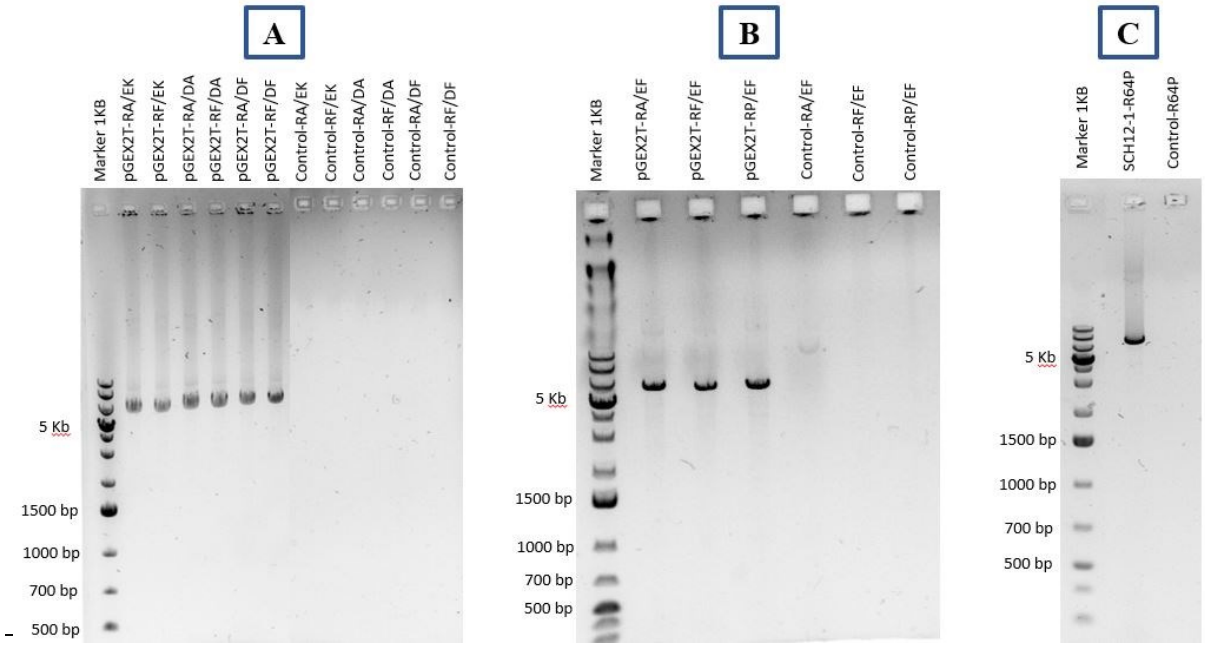

Figure 3.1 Confirmation of *Dpn*I-resistant DNA produced by QuikChange™ mutagenesis. Samples after electrophoresis on 0.8% agarose gels. Each lane contains the product of a QuikChange reaction as indicated. The control reactions lacked the DNA primers required for amplification and therefore should not generate any *Dpn*I-resistant product. The size marker is the 1 Kb$^+$ ladder (Thermo scientific). (A) pGEX2T-E189K, pGED190A13, and pGED190F16-2 derivatives, (B) pGEX2T-E189F derivatives, and (C) pSCH12-1 derivative.

To confirm that the expected nucleotide substitutions had been made, diagnostic restriction enzyme digestions were performed with samples and the products separated on 2% agarose gels

(Fig. 3.2). The oligonucleotides designed to convert residue 64 from arginine to proline, alanine or phenylalanine (Table 2.4) remove a *Dde*I site during mutagenesis such that two *Dde*I fragments of 228 bp and 433 bp appear as a single *Dde*I fragment of 661 bp when mutagenesis has been successful. So, clones containing the R64A, R64P or R64F substitution will show a 661 bp fragment that is absent in the plasmids with the original sequence coding for R64. Specifically, the 661 bp restriction fragment in lanes pGEX2T-RAEF and pGEX2T-RFEF (Fig. 3.2, panel A) indicates successful mutagenesis in these clones as does the 661 bp restriction fragment present in lanes pGEX2T-RAEK and pGEX2T-RFEK (Figure. 3.2, panel B). Finally, the 360 bp restriction fragment in lane pSCH2-1-R64P (Fig. 3.2, panel C) indicates successful modification of this plasmid as a *Dde*I restriction site which in the wild-type sequence generates 228 bp and 132 bp fragments is lost.

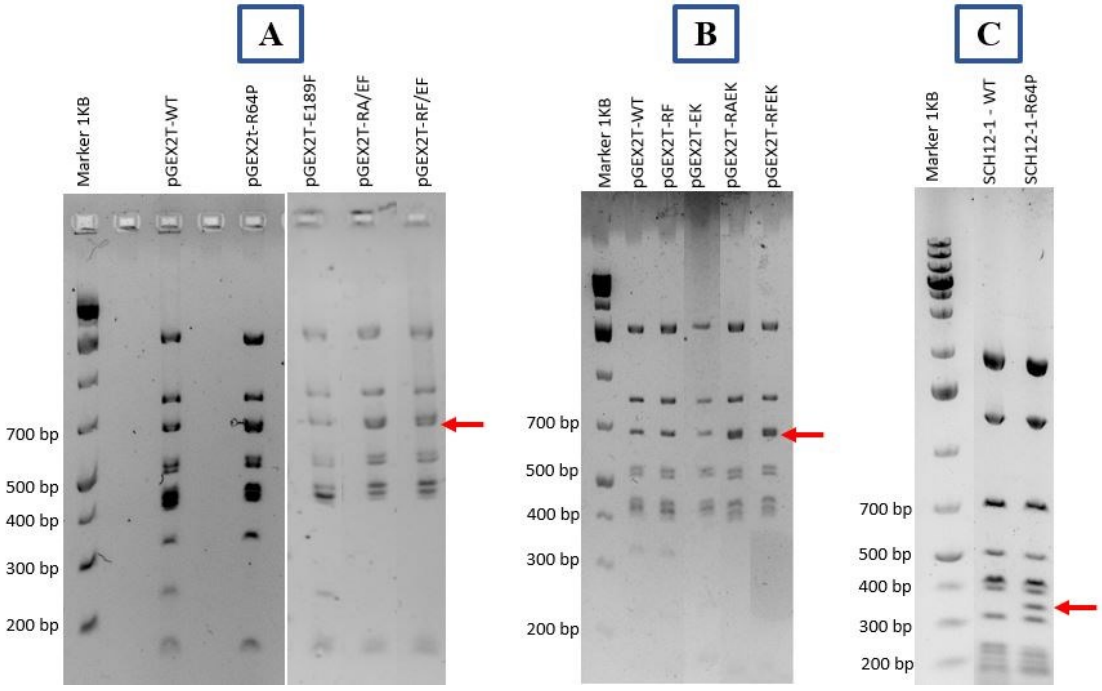

Figure 3.2 *Dde*I restriction digestion of *CCA1* variants in pGEX2T-Scr9-1 and pSCH12-1, made through site-directed mutagenesis. The novel restriction fragment that supports mutagenesis in pGEX-2T or pSCH12-1 is indicated by the red arrow. (A) Modification of pGEX2T-E189F to add mutation coding for R64A or R64F. (B) Modification of pGEX2T-E189K to add mutation coding for R64A or R64F. (C) Modification of pSCH12-1-WT to add mutation coding for R64P.

To confirm that substitutions had been made to convert residue 190 to alanine or phenylalanine, diagnostic restriction digestions were performed using *Hin*dIII or *Eco*RI (Fig. 3.3).

The variants containing D190A are expected to show fragments at 349 and 449 bp as a result of the introduction of a new *Hin*dIII restriction site (Table 2.4) into a 798 bp fragment. For the D190F variants, the oligonucleotides were designed (Table 2.4) to add a second *Eco*RI restriction site to the plasmid. After restriction digestion with *Eco*RI, two restriction fragments of the expected sizes (508 and 6041 bp) confirm that the mutagenesis had been performed successfully (Fig. 3.3).

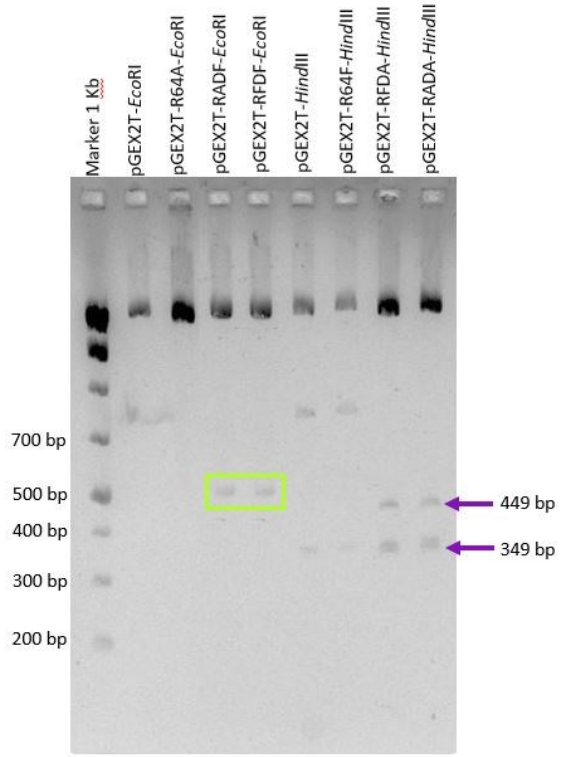

Figure 3.3 *Eco*RI and *Hin*dIII restriction digestion of *CCA1* variants in pGEX2T-Scr9-1. The restriction fragments at 449 and 349 bp (purple arrows) in the variants, but not in the control plasmid supports the presence of the D190A substitution in the R46 variants due to the presence of an additional *Hin*dIII restriction site. The restriction fragment at 508 bp (boxed) in the D190F variants but absent in the control samples supports the presence of the D190F substitution as an additional *Eco*RI restriction site has been introduced during mutagenesis.

To show that unexpected mutations had not been introduced into the DNA, sequence analysis of the variants was performed at the McGill University and Genome Quebec Innovation Centre when possible. The clones for which the sequencing is completed or in progress are listed in Table 3.1.

Table 3.1 Variant sequences

Variant	Expected sequence
R64A	Confirmed
R64F	Confirmed
R64P	Confirmed
R64A/E189F	Confirmed
R64A/E189K	In Progress
R64F/E189F	Confirmed
R64F/E189K	In Progress
R64P/E189F	Confirmed
R64A/D190A	Confirmed
R64F/D190A	In Progress
R64A/D190F	In Progress
R64F/D190F	Confirmed

3.2 Confirmation of Replacement of Wild-type DNA with Mutant DNA

QuikChange™ mutagenesis to introduce the R64A and R64F substitutions into the pSCH12-1 background was unsuccessful. Therefore, restriction digestion and ligation were used to transfer DNA fragments containing these mutations from the pGEX-2T plasmids to pSCH12-1. When the *Eco*RI-*Sal*I fragment containing the mutation that changes residue 64 to phenylalanine, proline or alanine in an E189F or E189K background was introduced into pSCH12-1-WT, a new *Dde*I restriction fragment of 360 bp was created as this DNA is missing a *Dde*I site found in the wild-type sequence (Fig. 3.4). A fragment at 360 bp was taken as diagnostic for correct insertion as it was difficult to see the fragments of 228 bp and 132 bp in the original clones. Compare pSCH12-1-WT to pSCH12-1-R64P, and pSCH12-1-E189F to pSCH12-1-RA/EF, RF/EF, RP/EF, or RA/EK (Fig. 3.4).

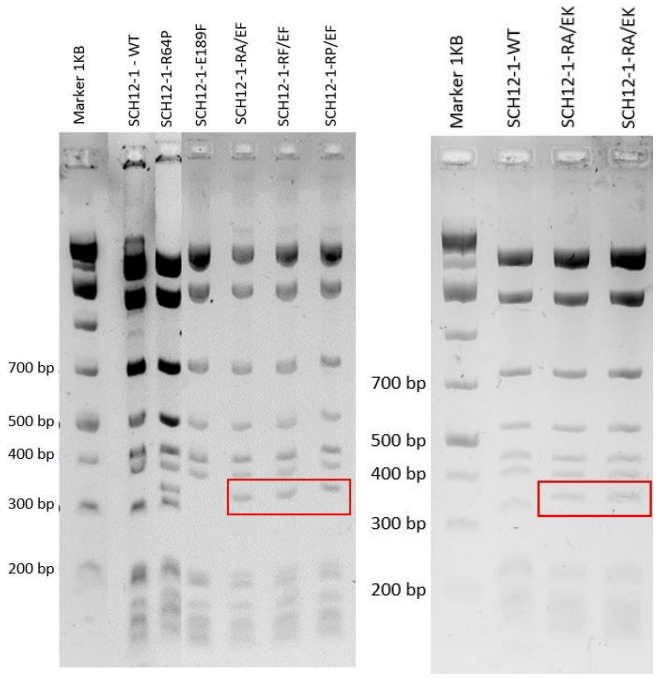

Figure 3.4 Agarose gels showing restriction digestions to confirm that restriction fragments containing the mutant DNA had replaced the original restriction fragment. Each lane is labeled with Molecular Weight Marker (Thermo scientific) or the name of the plasmid that has undergone restriction digestion. The presence of a fragment at 360 bp (red boxes) in the digestion pattern indicates that the fragment bearing the mutation has been introduced.

When the 1589 bp *Eco*RI-*Sal*I restriction fragment containing the mutation that converts D190 to A was successfully ligated into a plasmid lacking this mutation, a 798 bp restriction fragment was lost due to the introduction of an additional *Hin*dIII site which divides this fragment into fragments of 349 bp and 449 bp (Fig. 3.5). The absence of the 798 bp restriction fragment in pSCH12-1-D190A, pSCH12-1-RF/DA, or pSCH12-1-RA/DA was taken as diagnostic for the introduction of the restriction fragment containing the mutation generating the D190A substitution (Fig. 3.5).

As the mutagenesis that converts the aspartate residue at position 190 to phenylalanine introduces a new *Eco*RI restriction site (Table 2.4), transferring the fragment containing this mutation required a two-step ligation. The existing D190F variants were digested with *Eco*RI and *Sal*I and first the *Sal*I/*Eco*RI fragment (1081 bp) was ligated into the acceptor plasmid. Subsequently, the resulting plasmid was linearized with *Eco*RI and the *Eco*RI/*Eco*RI fragment (508 bp) inserted. As insertion of the *Eco*RI fragment could have been in either orientation, a *Bbs*I

digestion was used to confirm the orientation (Fig. 3.6). Insertion in the correct orientation results in *Bbs*I fragments of 3842 bp, 2417 bp and 1143 bp while insertion in the reverse orientation results in *Bbs*I fragments of 4232 bp, 2027 bp and 1143 bp (Fig. 3.6, panel A). Ligation of the *Eco*RI/*Eco*RI fragment in the correct orientation shows the same pattern of bands as wild-type, R64A and D190F on the gel (Fig. 3.6, panel B). If the direction had been reversed, three bands appear on the gel, but two show sizes different from the wild type (Fig. 3.6, red boxes in panel A).

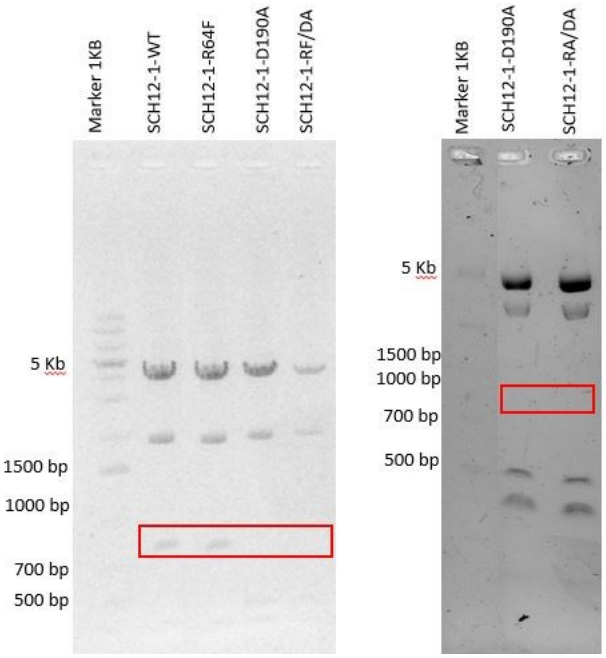

Figure 3.5 Agarose gels showing *Hin*dIII restriction digestions to confirm that restriction fragments containing the mutant DNA had replaced the original restriction fragment. Each lane is labeled with Molecular Weight Marker (Thermo scientific) or the name of the plasmid that has undergone restriction digestion. The loss of a fragment at 798 bp (red boxes) in the digestion patterns for SCH12-1-D190A, SCH12-1-RF/DA, and SCH12-1-RA/DA indicates that the fragment bearing the mutation has been introduced into these plasmids.

.

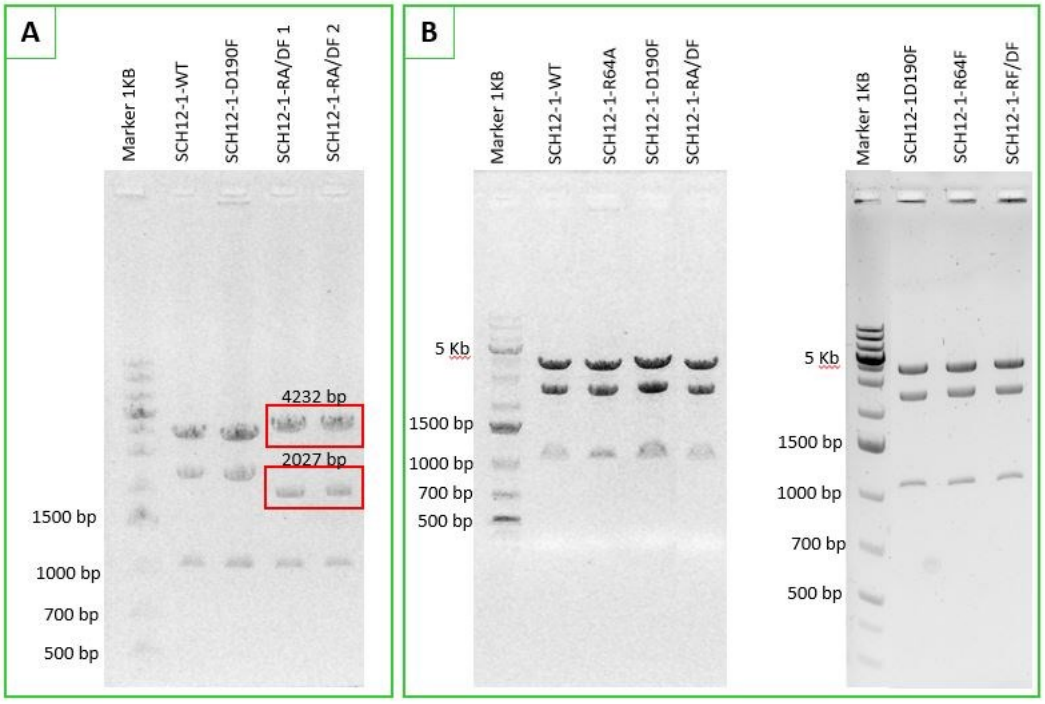

Figure 3.6 Agarose gel showing *Bbs*I digestions of pSCH12-1-R64A/D190F and pSCH12-1-R64F/D190F variants with controls. (A) Results showing the products of *Bbs*I digestion with *Bbs*I fragments from insertion of the *Eco*RI fragment in the reverse orientation boxed. (B) *Bbs*I digestions showing the correct orientation of insert in all samples.

3.3 Viability assay and phenotype determination

Plasmid shuffling was used to see what effect the various mutations had on yeast cell growth. Cells were replica plated appropriately and allowed to grow for up to three days at room temperature or at 37^{O}C (to assess the temperature-sensitive phenotype).

3.3.1 Effect of changes at position 64 on viability and temperature sensitivity in the native enzyme (Fig. 3.7).

As expected, the E189F variant showed a temperature-sensitive phenotype consistent with our earlier results (Shan *et al*., 2008). The native enzyme and the R64W variant allowed for growth at both temperatures as had been shown previously (Goring *et al*., 2013). The R64A and R64F variants generated here also grew well at the permissive temperature although the R64A variant showed an intermediate level of growth at the restrictive temperature as compared to the native

and E189F variants. The R64P variant, like the G131-2 control, was inviable at either temperature tested.

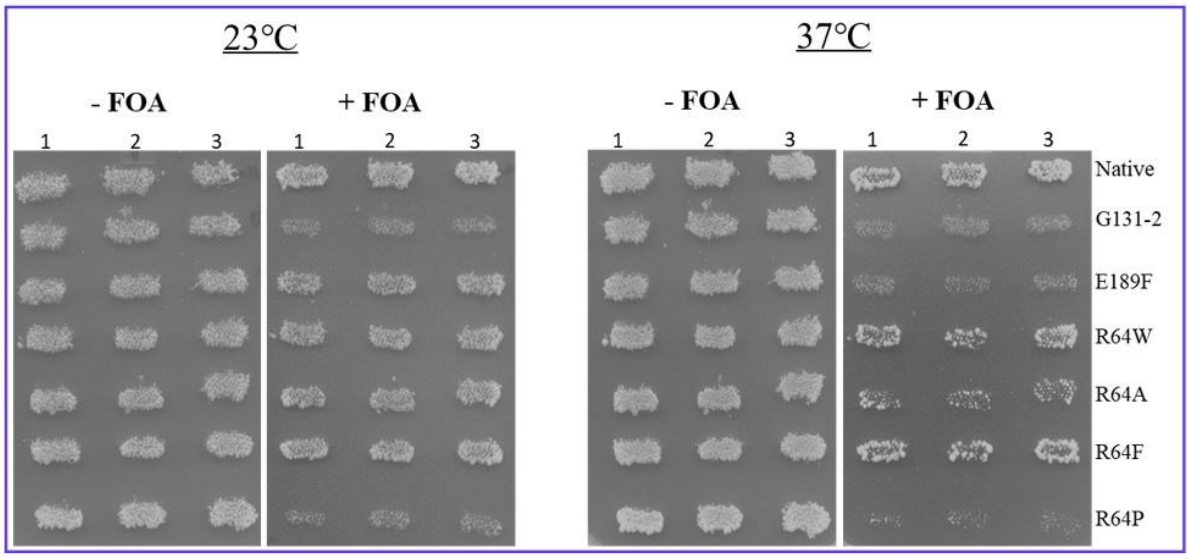

Figure 3.7 Growth of yeast expressing native and variant tRNA nucleotidyltransferases. Yeast strain SCDT8 was transformed with plasmids coding for the tRNA nucleotidyltransferase proteins indicated and three independent transformants were replica-plated to SC medium lacking uracil but with (+) or without (-) 5-fluoroorotic acid (FOA) and incubated at 22°C or 37°C to assess viability and temperature sensitivity.

3.3.2 Effect of changes at position 64 on viability and temperature sensitivity in the E189F variants (Fig. 3.8)

The R64P variant in the E189F background did not allow growth at either temperature as seen previously in the native background (Fig. 3.6). The R64F substitution, like the R64W substitution (Goring *et al.,* 2013), allows for growth at the permissive temperature and suppresses the E189F temperature-sensitive phenotype. While the R64A variant allows for growth at the permissive temperature, it does not suppress the *ts* phenotype partially, but not completely.

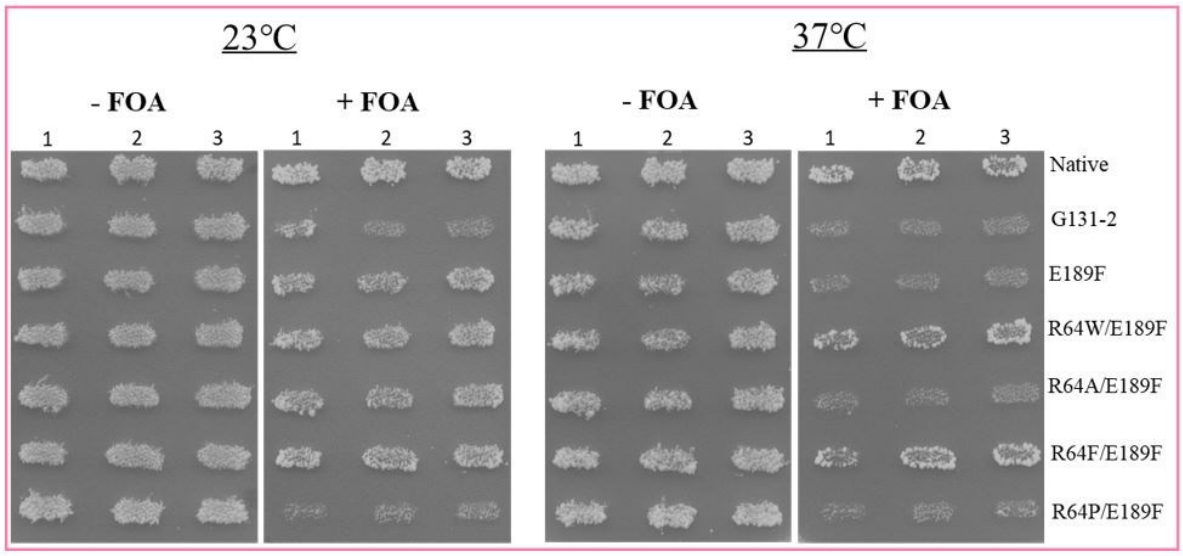

Figure 3.8 Growth of yeast expressing native and variant tRNA nucleotidyltransferases. Yeast strain SCDT8 was transformed with plasmids coding for the tRNA nucleotidyltransferase proteins indicated and three independent transformants were replica-plated to SC medium lacking uracil but with (+) or without (-) 5-fluoroorotic acid (FOA) and incubated at 22°C or 37°C to assess viability and temperature sensitivity.

3.3.3 Effect of changes at position 64 on viability and temperature sensitivity in the E189K variants (Fig. 3.9)

Conversion of R64 to A, or F in the E189K background showed the same results as seen for these substitutions in the E189F background. Both allow for growth at the permissive temperature, but while the R46F substitution assuages the *ts* phenotype as had been seen previously with the R64W substitution, the R64A change did not. As the R64P substitution was inviable in the native and E189F backgrounds it was not tested in any of the remaining backgrounds.

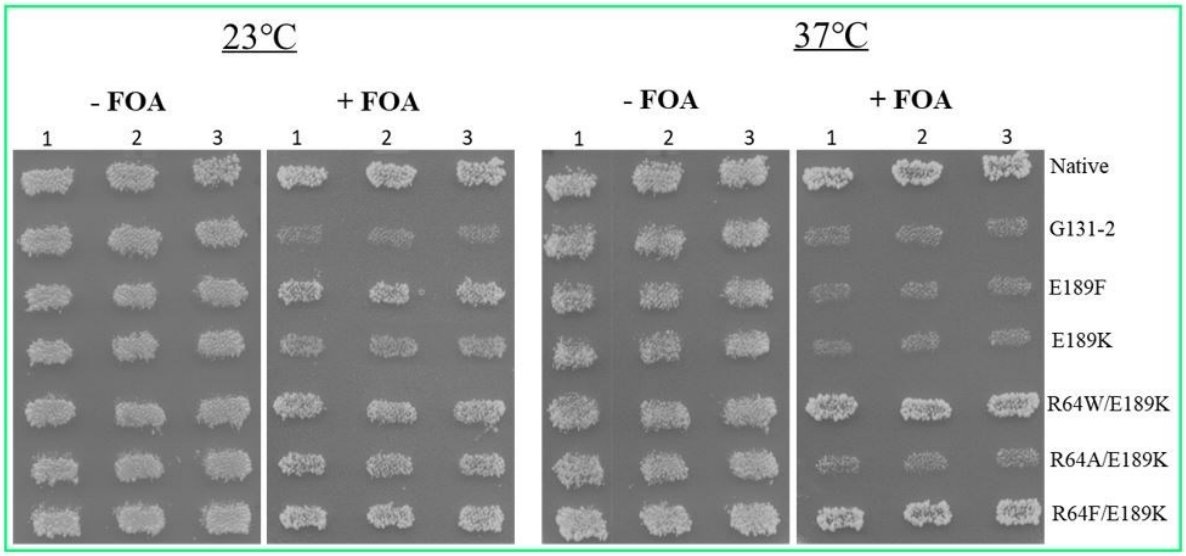

Figure 3.9 Growth of yeast expressing native and variant tRNA nucleotidyltransferases. Yeast strain SCDT8 was transformed with plasmids coding for the tRNA nucleotidyltransferase proteins indicated and three independent transformants were replica-plated to SC medium lacking uracil but with (+) or without (-) 5-fluoroorotic acid (FOA) and incubated at 22°C or 37°C to assess viability and temperature sensitivity.

3.3.4 Effect of changes at position 64 on viability and temperature sensitivity in the D190A variants (Fig. 3.10)

As shown previously (Rahman, 2017), the D190A variant is temperature sensitive and the R64W substitution can suppress this *ts* phenotype. The R64F or R64A substitutions in the D190A background do not suppress the *ts* phenotype. In the R64A substitution in combination with the D190A change not only the *ts* phenotype is not suppressed, but also these two amino acid substitutions together reduce growth at the permissive temperature.

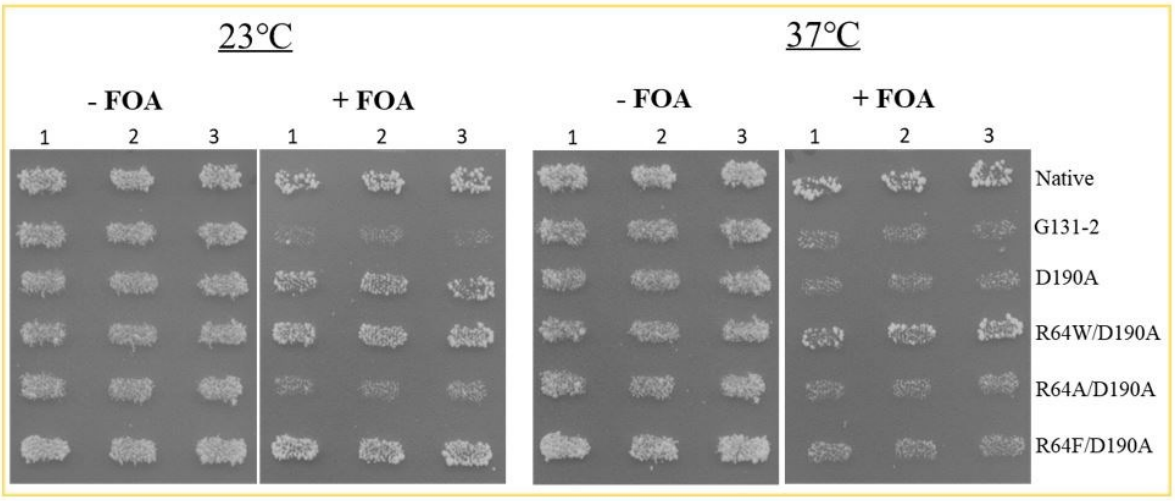

Figure 3.10 Growth of yeast expressing native and variant tRNA nucleotidyltransferases. Yeast strain SCDT8 was transformed with plasmids coding for the tRNA nucleotidyltransferase proteins indicated and three independent transformants were replica-plated to SC medium lacking uracil but with (+) or without (-) 5-fluoroorotic acid (FOA) and incubated at 22°C or 37°C to assess viability and temperature sensitivity.

3.3.5 Effect of changes at position 64 on viability and temperature sensitivity in the D190F variants (Fig. 3.11)

The D190F substitution dramatically reduces growth at both the permissive and restrictive temperatures as seen previously (Rahman, 2017). This is also the case for the R64A/D190F and R64F/D190F variants. This is in sharp contrast to what was seen previously with the R64W substitution which suppresses this growth phenotype at both the permissive and restrictive temperatures (Rahman, 2017).

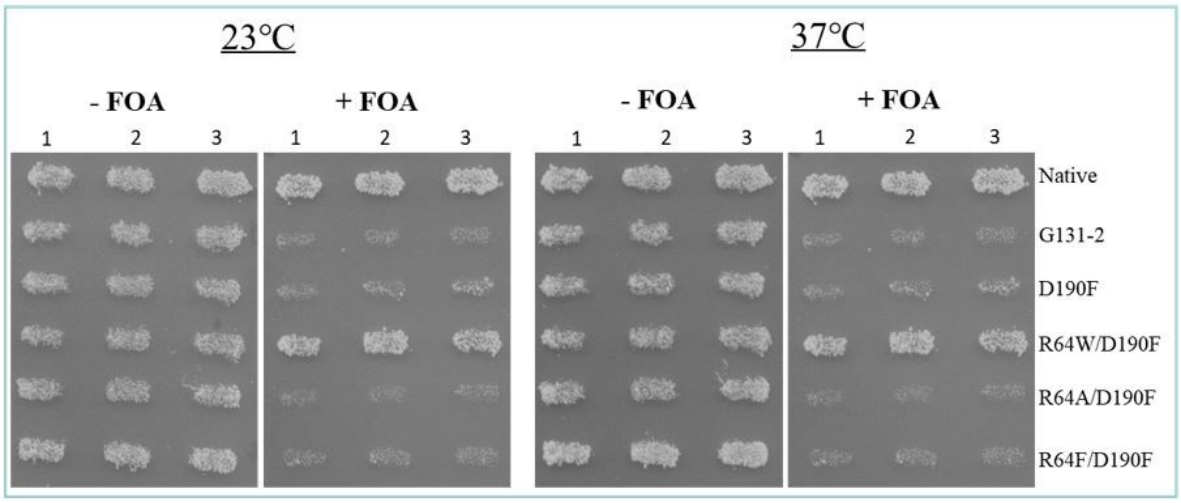

Figure 3.11 Growth of yeast expressing native and variant tRNA nucleotidyltransferases. Yeast strain SCDT8 was transformed with plasmids coding for the tRNA nucleotidyltransferase proteins indicated and three independent transformants were replica-plated to SC medium lacking uracil but with (+) or without (-) 5-fluoroorotic acid (FOA) and incubated at 22°C or 37°C to assess viability and temperature sensitivity.

The results of the viability and temperature-sensitivity assays are summarized in Table 3.2. A matrix reflecting the phenotypes observed with respect to changes in motifs A and C is shown in Table 3.3.

Table 3.2 Viability and temperature sensitivity results for the different variants

Variant	Viability Result	Reference
R64A	Viable	This work
R64A/E189F	Temperature sensitive	This work
R64A/E189K	Temperature sensitive	This work
R64A/D190A	Inviable	This work
R64A/D190F	Inviable	This work
R64F	Viable	This work
R64F/E189F	Suppressor	This work
R64F/E189K	Suppressor	This work
R64F/D190A	Temperature sensitive	This work

R64F/D190F	Inviable	This work
R64P	Inviable	This work
R64P/E189F	Inviable	This work
R64W	Viable	Goring *et al*., 2013
R64W/E189F	Viable	Goring *et al*., 2013
R64W/E189K	Viable	Goring *et al*., 2013
R64W/D190A	Viable	Rahman, 2017
R64W/D190F	Viable	Rahman, 2017
E189F	Temperature sensitive	Shan *et al.,* 2008
E189K	Temperature sensitive	Shan *et al.,* 2008
D190A	Temperature sensitive	Rahman, 2017
D190F	Inviable	Rahman, 2017

Table 3. 3 A comparison of the phenotypes observed as related to changes in Motifs A and C

Motif C / Motif A	E189	E189F	E189K	D190	D190A	D190F
R64	Viable	*ts*	*ts*	Viable	*ts*	Inviable
R64W	Viable	Suppressed	Suppressed	Viable	Suppressed	Suppressed
R64F	Viable	Suppressed	Suppressed	Viable	*ts*	Inviable
R64A	Viable	*ts*	*ts*	Viable	Inviable	Inviable
R64P	Inviable	Inviable	-	-	-	-

- Not tested

3.4 Protein purification

Aliquots from each step of protein purification and the final pure protein were analyzed by SDS-PAGE. The native enzyme (Fig. 3.12), and the R64F (Fig. 3.13) and R64F/E189F (Fig. 3.14) variants show purification to approximately 80%, 98% and 100% homogeneity, respectively. The GST-CCA fusion protein shows a major band at ~89 kDa (Panel A) as expected. Thrombin cleavage results in digestion of this protein into bands of ~ 62 kDa and 27 kDa indicating the tRNA-NT and GST-tag, respectively (Panel B). Passing the thrombin-cleaved samples through the GST column resulted in the removal of the GST protein and left a single band at ~62 kDa representing the pure protein (Panel C).

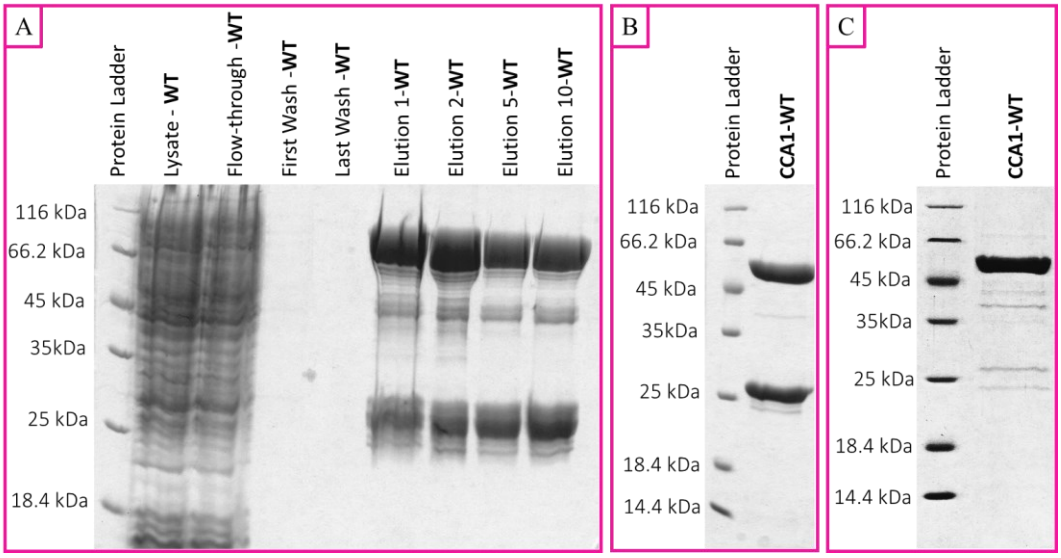

Figure 3.12 SDS-PAGE to follow purification of the native protein. A: collected samples at the end of cell lysis, passing the cell lysis through the Glutathione S-transferases (GST) column, washes, and four selected elution fractions. B: GST-tag cleavage by thrombin. C: GST-tag removal from the native protein by passing the dialyzed sample through the GST column. A band at ~62 kDa shows the pure protein.

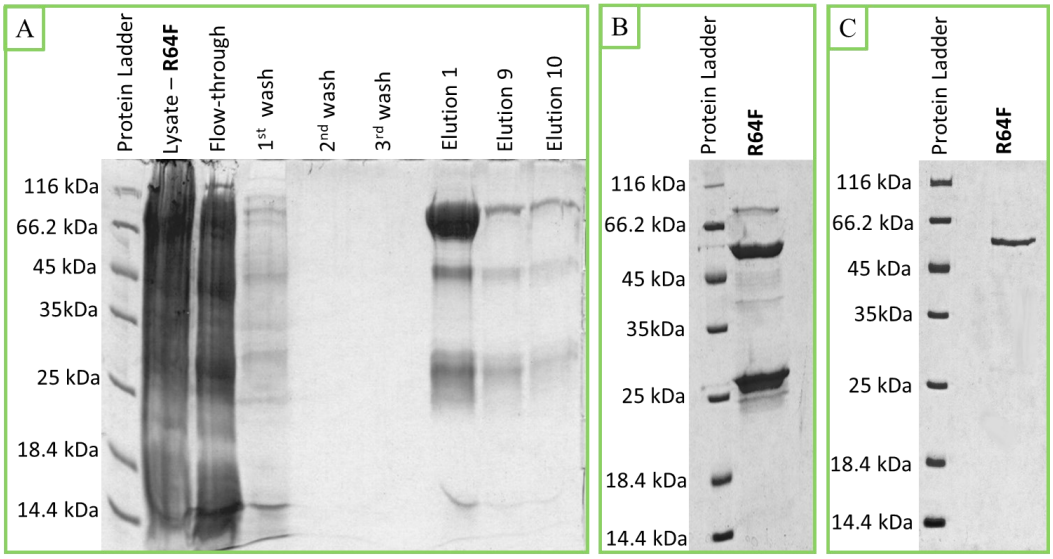

Figure 3.13 SDS-PAGE to follow purification of the R64F variant. A: collected samples at the end of cell lysis, passing the cell lysis through the Glutathione S-transferases (GST) column, washes, and four selected elution fractions. B: GST-tag cleavage by thrombin. C: GST-tag removal from the R64F variant protein by passing the dialyzed sample through the GST column. A band at ~62 kDa shows the pure protein.

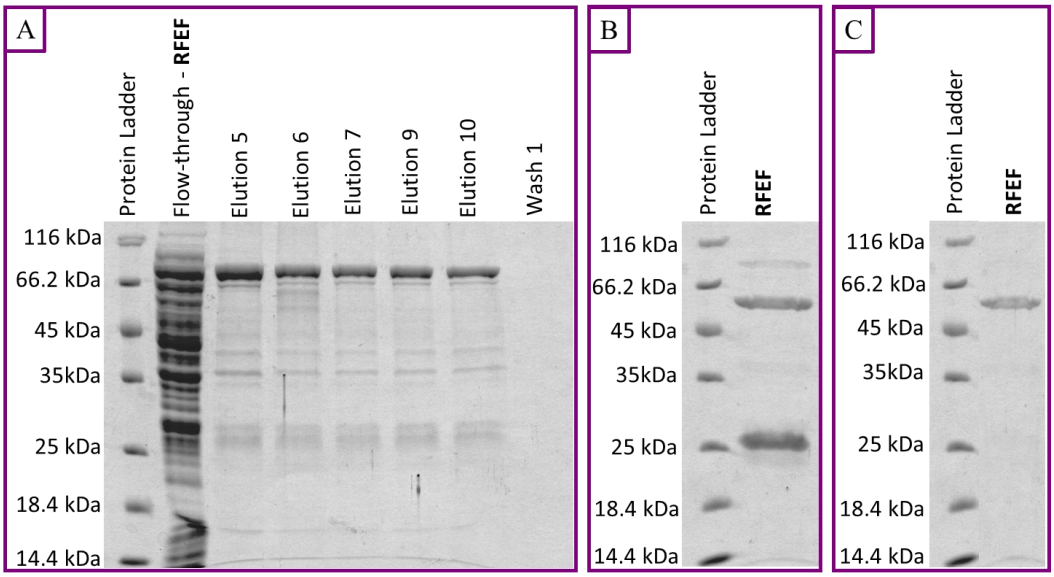

Figure 3. 14 SDS-PAGE to follow purification of the R64F/E189F variant. A: collected samples at the end of cell lysis, passing the cell lysis through the Glutathione S-transferases (GST) column, washes, and four selected elution fractions. B: GST-tag cleavage by thrombin. C: GST-tag removal from the R64F/E189F variant protein by passing the dialyzed sample through the GST column. A band at ~62 kDa shows the pure protein.

3.5 Biophysical Characterization

3.5.1 UV-visible spectroscopy

The absorbance of each sample at 280 nm and at 260 nm was recorded for all samples before and after RNAse A treatment. An increase in the ratio of A_{280} to A_{260} indicates elimination of nucleic acids by RNase A treatment as the major contributor to the A_{260} value is nucleic acids present in the sample. Loss of these nucleic acids (specifically tRNA) is evident in the increase in the A_{280}:A_{260} value seen for all samples tested (Fig. 3.15). These data also indicate that the native and variant enzymes retained nucleic acids during protein isolation suggesting that the amino acid substitutions do not decrease tRNA binding efficiency directly.

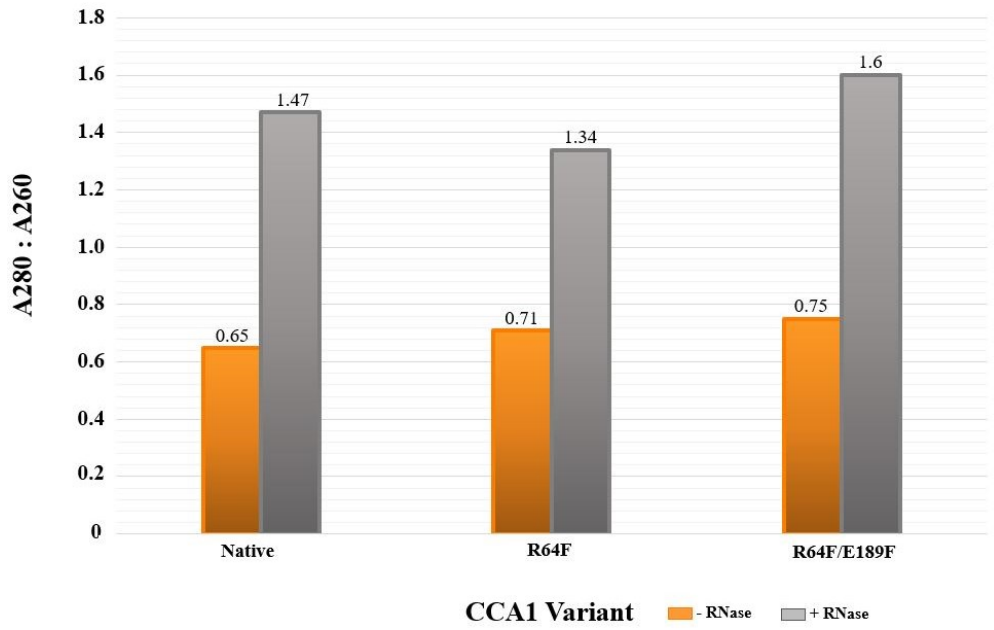

Figure 3.15 A280:A260 ratios of native and variant enzymes before and after RNaseA treatment. The UV absorbance at 280 nm and 260 nm was measured and the resulting ratios are indicated here. Before (orange) and after (gray) RNaseA treatment.

3.5.2 Circular dichroism spectroscopy

To check for possible changes in the secondary structure of the native and E189F variant due to the conversion of residue 64 to phenylalanine, circular dichroism spectroscopy was performed.

All proteins showed the double-trough spectrum with minima at 208 nm and 222 nm characteristic of primarily α-helix structure (Fig. 3.16) (Holzwarth and Doty, 1965). This supports the predicted structure of yeast tRNA-NT and is consistent with our previous observations (Goring *et al.,* 2013). The spectra of the R64F and R64F/E189F variants show minimal or no change in their spectra as compared to the native enzyme. Small differences in the spectra likely reflect a slight difference in the concentration of each protein.

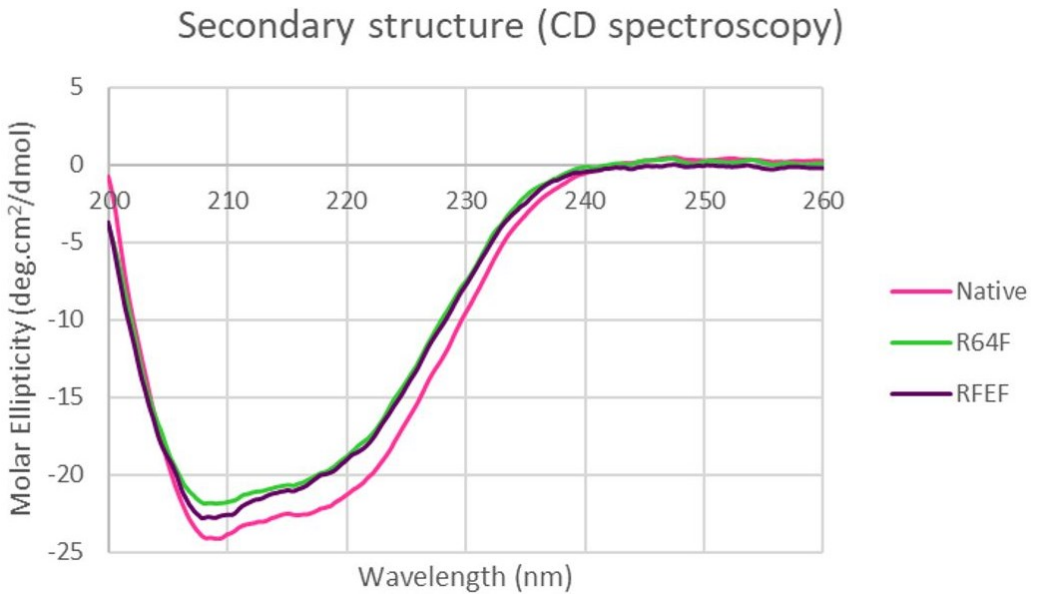

Figure 3.16 Circular dichroism spectra of native and R64F and R64F/E189F variant enzymes. Spectra are color coded as shown in the legend.

3.6 Activity assay

Activity assays were carried out for two minutes at 37ºC using 1.25 ng, 2.5 ng, 5 ng and 10 ng of the most pure protein fraction. For the native enzyme (Fig. 3.17), as little as 1.25 ng of enzyme resulted in more than 80% product formation for CMP addition to the tRNA-NC template or AMP incorporation to the tRNA-NCC template with 100% product formation with 2.5 ng, 5 ng, or 10 ng of enzyme. In contrast, when both CTP and ATP were added to the tRNA-NC template only about 20% of complete CCA addition was observed with 1.25 ng of enzyme. Near complete addition was seen with 2.5 ng protein and above.

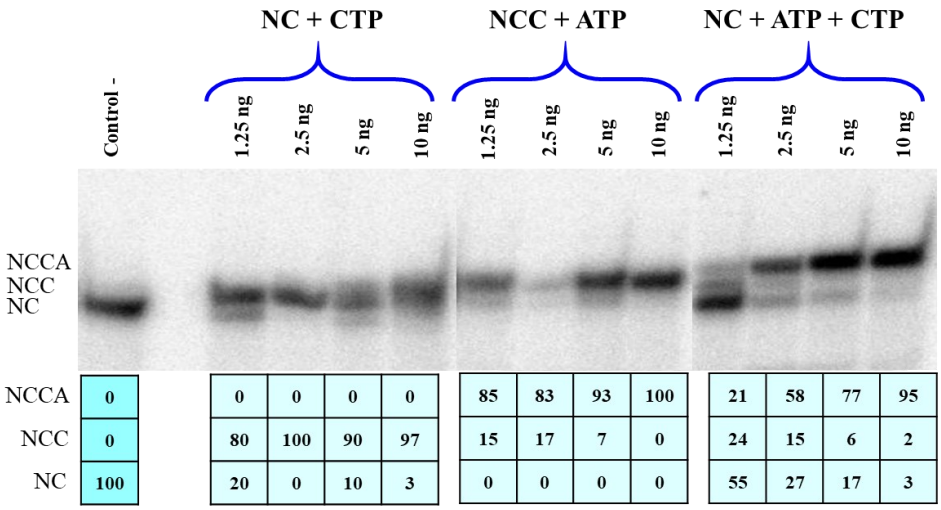

Figure 3.17 Denaturing polyacrylamide gel electrophoresis to show products of native enzyme activity assays. The amount of enzyme added is shown (in ng) above each lane. Radiolabelled tRNA-NC or tRNA-NCC was mixed with native enzyme and ATP, CTP, or ATP and CTP were added as indicated. The numbers below each lane show the results of densitometry to quantitate the relative amounts of tRNA substrate and products. Control is the boiled enzyme negative control.

For the R64F variant (Fig. 3.18) less than 25% incorporation of CMP into the tRNA-NC template or AMP into the tRNA-NCC template was seen with 1.25 ng of enzyme and at no protein level tested was there complete extension. At the 5 ng and 10 ng protein levels there was apparent misincorporation of CMP to generate 3-13% tRNA-NCCC product. When the R64F variant was supplied with both CTP and ATP and the tRNA-NC template only about 2% of the template showed complete extension with 1.25 ng of enzyme. This extension was increased to about 80% when 5 and 10 ng of enzyme were provided.

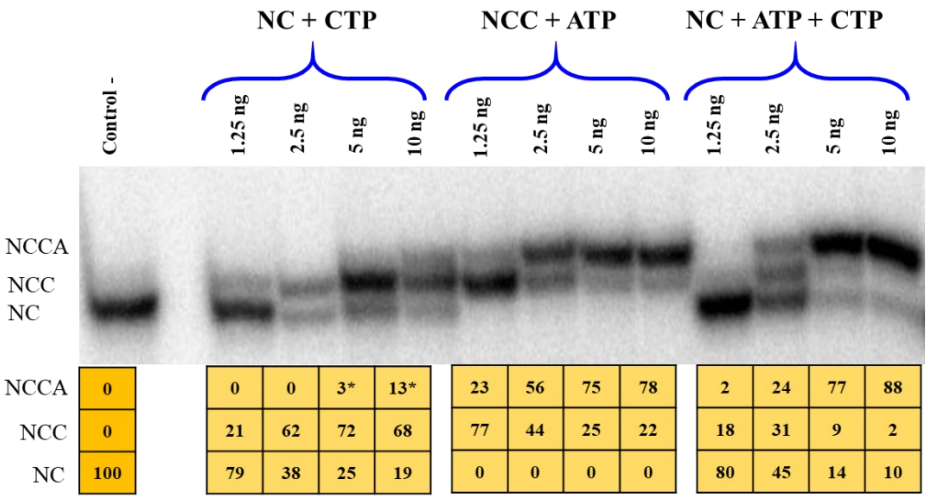

	Control -	NC + CTP				NCC + ATP				NC + ATP + CTP			
		1.25 ng	2.5 ng	5 ng	10 ng	1.25 ng	2.5 ng	5 ng	10 ng	1.25 ng	2.5 ng	5 ng	10 ng
NCCA	0	0	0	3*	13*	23	56	75	78	2	24	77	88
NCC	0	21	62	72	68	77	44	25	22	18	31	9	2
NC	100	79	38	25	19	0	0	0	0	80	45	14	10

Figure 3.18 Denaturing polyacrylamide gel electrophoresis to show products of R64F variant activity assays. The amount of enzyme added is shown (in ng) above each lane. Radiolabelled tRNA-NC or tRNA-NCC was mixed with the R64F variant and ATP, CTP, or ATP and CTP were added as indicated. The numbers below each lane show the results of densitometry to quantitate the relative amounts of tRNA substrate and products. Control is the boiled enzyme negative control. *signifies misincorporation of CMP at the terminal position.

The R64F/E189F variant (Fig. 3.19) showed the least activity with no apparent extension of the tRNA-NC or tRNA-NCC template until 2.5 ng of enzyme was added. Even at the highest protein level tested (10 ng) the tRNA-NC template showed only about 50% of tRNA-NCC product formation by CMP incorporation while the tRNA-NCC template only showed 45% extension to tRNA-NCCA by AMP incorporation. Only about 10% of tRNA-NC template was fully extended when supplied with both CTP and ATP even at the highest protein level (10 ng) tested.

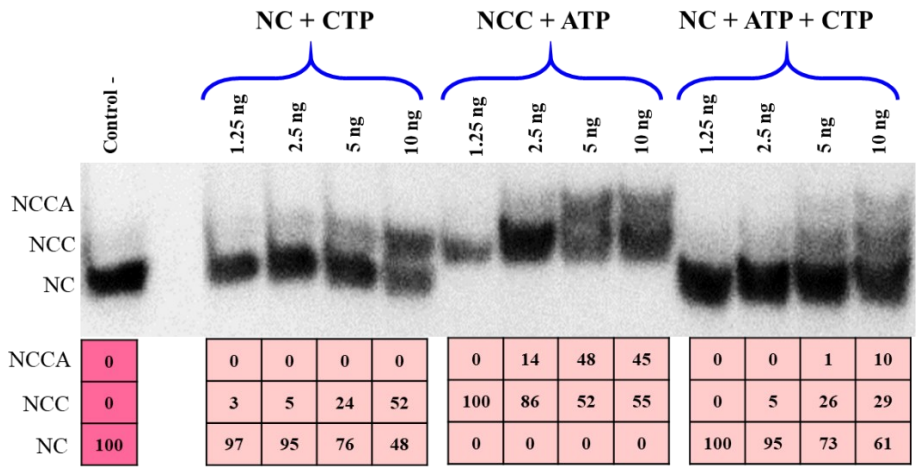

Figure 3.19 Denaturing polyacrylamide gel electrophoresis to show products of R64F/E189F variant activity assays. The amount of enzyme added is shown (in ng) above each lane. Radiolabelled tRNA-NC or tRNA-NCC was mixed with the R64F/E189F variant and ATP, CTP, or ATP and CTP were added as indicated. The numbers below each lane show the results of densitometry to quantitate the relative amounts of tRNA substrate and products. Control is the boiled enzyme negative control.

3.7 Computational analysis of model structure

As described in the introduction to this thesis, the organization of motifs A and C in *Saccharomyces cerevisiae* tRNA-NT has been modelled based on the existing crystal structure of the *Thermotoga maritima* tRNA-NT (Toh *et al.,* 2009). Here, I show the model structures of the variants that I generated in this thesis.

3.7.1 Comparison of the structures of the R64 variants and the native enzyme

Our model structure for the protein with the arginine residue at position 64 converted to tryptophan (Fig. 1.11) shows changes in the spacing of these two side chains but no dramatic difference in their orientation (compare Fig. 1.10 to Fig. 1.11) which suggests that the potential for any predicted electrostatic interactions has been disrupted and any H-bonding potential had been reduced. When I converted the arginine residue at position 64 in β1 in the native enzyme to alanine, phenylalanine, or proline these model structures also show a change in the spacing between the side chains of residues 64 and 189, but more importantly in each case, the model predicts a change in the orientation of the side chain of glutamic acid, E189, in β7 such that any interaction with R64 is lost and new interactions with N182 in the β-turn between β6 and β7 could

arise (Fig. 3.20). These changes could alter the structure of this region of the protein and particularly the non-covalent interactions involved in the organization of β-strands β1, β2, β6 and β7 in this β-sheet (Fig. 3.20, compare native to variants). This would be particularly important in the case of the R64P variant were β1 is truncated by the R64P substitution.

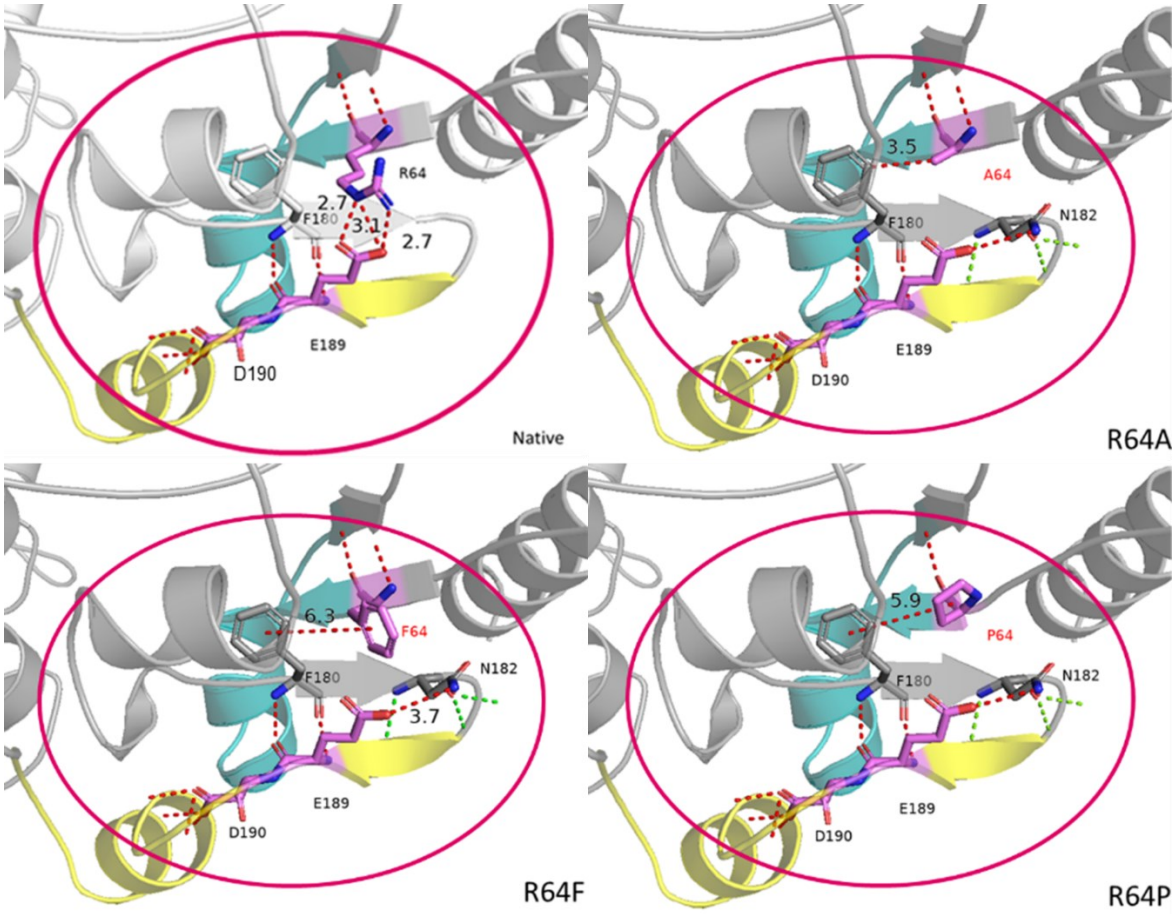

Figure 3.20 The model structure of *S. cerevisiae* native tRNA-NT and the R64A, R64F and R64P variants. The R groups of residues of interest in motifs A and C are shown and the distances between atoms of interest are indicated. Red circles show the important regions in each structure.

3.7.2 Comparison of the structures of the native enzyme and the E189F variant

Our comparison of the models of the native enzyme and the E189F variant (Fig. 3.21) suggests major changes in this region of the protein upon conversion of the charged glutamate at this position to the aromatic and hydrophobic phenylalanine. Converting E189 to phenylalanine is

predicted to eliminate interactions between E189 and R64 and introduce new interactions between E187 and R64 as well as novel interactions between residue F189 at the end of β7 and residue F180 in β6.

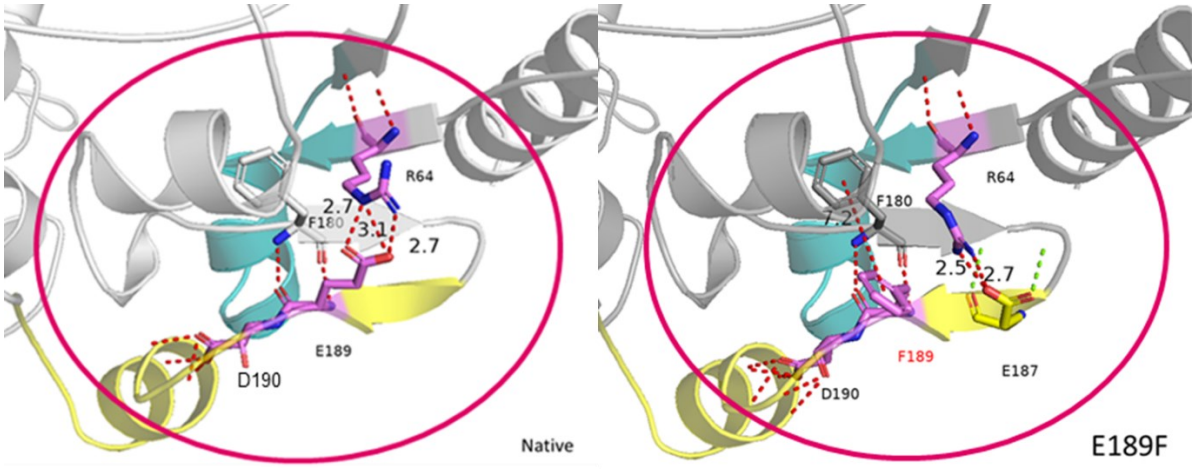

Figure 3.21 The model structure of *S. cerevisiae* native tRNA-NT and the E189F variant. The R groups of residues of interest in motifs A and C are shown and the distances between atoms of interest are indicated. Red circles show the important regions in each structure.

3.7.3 Comparison of the structures of the R64 variants in the E189F background

Our comparisons of the models of the R64W, R64A, R64F and R64P variants in the E189F background show that only in the R64P variant is there the potential for fewer interactions between the residue at position 64 and residue A85 in β2.

As we introduced hydrophobic and/or aromatic residues at positions 64 and 189, there is the potential for new hydrophobic or π-π stacking interactions including with residue F180 at the beginning of β5.

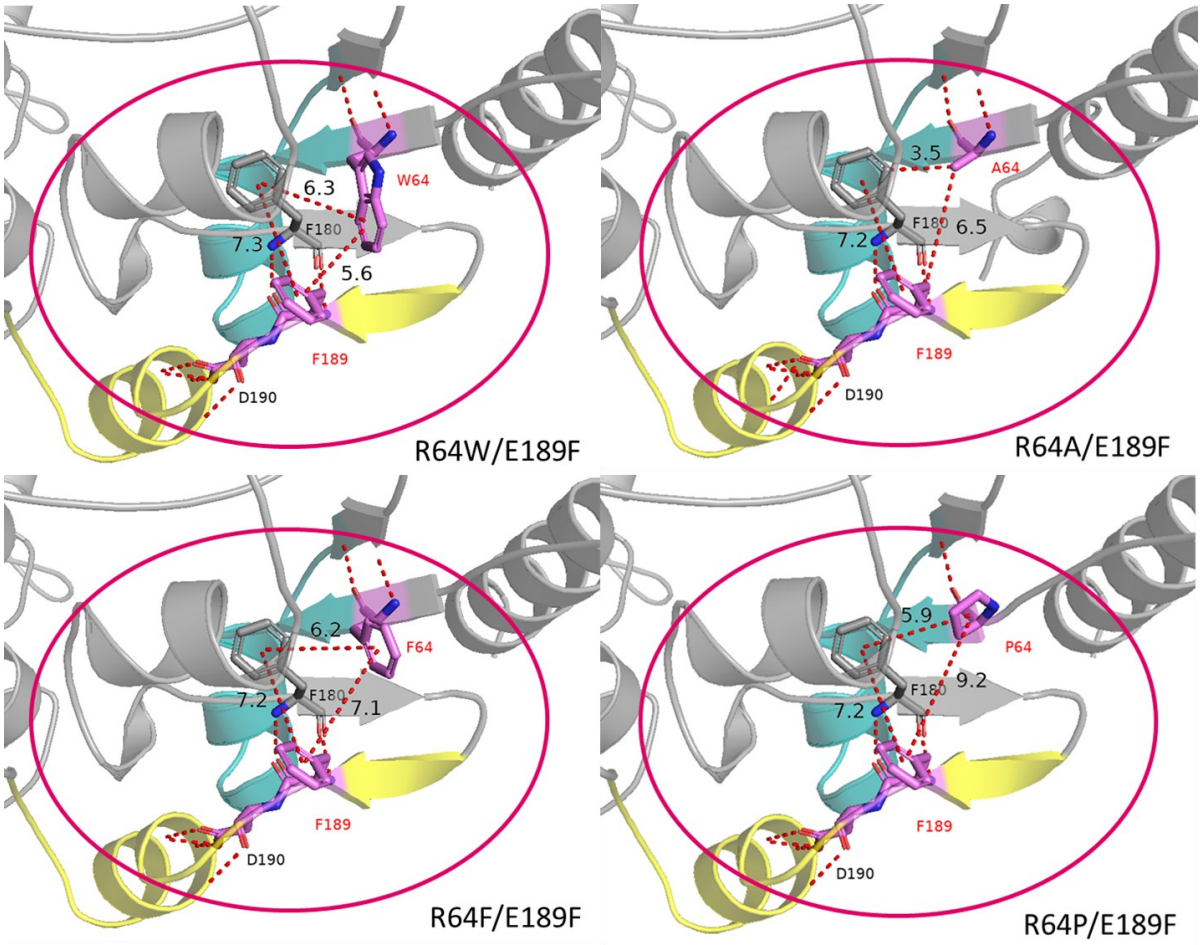

Figure 3.22 The model structure of *S. cerevisiae* tRNA-NT R64W, R64A, R64F and R64P variants in the E189F background. The R groups of residues of interest in motifs A and C are shown and the distances between atoms of interest are indicated. Red circles show the important regions in each structure.

3.7.4 Comparison of the structures of the native enzyme and the E189K variant

Molecular modelling suggests that converting the glutamate residue at position 189 to lysine results in the loss of any potential interactions between residue 189 in β7 and the arginine at position 64 in β1, but that K189 may then interact with the main chain of β5 (Fig. 3.23).

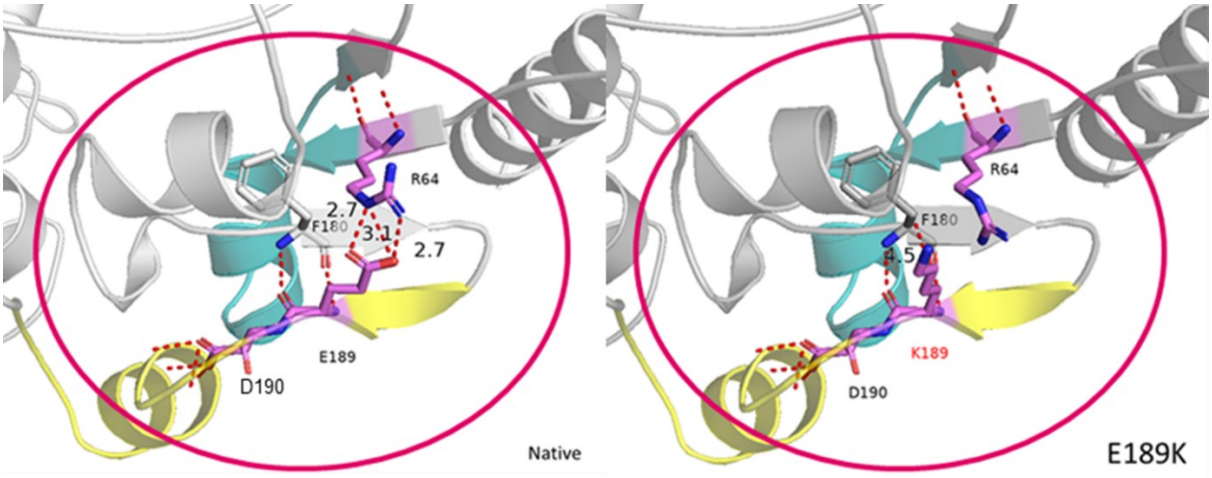

Figure 3.23 The model structure of *S. cerevisiae* tRNA-NT native and the E189K variant. The R groups of residues of interest in motifs A and C are shown and the distances between atoms of interest are indicated. Red circles show the important regions in each structure.

3.7.5 Comparison of the structures of the R64 variants in the E189K background

Comparison of the model structures of R64W/E189K, R64A/E189K, R64F/E189K, and R64P/E189K (Fig. 3.24) shows first that β2 is disrupted by the conversion of the arginine at position 64 to proline. This is the most dramatic alteration in structure seen in any of the variants characterized to this point. With the other variants you see an increased potential for interaction with the main chain of β5 and an increase in the potential for hydrophobic interactions with residue F180 at the beginning of β5.

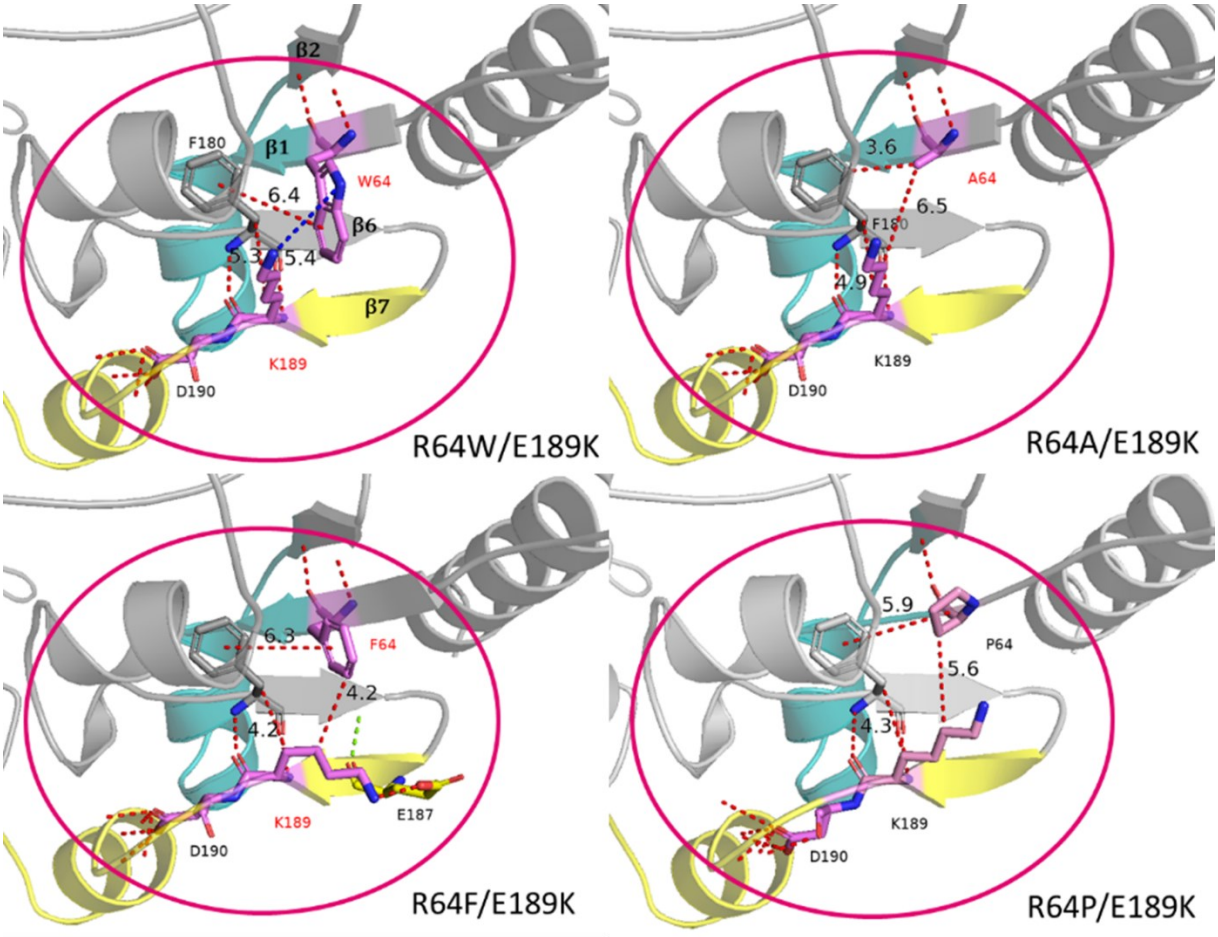

Figure 3.24 The model structure of *S. cerevisiae* tRNA-NT R64W/E189K, R64A/E189K, R64F/E189K, and R64P/E189K variants. The R groups of residues of interest in motifs A and C are shown and the distances between atoms of interest are indicated. Red circles show the important regions in each structure.

3.7.6 Comparison of the structures of the native enzyme and the D190A variant

The model structure of D190A variant in comparison to the native enzyme shows a closer approach of E189 to R64 by up to 0.4 Å. This may reflect that there are fewer interactions between A190 and residues at the terminus of α6 as compared to D190 and this helix which would allow β7 to move slightly closer to β2. No novel interactions are evident in this variant.

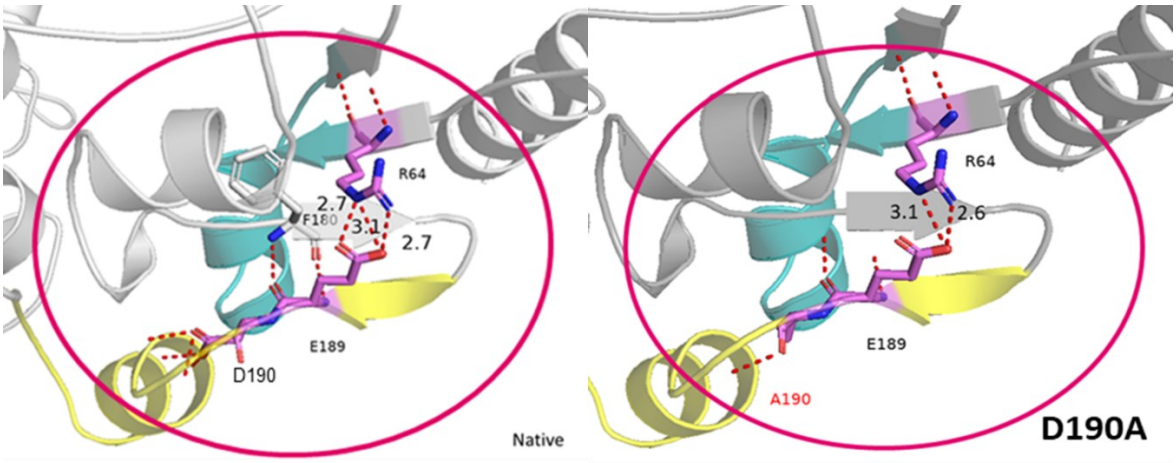

Figure 3.25 The model structure of *S. cerevisiae* tRNA-NT native and the D190A variant. The R groups of residues of interest in motifs A and C are shown and the distances between atoms of interest are indicated. Red circles show the important regions in each structure.

3.7.7 Comparison of the structures of the R64 variants in the D190A background

Model structures of the R64W/D190A, R64A/D190A, R64F/D190A, and R64P/D190A variants (Fig. 3.26) suggest, in all cases, the reduction of potential interactions between residue 64 and E189. The R64W and R64F variants again show potential interactions with F180 as seen in the E189F (Fig. 3.22) and E189K (Fig. 3.24) variants. The R64A and R64P variants allow for a potential reorganization of E189 such that it could interact with N182 in the β-turn between β-strands β6 and β7.

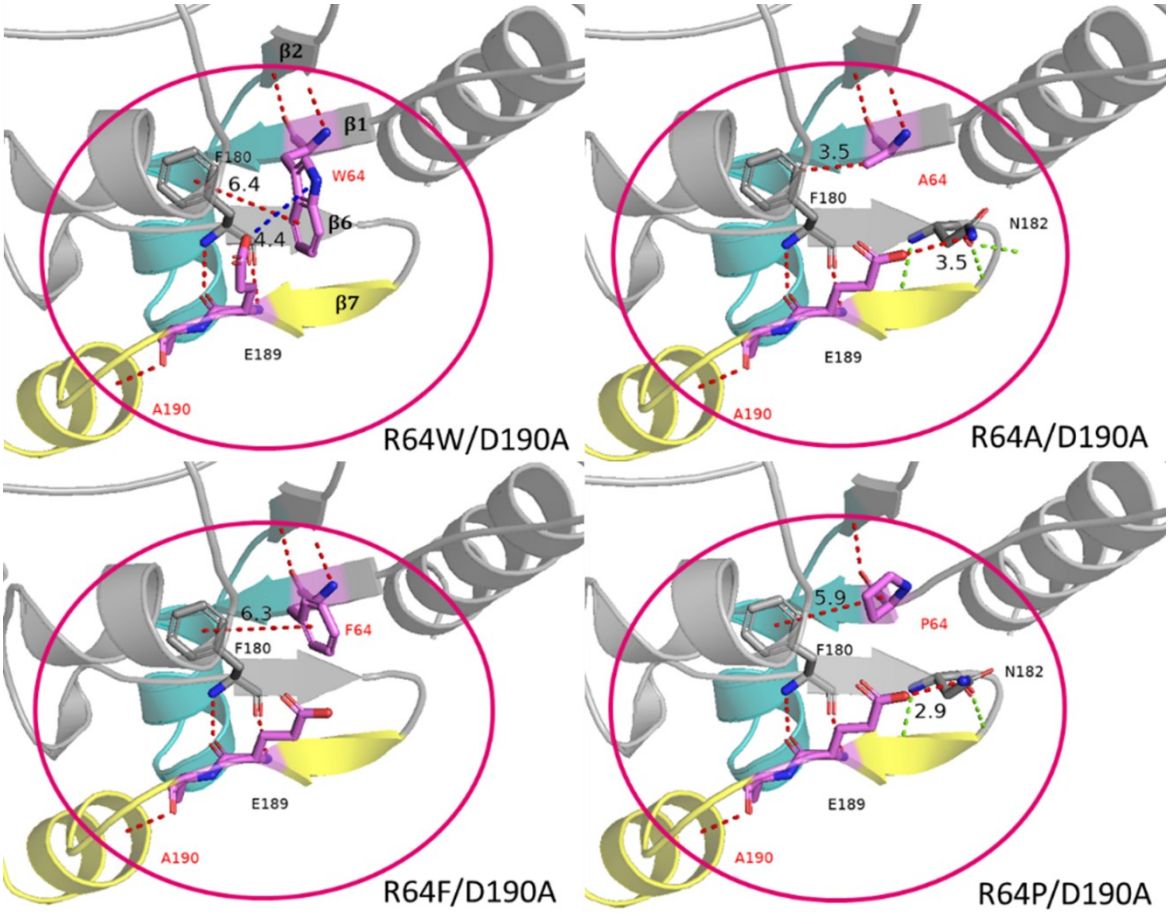

Figure 3.26 The model structure of *S. cerevisiae* focusing on the motif A and C and interactions in the R64W/D190A, R64A/D190A, and R64F/D190A variants. The R groups of residues of interest in motifs A and C are shown and the distances between atoms of interest are indicated. Red circles show the important regions in each structure.

3.7.8 Comparison of the structures of the native enzyme and the D190F variant

Based on these models, the D190F variant shows the most dramatic rearrangement of potential interactions of all of the variants examined (Fig. 3.27). This may not be surprising as the D190F substitution lead to the most dramatic change in cell viability with little or no growth at both the permissive and restrictive temperatures (Fig. 3.11). As with the D190A variant, our model structure shows a closer approach of E189 to R64 but only at the level of 0.1 to 0.2 Å. This again may reflect fewer interactions between F190 and residues at the terminus of α6. It also may reflect a new potential interaction with N182 in the β-turn between β6 and β7 as seen in the D190A

variant. Finally, this variant is the first to show the potential for new hydrophobic interactions with residue V188 in β7.

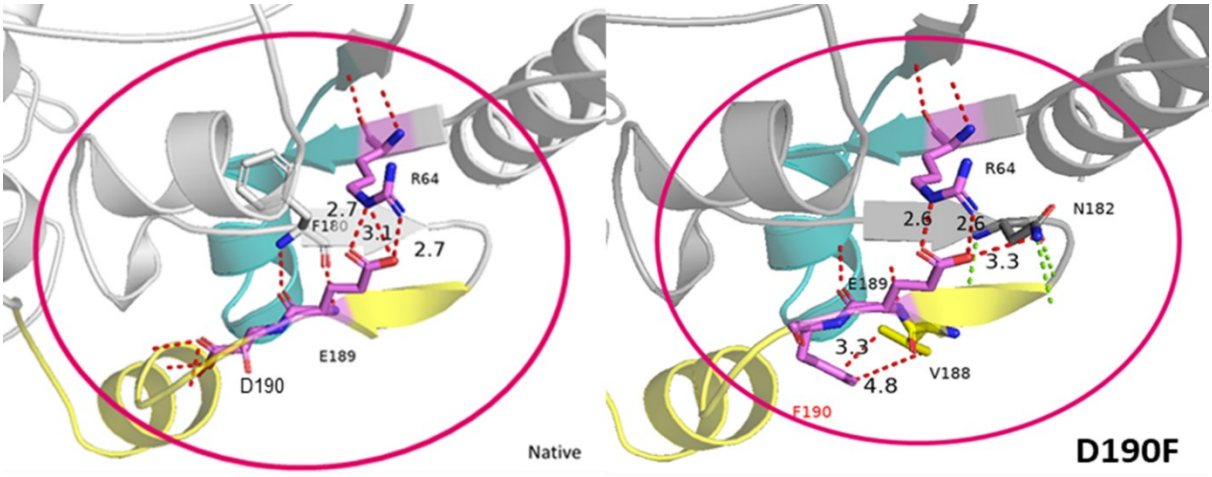

Figure 3.27 The model structure of *S. cerevisiae* tRNA-NT native and the D190F variant. The R groups of residues of interest in motifs A and C are shown and the distances between atoms of interest are indicated. Red circles show the important regions in each structure.

3.7.9 Comparison of the structures of the R64 variants in the D190F background

Comparisons of the predicted structures of R64W/D190F, R64A/D190F, R64F/D190F, and R64P/D190F variants (Fig. 3.28) show that β2 is disrupted in the conversion of the arginine at position 64 to proline as seen in the R64P/E189K variant (Fig 3.24). Aside from this the most interesting change in the structure is reflected in the role that F180 in β5 may play in the organization of this region of the protein again as seen previously in the E189K variants (Fig. 3.24). Each of these variants also shows the loss of any interactions between F190 and α6 as seen in the D190F variant. So, in none of these double variants are the potential hydrophobic interactions between positions 190 and 188 in β7 in the D190F variant eliminated.

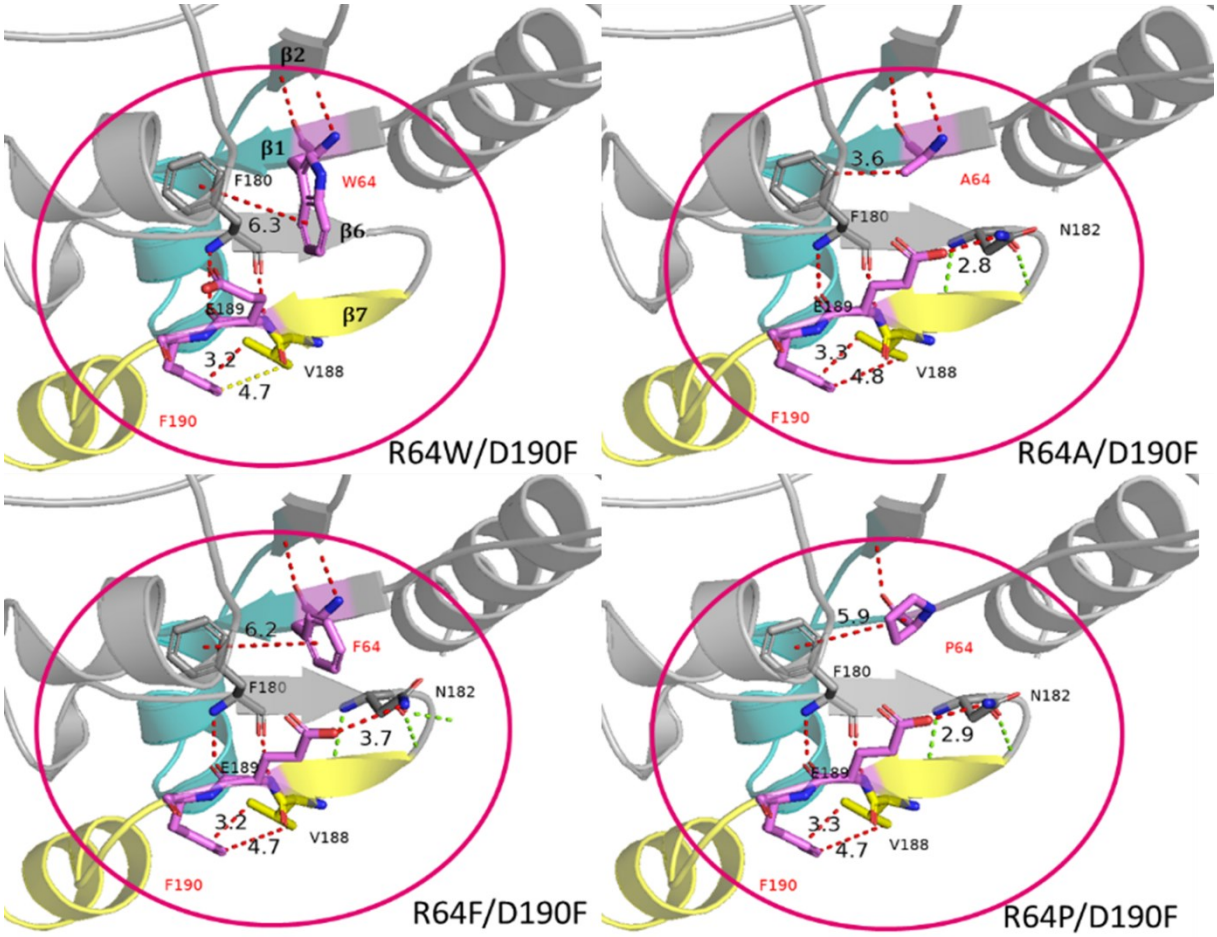

Figure 3.28 The model structure of *S. cerevisiae* focusing on the motif A and C interactions in R64W/D190F, R64A/D190F, R64F/D190F, and R64P/D190F variants. The R groups of residues of interest in motifs A and C are shown and the distances between atoms of interest are indicated. Red circles show the important regions in each structure.

4.0 DISCUSSION

4.1 The importance of Motif C

Based on the initial crystal structures (Li *et al.,* 2002; Cho *et al.,* 2007) and the lack of sequence conservation among organisms, motif C (Fig. 1.6) in the head and neck region of tRNA nucleotidyltransferase initially was thought to serve as a simple connector between the head and neck domains of the protein. Subsequent studies in our lab (Shan *et al*., 2008) showed, through genetic and biochemical experiments, the importance of motif C in enzyme activity and protein stability. A glutamate to lysine substitution at position 189 in the yeast enzyme was shown to reduce enzyme activity and thermostability and led to a temperature-sensitive phenotype.

Further biochemical and crystallographic experiments (Toh *et al*., 2009, Yamashita and Tomita, 2016) resulted in motif C being called a "springy hinge" that controls the processivity and specificity of nucleotide incorporation. Specifically, in the *Thermotoga maritima* enzyme (upon which our yeast model structure is built) β4 and β5 in the single β-sheet that defines Class II tRNA nucleotidyltransferases are connected by a β hairpin (amino acid residues 81–87) that moves as the enzyme goes from CMP incorporation to AMP incorporation. Moreover, the crystal structure suggests that in addition, the organization of the loop region (amino acid residues 102–121) between β6 and α5 also changes (Toh *et al*., 2009).

That motif C plays a role in the reorganization of the entire head and neck region of the protein was further supported by genetic and biochemical experiments in our lab where mutations that suppressed the *ts* phenotype and restored enzyme activity were mapped to amino acid substitutions in motif A (Goring *et al*., 2013). These amino acid substitutions were in motif A which plays a crucial role in nucleotide binding and catalysis (Holm and Sander, 1995). Additional experiments with the yeast enzyme (Sandhu, 2014) suggested that the initial mutation in motif C disturbs the precise positioning of motif A and B residues leading to a reduced k_{cat} defining reduced enzyme activity. This was proposed to be due to an increase in the size of the residue in motif C (Sandhu, 2014).

More recently, EPR spectroscopy with the human tRNA-NT (Ernst *et al.,* 2015) showed a measurable change in organization of the head and body domains. These authors proposed that

during enzyme activity motif C adjusts the catalytic core of the enzyme and the tRNA binding site for the binding and addition of each NTP. Reflecting back on the springy hinge model, these authors suggest that motif C expands on tRNA binding to allow for CMP and AMP incorporation and then after AMP incorporation contracts to limit extension of the tRNA. It is the change in motif C that allows for reorganization of the active site and catalysis to occur. These authors used site-directed mutagenesis to show that changing an aspartic acid residue (D139) in motif C resulted in decreased catalysis but no change in substrate binding (Ernst *et al.,* 2015).

We subsequently carried out a detailed kinetic analysis of the yeast enzyme by changing E189 (identified in yeast through the *ts* phenotype) and D190 (corresponding to D139 in the human enzyme) to show that as in the human enzyme site-directed mutagenesis at these positions in motif C did not alter substrate binding (K_m) for ATP, CTP or tRNA, but did dramatically reduce turnover number (k_{cat}) (Rahman, 2017). Finally, Ernst *et al*. (2015) argued that the flexible spring element in motif C does not act alone but instead acts through hydrogen bonding with two neighboring α-helices, α8 and α11 (Fig. 4.1), to help to define the number of nucleotides added to the tRNA. So, we are beginning to get an understanding of the role of motif C in enzyme activity.

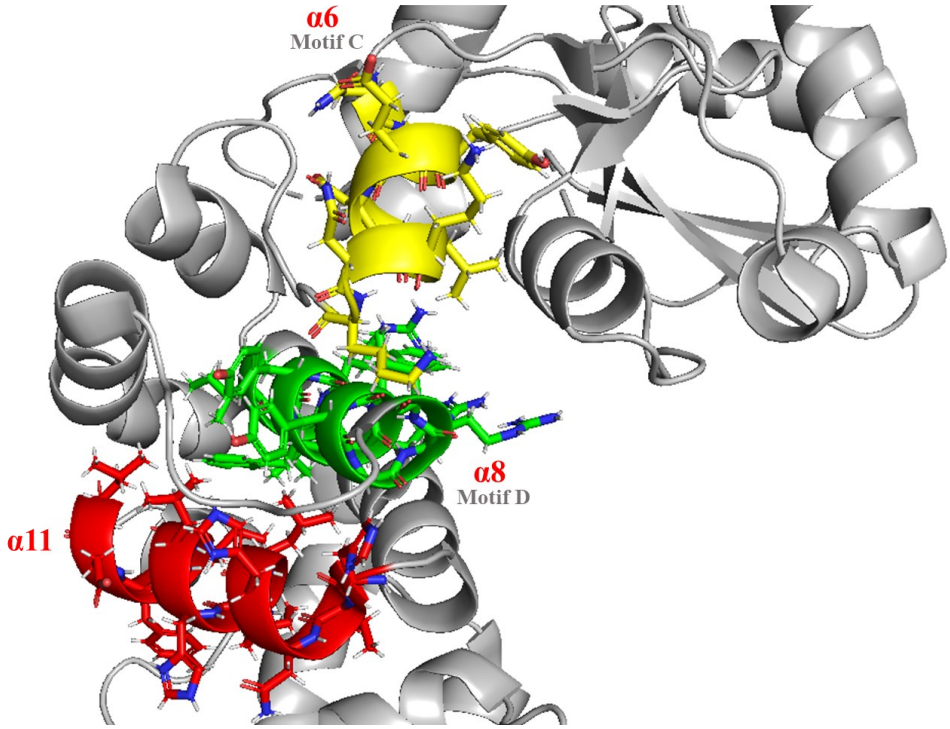

Figure 4.1 The structure of human TRNT1, showing motif C (yellow) and α8 (green) and 11 (red) in motif D and the body domain, respectively.

As described above, we were the first group to identify any specific residues outside of motif C that may be involved in its activity. Specifically, we showed that a suppressor mutation that converted residue 64 from arginine to tryptophan in β1 in motif A increased enzyme activity in the E189F variant and suppressed the *ts* phenotype (Goring *et al*., 2013). We then showed that this arginine to tryptophan substitution at position 64 on its own did not result in a *ts* phenotype (Goring *et al*., 2013) and showed no major change to either k_{cat} or K_m as compared to the native enzyme (Sandhu, 2014). We further showed that changing residue 64 to glutamate showed no phenotype in the native background but could not suppress the *ts* phenotype in the E189F or E189K background (Goring *et al*., 2013). Finally, we showed that the R64W substitution could affect the activity of E189F, E189K, E189A, D190F and D190A variants suggesting that the role of R64 is not limited to a defined interaction with a specific residue in motif C.

In this project, I expanded upon this finding to develop a stronger understanding of the role of residue 64 in the suppression of the *ts* phenotype and in enzyme activity. Specifically, I changed residue 64 to alanine (small and hydrophobic), phenylalanine (large and hydrophobic) or proline (which should disrupt a β-strand) and then characterized these variants in a native, E189F, E189K, D190A or D190F background. Each R64 variant will be discussed individually and then general conclusion based on the comparisons of these different amino acids will be proposed.

4.2 Characterization of R64F variants

4.2.1 The R64F substitution in the native background

As expected, based on our studies with the R64W variant, we saw no difference in growth with the R64F variant as compared to the native background (Fig. 3.7). Moreover, the R64F variant did not show a *ts* phenotype (Fig. 3.7). Its activity levels (compare Fig. 3.17 and 3.18) were sufficient to explain why we did not see a *ts* phenotype. We saw roughly 25% of the activity for CMP incorporation into the tRNA-NC template or AMP incorporation into the tRNA-NCC template in the R64F variant as compared to the native enzyme at the lowest enzyme amount tested (1.25 ng). When the enzyme level was increased to 2.5 ng we saw more than 60% incorporation of CMP or AMP into the appropriate template as compared to the native enzyme. One feature of incorporation into the R64F variant is noteworthy. Improper incorporation of CMP into the final

position of the tRNA is more prevalent in the R64F variant than in the native enzyme with up to 10% of the final product in the R64F variant containing a third C at the highest amount of protein tested (Fig. 3.18). This is consistent with what had been seen previously with the R64W variant (Goring *et al*., 2013, Rahman, 2017). We have argued that given that residue 64 is found in motif A and that this motif contains the two aspartate residues required to coordinate the metal ions required for catalysis, this change in misincorporation could be an indication of changes in the orientation of the metal ions that alters enzyme activity (Rahman, 2017). However, given that nucleotide recognition is mediated by motif D (Li *et al*., 2002, Cho *et al*., 2007) perhaps a change at residue 64 could alter the organization of motif D relative to motif A.

We did not expect to see any alterations in tRNA binding as a result of the R64F substitution as this change is in the head domain of the protein and tRNA binding is primarily through the body and tail domains of the protein (Li *et al*., 2002, Tomita *et al*., 2004, Xiong *et al*., 2003, Xiong *et al*., 2004, Betat *et al*., 2004, Leibovitch *et al*., 2013, Yamashita *et al*., 2015, Yamashita and Tomita, 2016, Leibovitch *et al*., 2019). When we compared the nucleic acid (presumably tRNA) associated with the protein after purification (Fig. 3.15) as a crude indicator of complexation of tRNA and protein we find similar A_{280}:A_{260} ratios both before and after RNaseA treatment with a roughly two-fold increase on RNaseA treatment, suggesting that both proteins were purified with associated RNA.

A comparative analysis of the models of the native enzyme (Fig. 1.10) and the R64W variant (Fig. 1.11) show an apparent interaction between residues 64 and 189 although there appear to be fewer interactions between W64 and E189 than between R64 and E189. This reduced number of interactions may be linked to the change in the conformation of the active site that results in the reduced activity. So, the R64W change could disturb the enzyme but, instead of altering the active site including a catalytically important residue of motif A, it alters the two hinge regions (described above) linking motifs C and E which have been proposed to play a role in catalysis in the context of altering the conformation of the active site to allow AMP incorporation at the terminal position of the tRNA (Ernst *et al*., 2015).

In contrast, when residue 64 is converted to phenylalanine, we see a more dramatic rearrangement in the protein (Fig. 3.20). Here the interactions between residues 64 and 189 are completely lost and in fact residue 189 is shown to interact with residue N182 in the β-turn between

β6 and β7 (Fig. 3.20). This change in bonding pattern could alter the organization of the active site and lead to the reduction in enzyme activity seen for both CMP and AMP incorporation (Fig. 3.18). However, the loss of these interactions and the new interaction with respect to N182 do not sufficiently disable the enzyme to generate the *ts* phenotype (Fig. 3.7).

4.2.2 Characterization of the R64F substitution in the temperature-sensitive backgrounds

4.2.2.1 The R64F substitution in the E189F background

While the R64F substitution at residue 64 in the native background resulted in reduced activity in terms of both CMP and AMP incorporation (Fig. 3.18) this loss of activity (to about 25% that of the native enzyme) was not sufficient to generate a *ts* phenotype (Fig. 3.7). In contrast, if the interactions between residues 64 and 189 are disrupted by the conversion of glutamate 189 to phenylalanine a *ts* phenotype does arise (Fig. 3.8). This E189F variant shows only about 4% activity as compared to the native enzyme (Shan *et al*., 2008) and it is this more dramatic reduction in activity that was linked to the generation of the *ts* phenotype (Goring *et al*., 2013). These results support our earlier hypothesis that the change in enzyme activity is linked to more than just an interaction between residues 64 and 189 (Goring *et al*., 2013, Rahman, 2017). If it was that simple, then one would expect a similar response whether the interactions were disrupted by altering residue 64 or 189. If one compares the model structures of the native enzyme and the E189F variant (Fig. 3.21) a dramatic alteration of the organization of the protein around residue 189 is apparent. There is a loss of interactions between residues 64 and 189 as we saw in the R64F variant, but more importantly there are new interactions formed between E187 and R64 as well as novel interactions between residue F189 at the end of β6 and residue F180 in β5. This suggests that the organization of this region of the protein is altered more dramatically in the E189F variant than in the R64W or R64F variant. When we (Rahman, 2017) explored the specific changes in enzyme activity linked to the E189F substitution we found that turnover number was reduced on the order of 100 fold while K_m was not altered. This indicates that it is not substrate binding but catalytic activity that is altered. This observation agrees well with observations of other researchers working with the human tRNA-NT (Ernst *et al*., 2015) where a change in the residue adjacent to the human equivalent of E189 in motif C also resulted in no change in substrate binding but led to a 15-fold reduction in AMP incorporation.

When residue 64 was converted from arginine to phenylalanine in the E189F background we found that this R64F/E189F variant (Fig. 3.19) showed less activity than the native enzyme (Fig. 3.17) or R64F variant (Fig. 3.18). When supplied with 10 ng of enzyme, product formation from CMP addition to the tRNA-NC template showed only about 50% of tRNA-NCC. Similarly, there was only about 45% product formation to tRNA-NCCA by AMP incorporation. When the assay was carried out with the tRNA-NC template and both CTP and ATP only about 10% of the complete product was shown even at the highest protein level (10 ng) tested. Even so, the important point to note here is that even with this level of activity, the *ts* phenotype in the E189F variant is suppressed (Fig. 3.8). This is an interesting observation as it was noted previously that the reduction in k_{cat} of the E189F variant was to about 1% that of the native enzyme and this variant showed the *ts* phenotype (Rahman, 2017). In those same experiments the R64W/E189F variant showed a k_{cat} of 13% that of the native enzyme and was able to grow at the restrictive temperature (Rahman, 2017) in good agreement with what we saw here. So, the E189F substitution leads to a dramatic reduction in turnover number but a limited change in substrate binding, while the conversion of residue 64 to tryptophan or phenylalanine increases the activity of this variant by 10-fold to approximately 10% of that of the native enzyme. This increase is activity, then is sufficient to suppress the *ts* phenotype. It will be important to carry out a more detailed kinetic analyses on the R64F/E189F variant when conditions allow to see if as in the R64W/E189F variant it is k_{cat} and not K_m that is altered.

If we compare the models of the R64W and R64F variants in the E189F background (Fig. 3.8) we see that as both substitutions introduce hydrophobic and/or aromatic residues at positions 64 and 189, there is the potential for new hydrophobic or π-π stacking interactions. Comparing both variants shows very similar predicted structures consistent with the activity and suppression of the *ts* phenotype that we observed. Both variants show a novel interaction not seen previously between residue F180 at the beginning of β6 and F189 of β7. However, they lack the interaction between R64 and E187 seen in the E189F variant (compare Fig. 3.21 and Fig. 3.22). Again, this suggests the importance of the organization of β6 and β7 in enzyme activity.

4.2.2.2 The R64F substitution in the E189K background

The conversion of the negatively-charged glutamic acid residue at position 189 to a positively-charged lysine should disrupt any potential electrostatic interactions that existed between the glutamate at position 189 in β7 and the arginine at position 64 in β1. Our molecular model suggests that this indeed is the case (Fig. 3.23). However, in this variant the lysine at position 189 which does not now interact with R64 is available to interact with the main chain of β6. So, again this amino acid substitution results in the potential for rearrangements about β1, β6 and β7. Once again, this substitution results in reduced enzyme activity with in this case activity being reduced to 5% that of the native enzyme (Shan *et al*., 2008) and this drop in activity is thought to lead to the *ts* phenotype (Goring *et al*., 2013) observed (Fig. 3.9).

As with the E189F variant discussed above, the R64F substitution in the E189K background suppressed the *ts* phenotype (Fig. 3.9). A comparison of the R64W variant with the R64F variant in the E189K background suggests an increased potential for interactions with the main chain of β6 and an increase in the potential for hydrophobic interactions with residue F180 at the beginning of β6. Again, this points to the organization of β6 and β7 and how residues in β1 may alter these interactions. The similarities in these variants is linked well with the suppression of the *ts* phenotype seen with both amino acid substitutions. Again, this suggests that it is not a direct interaction between residues 64 and 189 that is important but instead the arrangement of the higher order structures in this region of the protein.

4.2.2.3 The R64F substitution in the D190A background

Converting the aspartic acid residue at position 190 to alanine resulted in a temperature-sensitive phenotype (Fig. 3.10). When the model structure of the D190A variant was compared to the native enzyme, potential interactions between R64 and E189 were still evident. This suggests that the *ts* phenotype is not dependent on specific R64/E189 interactions but instead is dependent on the organization of this region of the protein. The D190A variant also shows fewer interactions between A190 and residues at the beginning of α6 as compared to D190. Decreasing how tightly β7 is bound to this helix by reducing the potential bonds may allow β7 to move slightly closer to β2. No new interactions are evident in this variant.

Previous studies with the human tRNA-NT showed that the aspartic acid that corresponds to D190 in the yeast enzyme is involved in maintaining the spring derived from motif C (Ernst *et al*., 2015). These authors showed that converting this position from aspartic acid to alanine resulted in a 15-fold reduction in turnover number, but no major change in K_m. They also saw that this amino acid substitution altered the movement of the head and body domains with respect to one another as measured by EPR spectroscopy. They proposed that D139 plays a role in helix-capping to stabilize the adjacent small α-helix by allowing the terminal carboxylic acid group of the aspartic acid residue to interact with the main chain nitrogens of G143 and Y144 (Ernst *et al*., 2015). When D139 is converted to alanine the capping interaction is lost, such that the helix is destabilized, and its positioning is altered contributing to the loss of activity observed. Taking these data together, the authors concluded that motif C plays a role in the structural reorganization of the enzyme during CCA-addition such that it arranges in space the ATP and tRNA-CC substrates such that the terminal AMP can be incorporated into the protein. They also suggest that motif C could play a broader role in the organization of the active site. Using their own computational models, they showed that when the aspartate was converted to alanine this leads to a tilting motion of the head domain away from motif C with subsequent reorientation of the β-sheet region in the head domain. This change alters the structure of the active site such that the enzyme is unable to switch from the structure required for CMP incorporation to the structure required for AMP incorporation (Ernst *et al*., 2015). They suggest that the spring element made of motif C and surrounding α-helices plays an important role in stabilizing and adjusting the positions of the head and body domains for specific nucleotide incorporation. These observations are consistent with our modelling studies which also show the potential reorganization of the corresponding β-sheet in the yeast enzyme. We hoped to see what new information we could gain by making changes at position 64.

When R64 was converted to tryptophan (Rahman, 2017) or phenylalanine (Fig. 3.26) our models show fewer interactions between residues 64 and 189 and new interactions with F180 as previously seen in the E189F (Fig. 3.22) and E189K (Fig. 3.24) variants. While the R64W variant suppressed the *ts* phenotype the R64F variant did not (Fig. 3.10). This may reflect the fact that the R64F variant shares fewer interactions with E189 (Fig. 3.26) as the replacement of the indole component of the side chain with a phenyl ring would result in the loss of the potential hydrogen bond with the ring nitrogen in tryptophan. More simply it could reflect the reduction in size of the

side chain and steric issues. It will be interesting to see what happens when R64 is converted to the much smaller alanine.

When the activities of the D190A variant and the R64W/D190A variants were assayed the D190A variant showed a decrease in k_{cat} to 15% of that of the native enzyme while the R64W/D190A variant restored activity to 56% of that of the native enzyme (Rahman, 2017). This suggests that changing the residue at position 64 can alter the structure of this region of the protein containing motif C and the adjacent helices and alter the activity of the enzyme. Again it will be useful to see the activities of the R64F variants and to define more precisely the kinetic parameters for the R64F/D190A variant to see how they differ from those of the R64W/D190A variant to explain why R64F does not suppress the *ts* phenotype while the R64W variant does.

4.2.3 Characterization of the R64F substitution in the inviable background

4.2.3.1 The R64F substitution in the D190F background

Ernst *et al.* (2015) have shown that converting the aspartic acid residue at position 139 (corresponding to D190 in the yeast enzyme) to the much smaller alanine resulted in detrimental changes in catalytic activity and protein structure. We previously had shown that increasing the size of E189 (by replacing it with phenylalanine or lysine) resulted in a dramatic reduction in enzyme activity and reduced thermal stability (Shan *et al*., 2008). Based on these observations we wanted to see what effect increasing the size of residue 190 would have on enzyme structure and function. Therefore, we introduced a phenylalanine at position 190 and showed a reduction in k_{cat} of ~100 fold (Rahman, 2017). As expected, this decrease in enzyme activity was linked to an inability for yeast carrying this substitution to grow even at the permissive temperature (Fig. 3.11).

Our modelling suggests that in the D190F variant there is an extensive rearrangement of potential interactions (Fig. 3.27). E189 still interacts with R64 but in the variant also with N182. This variant is the first to show the potential for new hydrophobic interactions with residue V188 in β7. Moreover, any interactions with α6 are lost in the D190F variant. Given the role for motif C and the adjacent helices in enzyme function, these changes in the structure seem important.

When R64 in the D190F variant was converted to tryptophan k_{cat} was increased to 7% of that of the native enzyme (Rahman, 2017) and growth occurred at both the permissive and restrictive temperatures (Fig. 3.11). In the R64W/D190F variant there is a new interaction between E189 and F180 and the loss of the interaction between E189 and N182 (Fig. 3.28). Again, perhaps it is the rearrangement in this region of the protein that increases enzyme activity to allow the cells to grow. In the R64F/D190F variant, which is unable to grow at either temperature, the interaction with N182 remains while there is an altered interaction with F180 (Fig. 3.28). This may suggest that the interaction between E189 and N182 is what alters the structure to reduce the activity of the enzyme.

4.3 Characterization of R64A variants

We previously have shown that increasing the size of the residue at position 64 from arginine to tryptophan does not have a dramatic effect on the catalytic properties of the native enzyme but will increase the turnover number of several *ts* variants and allow their growth at the restrictive temperature (Rahman, 2017). I showed (section 4.2) that converting position 64 to phenylalanine reduces the activity of the native enzyme (Fig. 3.18) but increases the activity of the E189F variant (Fig. 3.19) such that it can suppress this *ts* phenotype (Fig. 3.8). This R64F substitution also suppresses the *ts* phenotype in the E189K variant (Fig. 3.9), but unlike the R64W variant will not suppress the *ts* phenotype in the D190A variant (Fig. 3.10) or restore viability to the D190F variant (Fig. 3.11). One possible explanation for this observation is that the size of the residue at position 64 plays an important role in restoring enzyme activity and allowing for viability at the permissive and restrictive temperatures. To address this question, I placed an alanine at position 64. This substitution essentially removes the indole ring from the tryptophan side chain and leaves on the methyl group.

4.3.1 Characterization of the R64A substitution in the native background

While the R64A variant shows growth comparable to that of the native enzyme at the permissive temperature, it shows an apparent reduced growth rate at the restrictive temperature suggesting that this substitution on its own leads to a *ts* phenotype (Fig. 3.7). A comparative analysis of the models of the native enzyme (Fig. 1.10) and the R64A variant (Fig. 3.20) shows no

apparent interactions between residues A64 and E189 on β1 and β7 although the potential for main chain interactions between strands β1 and β2 remains. Moreover, as in the R64F variant (but not the R64W variant) we also see that E189 could interact with N182. This again suggests that an interaction with N182 is detrimental to enzyme activity but as both the R64F and R64A variant possess this interaction there must be more involved than this alone as R64A grows poorly at the restrictive temperature while R64F shows no phenotype (Fig. 3.20). Perhaps this directly reflects a contribution of the size of the side chain in defining the structure of this region of the protein. It is important to determine the activity of the R64A variant to see if a link can be found between the apparent reduced growth rate at the restrictive temperature and the activity retained in this variant.

4.3.2 Characterization of the R64A substitution in the temperature-sensitive backgrounds

4.3.2.1 The R64A substitution in the E189F background

In the E189F background the R64A substitution is not able to suppress the *ts* phenotype (Fig. 3.8). Given that we saw a reduced growth rate in the strain expressing the R64A variant (Fig. 3.7) this is not surprising. If we examine the predicted structure of the R64A variant (Fig. 3.22) we see that it resembles more closely that of the R64F variant than the R64W variant. This is especially in the context of the distance between residues 64 and 189. One could imagine an orientation of the phenylalanine residues in the R64F/E189F variant to generate new hydrophobic or π-π stacking interactions that would not be possible in the R64A/E189F variant. Perhaps these interactions are what allows the R64F variant to suppress the *ts* phenotype while the R64A variant cannot.

4.3.2.2 The R64A substitution in the E189K background

There is no apparent change in growth at the permissive temperature for the R64A/E189K variant as compared to the E189K variant (Fig. 3.9) but unlike the R64W and R64F substitutions, the R64A substitution is unable to suppress the *ts* phenotype (Fig. 3.9). Again, this agrees with what was seen with the E189F variant where the R64A substitution was unable to suppress the *ts* phenotype (Fig. 3.8) and may again reflect that the reduced activity of the E189K variant that leads to the *ts* phenotype is further reduced in the R64A/E189K variant. If one compares the predicted structures of the R64A variant and the R64F and R64W variants the most obvious difference is

that there are no possible interactions with the side chain of the R64A variant (Fig. 3.24). While there are potential hydrophobic interactions between the aliphatic side chain of lysine 189 and aromatic ring of phenylalanine 64, and both hydrophobic and hydrogen bonding interactions between W64 and K189, the only potential for interactions with A64 is weak hydrophobic interactions with the methyl group of alanine, or more likely with the main chain atoms. Again, a rearrangement of interactions in this region of the protein may be linked to structural changes in the active site of the enzyme.

4.3.2.3 The R64A substitution in the D190A background

The R64A substitution did not suppress the *ts* phenotype in the D190A variant and in fact these cells showed poorer growth than the D190A variant even at the permissive temperature (Fig. 3.10). One major difference between the R64A variant and the R64W or R64F variants is that there is no potential interaction between the side chains of these or other residues with R64A (Fig. 3.26). F180 which interacts with the side chains of W64 or F64 can only interact with the backbone atoms of E189. The second striking difference in the R64A variant is that in this variant (but not in the R64W or R64F variants) E189 is able to interact with N182. This again points to the role of N182 and the loop in which it is contained in organizing the structure of the enzyme.

4.3.3 Characterization of the R64A substitution in the inviable background

4.3.3.1 The R64A substitution in the D190F background

Reducing the size of the residue at position 64 clearly does not compensate for an increase in the size of the residue at position 190 as the R64A/D190F variant is inviable at either temperature tested (Fig. 3.11). As in the D190A variant in this case there are no interactions with the A64 side chain and residue E189 can interact with N182 (Fig. 3.28). This again suggests the importance of this loop between strands β6 and β7.

4.4 Characterization of R64P variants

The most important feature of a proline residue is that it would be predicted to disrupt an α-helix or a β-strand as it is an imino acid that limits rotation about the main chain of the polypeptide (Voet and Voet, 2005). Therefore, by introducing this residue into position 64 we anticipate that β1 in motif A will be disrupted. Given the importance of motif A in enzyme activity (Holm and Sander, 1995, Steitz, 1998, Li *et al*., 2002, Xiong *et al*., 2003), we expected that this substitution would have a dramatic effect on tRNA-NT activity.

4.4.1 Characterization of the R64P substitution in the native background

As we expected, conversion of the arginine at position 64 to proline does lead to inviable cells at both the restrictive and permissive temperatures (Fig. 3.7). This is the first substitution at position 64 that caused lethality. While it seems likely that disruption of β1 leads to the non-viable phenotype, replacement of the large hydrophilic arginine at position 64 with the smaller and non-polar proline could also disrupt possible interactions between position 64 and other residues as compared to the native enzyme model structure (Fig. 3.20) generating the phenotype observed. Based on the R64P model structure which shows the same interaction between E189 and N182 as seen in the R64A and R64F variants (which we proposed to have a role in decreasing enzyme activity) we cannot discount the role that this interaction may also play in the R64P variant (Fig. 3.20).

In addition to the loss of the interactions between positions 64 and 189 in the R64P variant, we also noticed that the potential main chain interactions between P64 in β1 and alanine 85 in β2, are decreased as compared to the native enzyme and other variants (Fig. 3.20). Together these changes may alter the secondary structure of the enzyme even though the main chain interactions between E189 and F180 remains. Disruption of β1 alters multiple interactions in this region of the enzyme that impact negatively on enzyme structure or function leading to the non-viable phenotype that we observed.

4.4.2 Characterization of the R64P substitution in a temperature-sensitive background

Given that the R64P substitution generated a non-viable phenotype, we tested this substitution in only one variant background. As expected, the R64P substitution in the E189F *ts* background did not suppress the *ts* phenotype (Fig. 3.8). Molecular modelling suggests that in this background (Fig. 3.22) as well as in the E189K (Fig. 3.24), D190A (Fig. 3.26) and D190F (Fig. 3.28) you see the reduced interactions between β1 and β2 as observed in the native background. In fact, in the E189K and D190F backgrounds β1 is lost completely (Fig. 3.24). Also, other potential interactions in the E189F, E189K and D190F are shared by the R64F, R64A and R64P variants. The R64F, R64A and R64P variants all show the potential for an interaction between E189 and N182 in the D190F background while only R64A and R64P show this potential interaction in the D190A background. This also suggests the importance of the loop that contains N182.

4.5 General conclusions

When we identified the *ts* mutation that first suggested a role for motif C in tRNA-NT activity we suggested that amino acid substitutions at this position led to the *ts* phenotype because of an increase in the size of the amino acid at this position (Shan *et al*., 2008). We saw an excellent correlation between the Van der Waals' volume (Richards, 1974): Glu (109Å^3), Gln (114 Å^3), His (118 Å^3) and Lys and Phe (135 Å^3 each) of the amino acid at position 189 and the decrease in enzyme activity seen in each variant. Based on the available crystal structures at the time, we proposed that this residue was positioned in a β-turn connecting β7 with α6 in the yeast enzyme (Fig. 4.2) at or near the junction of the head and neck domains important for enzyme activity.

Figure 4.2 Alignment of the head and neck domains of the human, yeast and *Thermotoga maritima* tRNA-NTs. The conserved motifs are labelled and boxed according to the colours scheme in Fig. 1.1. Secondary structures defined from the human and *T. maritima* crystal structures are shown in blue and green, respectively. The predicted secondary structures in the yeast protein are shown in pink. The α-helices and β-strands are labelled α or β and numbered in sequential order. The numbers on the right represent the positions of the amino acids in the primary sequence.

Given the conservation of this motif in tRNA nucleotidyltransferases, it seemed reasonable to us that the mutation in the yeast *CCA1* gene led to steric constraints in the enzyme that altered the organization of this motif, changing the overall structure of the protein, affecting its activity and

stability and leading to the *ts* phenotype. Later we showed that the loss of activity was defined by a decrease in catalytic activity rather than a change in substrate binding (Sandhu, 2014, Rahman, 2017). Subsequently, Toh *et al*. (2009) used crystal structures to show the rearrangement of the head and neck domains of the *Thermotoga maritima* tRNA-NT on substrate binding and proposed a "springy hinge" model for the role of motif C that helps to correctly position the head (with motifs A and B) and neck domains (motif D) for proper catalysis.

More recently, Ernst *et al*. (2015) showed that in the human enzyme the conversion of D139 (corresponding to D190 in the yeast enzyme) (Fig. 4.2) to alanine resulted in a decrease in the ability of AMP to be incorporated into the growing tRNA. We also showed that in yeast the D190A substitution reduced the turnover number and that a D190F substitution did so even more dramatically (Rahman, 2017) suggesting that a larger residue in this region of the protein may also have steric effects reducing enzyme activity. Ernst *et al*. (2015) proposed that the reduced catalytic activity that they saw resulted from an inability of the catalytic residues to arrange correctly to allow the substrates to be organized appropriately for catalysis. Further they suggested that this results from a reorganization of the active site due to the loss of the stabilizing role of the helix-capping of D139 on α6 (Fig. 4.2) and that this and adjacent helices are rearranged (Fig. 4.1). Our observations in yeast are consistent with this model. Taken together these data support the role of motif C in organizing the active site to allow for catalysis.

A loss of catalytic activity in variant enzymes may be mediated by a change in motif C that alters the organization of other regions of the active site without a direct interaction with residues in motif C, or by changing specific interactions between residues in motif C and those in other regions of the protein. To begin to address these possibilities we identified a mutation that suppressed the *ts* phenotype in yeast (Goring *et al*., 2013). This mutation resulted in the replacement of an arginine residue at position 64 with a tryptophan. R64 is found in β1 in motif A in the yeast enzyme (Fig. 4.2). Given the crucial role of the DxD sequence (adjacent to β2 in motif A) in coordinating the metal ion required for catalysis (Steitz, 1998; Li *et al.,* 2002; Betat *et al.,* 2010) it is perhaps not surprising that a second substitution in this region of the protein could restore enzyme activity and suppress the *ts* phenotype (Goring *et al*., 2013). However, this did not distinguish between the possibilities that the amino acids in motifs A and C interact directly with one another to suppress the *ts* phenotype, or that the first amino acid change (position 189 or 190

in motif C) that leads to the *ts* phenotype causes a change in the protein which is compensated for by a completely independent change in the protein resulting from the second amino acid change (position 64 in motif A). To address these possibilities here, I altered position 64 specifically to reduce its size to see what effect this would have on enzyme structure or function.

When position 64 was converted from arginine to phenylalanine no *ts* phenotype was observed (Fig. 3.7) and the R64F substitution suppressed the E189F (Fig. 3.8) and E189K (Fig. 3.9) *ts* phenotypes. However, this substitution was unable to suppress the *ts* phenotype in the strain expressing the D190A variant (Fig. 3.10) and the R64F/D190F variant was inviable (Fig. 3.11). When position 64 was converted from arginine to alanine an apparent slow growth phenotype was observed at the restrictive temperature (Fig. 3.7) and neither the *ts* nor inviable phenotypes were suppressed (Fig. 3.8 to 3.11). Finally, conversion of position 64 to proline resulted in non-viable cells under any conditions tested (Fig. 3.7 and 3.8).

If we look at the characteristics of the amino acid side chains at position 64, we see that the size of the side chain seems to be important. With the arginine (148 $Å^3$) at this position in the native enzyme we see the *ts* or inviable phenotypes that result from changes at position 189 or 190. Except in the case of the D190 variants, if position 64 is converted to phenylalanine (135 $Å^3$) the same phenotypes are observed in R64F/E189F and R64F/E189K, but all of these phenotypes are suppressed when this position is converted to tryptophan (163 $Å^3$). When position 64 is an alanine (67 $Å^3$) none of the 189 or 190 phenotypes are suppressed and actually the R64A variant grows more slowly than the native enzyme at the restrictive temperature. Based on these observations, there is a good correlation between the size of the residue at position 64 and the ability of the enzyme to suppress the phenotype observed. The largest side chain suppresses all of the phenotypes tested while the smallest side chain suppresses none and on its own impairs growth at the higher temperature. This raises the possibility that there are steric constraints on the residue at position 64 as we have proposed for changes at position 189. Perhaps the β-turn between β1 and α3 is altered causing a change in this region of the protein altering structure or function. Certainly, based on these data the deleterious effect of a larger residue at position 189 (E189F, or E189K) is not compensated for by a smaller residue at position 64 (R64A). This may argue against a direct interaction between residues 64 and 189 in the variants. We saw this previously when we generated the R64E/E189R variant that was viable, but retained a *ts* phenotype (Goring *et al*., 2013). The

fact that the R64W substitution can suppress any of the phenotypes resulting from changes at residues 189 and 190 (Fig. 3.7 to 3.11) also argues against any direct interactions as no available models show any interactions between residues 64 and 190.

The proline (90 $Å^3$) residue is intermediate in size between the alanine and the phenylalanine yet results in inviable cells under any conditions tested (Fig. 3.7 and 3.8). This likely reflects the fact that introducing this imino acid into β1 disrupts this β-strand and this region of the protein (Fig. 4.2). As the two aspartic acid residues required for catalysis are found in motif A, disrupting this region of the protein could have dramatic effects on catalytic activity.

Before we discount completely the role of a possible direct interaction between residues 64 and 189, we need to look at the other features of the side chains. That R64W can suppress the *ts* phenotype in the E189F or E189K variant and restore enzyme activity (Goring *et al*., 2013, Rahman, 2017) may not be limited simply to its size. The indole ring would be able to be involved in hydrophobic and/or π-π stacking interactions with a phenylalanine residue and would be able to potentially hydrogen bond with the terminal amino group of a lysine residue. My observations in this study suggest that the large hydrophobic substitution at position 64 (R64F) may compensate through hydrophobic and/or π-π stacking interaction for the electrostatic or hydrogen bonding interactions lost in the E189F and E189K variants, such that the *ts* phenotypes of these variants are suppressed. Indeed, when tested, the activity of the R64F/E189F (Fig. 3.19) variant seemed higher than that previously reported for the E189F variant (Rahman, 2017). This may reflect a direct hydrophobic or π-π stacking interaction between the aromatic rings at these two positions. An explanation of the R64F suppressor phenotype in the E189K background is not so straightforward but may involve a hydrophobic interaction between the aliphatic portion of the long side chain of lysine and the aromatic ring of phenylalanine. The inability of the alanine at position 64 to suppress any of the phenotypes and to give itself a slow growth phenotype at the higher temperature may reflect an inability of this residue to interact with either the glutamate in the native enzyme or the lysine or phenylalanine in the variants, but it may more simply reflect a small residue at position 64 that alters the structure or organization of motif A.

Based on these analysis it appears that while a direct interaction between R64 and E189 may be important in the structure and activity of the native enzyme, restoration of this interaction can compensate somewhat for the loss of activity when these interactions are disrupted. This does not

explain the phenotypes observed in the variants with changes at position 190, *e.g*., D190A, D190F. To understand how these changes are compensated for by changes elsewhere in the protein requires an additional explanation.

My molecular modelling of the native and variant enzymes (Fig. 3.20 to 3.28) predicts altered interactions between amino acids that could be linked to the changes in the organization of the enzyme. In some instances, specific interactions seem to be linked to specific phenotypes. For example, the major difference between the R64W/D190F and R64F/D190F variants is the orientation of E189. In the R64W/D190F variant E189 interacts with the main chain of F180, while in the R64F/D190F variant E189 interacts with N182 which is at the end of β6 in motif B and near the loop between motifs B and C. This change in organization with respect to motif B and C could be linked to the differences in the suppressor abilities of R64F and R64W with respect to the D190 variants. The importance of interactions with N182 and the lack of suppression is seen in models of many of the variants (Fig. 3.20, 3.27, 3.28) where the presence of this interaction is linked to a nonviable phenotype, reduce growth or a loss of the suppressor.

Specifically, in the case of the D190F variant, residue D190 is found in motif C at the end of β7 and near the beginning of α6 (Fig. 4.2). Converting the aspartic acid at this position to phenylalanine eliminates stabilization of α6 by D190 through helix capping mediated by the aspartic acid residue as it was predicted in the molecular model (Fig. 3.27). If this indeed is the case, then this may allow a destabilization of that helix and a shift in its position as seen for the D139A human variant (Ernst *et al*., 2015). As α6 is linked to β7 by a short loop (Fig. 4.2, Fig.4.3), the movement of α6 may be linked to a shift in the position of β7 to rearrange the relative organization of the single β-sheet in the head domain leading to reduced enzyme activity (Rahman, 2017) and the lethality observed in the D190F variant (Fig. 3.11).

A second feature seen in the D190F variant that is absent from the native enzyme is an interaction between E189 and N182 (Fig. 3.27). N182 is found at the end of β6 adjacent to the small loop connecting β6 to β7 (Fig. 4.2, Fig. 4.3). Again, the reorganization of strands β6 to β7 may be what leads to the lethal phenotype observed as altering the positioning of these strands would alter the relative positioning of motif B and motif C. My studies further showed that substitution of R64 with phenylalanine or alanine was unable to suppress this phenotype (Fig. 3.11), but we previously had shown that the R64W variant could suppress it (Rahman, 2017).

Based on my models, the difference between the R64W/D190F variant and the R64F/D190F and R64A/D190F variants is that in the R64W variant (but not in the R64F or R64A variants), the interaction between E189 and N182 is lost (Fig. 3.28). This suggests that the interaction between E189 and N182 in any of these variants is what causes the changes in the protein structure that leads to the phenotype observed. Only in the R64W variant is the side chain at position 64 sufficiently large to prevent E189 from interacting with N182. Therefore, it is a steric constraint introduced by the mutation in motif A that blocks the rearrangement introduced by the D190F substitution in motif C such that the phenotype is suppressed.

Clearly, it is a combination of effects that leads to the phenotypes observed. For example, the D190A variant is temperature sensitive (Fig. 3.10), but modeling suggests that it does not contain the E189-N182 interaction (Fig. 3.25). However, in the R64A/D190A double variant the cells are dead at both the permissive and restrictive temperatures (Fig. 3.10) and molecular modelling suggests the presence of this E189-N182 interaction (Fig. 3.26). In the case of the D190A variant, the structural rearrangements are such that R64F, in this case, shows no suppression (Fig. 3.10). Perhaps this is a case of the original D190A substitution causing a rearrangement of α6 and β7 that somewhat destabilizes the β-sheet leading to the *ts* phenotype. However, because of the size of the alanine residue the rearrangements are not as dramatic as those seen in the D190F variant (compare Fig. 3.25 and Fig. 3.27) such that the change in the relative positions of β6 and β7 and in the structure of the β-sheet are changed sufficiently to induce the *ts* phenotype, but not sufficiently to lead to cell death. Again, as we have suggested previously (Goring *et al*., 2013) the difference in the phenotype observed likely reflects the relative catalytic activity of the protein. So, while the D190F variant likely retained little or no activity, the D190A variant retained enough activity to allow the cell to survive at the permissive temperature, it was not enough for viability at the restrictive temperature. When the residue at position 64 was converted from arginine to alanine in the D190A background this further destabilized the structure of the β-sheet because it allowed for the formation of the E189-N182 interaction (Fig. 3.26) and this presumably reduced the activity of the enzyme even further and led to the lethal phenotype observed (Fig. 3.10). In the D190A background the R64F substitution was unable to suppress the *ts* phenotype but did allow growth at the permissive temperature (Fig. 3.10). The ability of the R64F/D190A variant to grow at the permissive temperature may be linked to the lack of the E189-N192 interaction seen in the R64A/D190A variant (Fig. 3.26). Although this variant lacks the E189-N182 interaction it

maintains the *ts* phenotype supporting the contention that the *ts* phenotype is mediated by changes in more than one specific interaction.

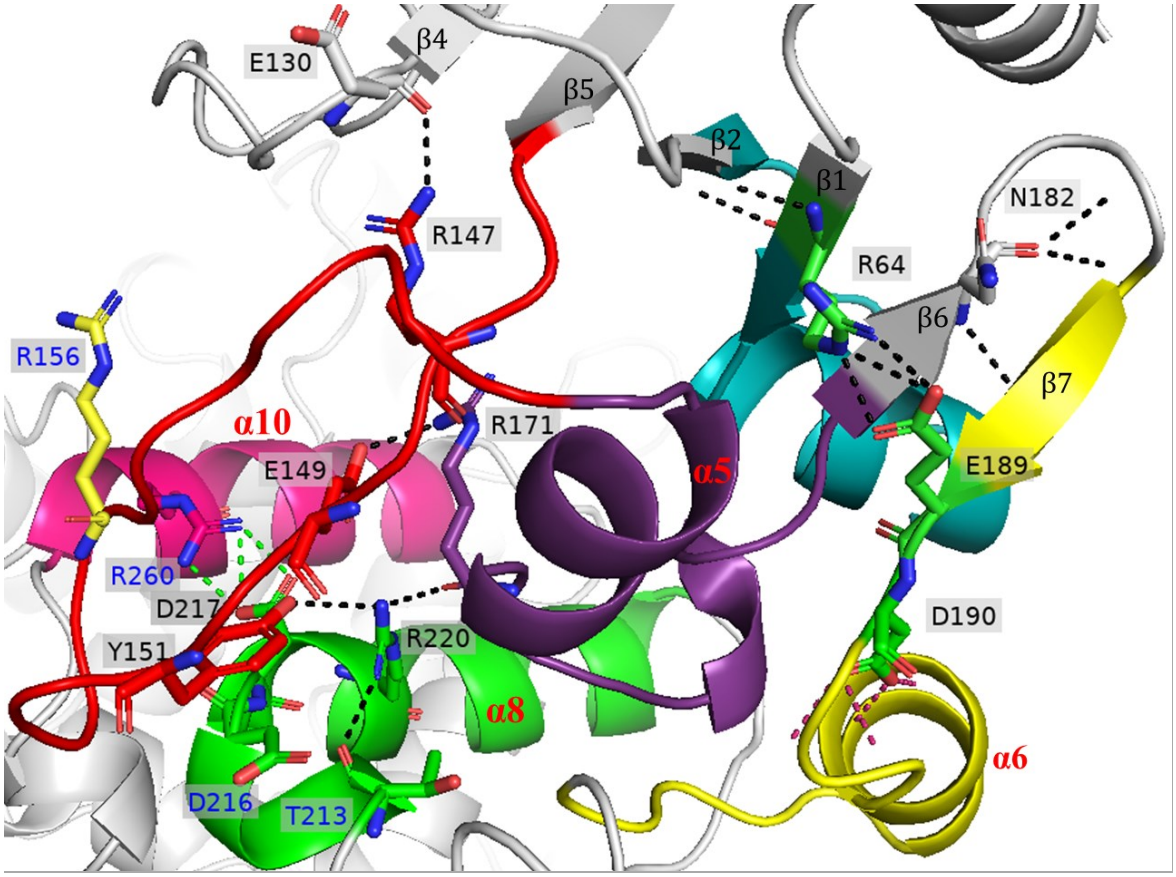

Figure 4.3 The model structure of the catalytic head domain of *S. cerevisiae* tRNA nucleotidyltransferase showing the connection of the head and neck domain though the flexible loop region (red). Residues are shown based on important residues identified by Toh *et al.* (2009).

5.0 SUMMARY AND FUTURE WORK

This study was conducted to better understand the role of position 64 in yeast tRNA nucleotidyltransferase. It was hoped that this would provide additional information about the interaction of motifs A (where position 64 is found) and C (where position 189 is found) in enzyme activity. I was particularly interested in discovering the mechanism of suppression by characterizing novel R64 variants (R64F, R64A, R64P) that I generated. Among these newly generated variants, only R64F showed the ability of suppress a *ts* phenotype, but not in all *ts* backgrounds. Specifically, it suppressed the *ts* phenotype in E189F and E189K variants, but had no effect on the phenotypes of the D190 variants. The R64A variant was unable to suppress any phenotype and showed low growth at the restrictive temperature. The R64P variant resulted in a lethal phenotype.

Molecular modelling of the predicted structures of the variant enzymes suggests that the phenotypes observed, and the suppression of those phenotypes is not limited to an interaction between only two specific residues but must involve interactions with other residues. Motif C modulates the organization and orientation of the head domain relative to the neck and body domains. Changes in this organization are required for NMP incorporation (CMP or AMP) at the 3' terminus of the growing tRNA. The consecutive addition of these nucleotides is mediated by interactions between the head and neck domains of the enzyme which position the catalytic residues so that they can perform the necessary chemistry. Disruption of any of these interactions can affect enzyme activity and NMP incorporation.

This study showed that the introduction of a large and hydrophobic residue at position 64 (R64F) allowed for suppression of the *ts* phenotype in the E189F and E189K variants, but did not suppress the lethal phenotype in the D190A and D190F variants. This may suggest the importance of a direct interaction between positions 64 and 189 in motifs A and C, respectively. The *ts* phenotype is suppressed by potential interactions between F64 and F189 that replace the original interactions between R64 and E189. Although the R64F variant showed less activity than the native enzyme indicating that the variant enzyme is altered in its active site, the R64F/E189F variant showed more activity than we had seen previously in the E189F variant suggesting that the suppressor mutation altered the protein to partially restore activity. Moreover, the R64F variant showed increased misincorporation of CMP to generate the tRNA-NCCC product again suggesting

that some aspect of the active site has been altered to favor CMP incorporation over AMP incorporation at the last position of the tRNA.

Once I had analyzed the data from the variants carrying the R64F substitution, I could compare those results to the results of the previously characterized R64W variant. The most interesting observation here was that unlike the R64F variant, cells expressing the R64W variant showed no phenotype different from that of the native enzyme. This suggests that in the case of the R64W variant where the tryptophan side chain is larger than and has more hydrogen-bonding potential than that of phenylalanine, its effects on structure and function are more dramatic. The R64W substitution ameliorated the changes resulting from substitutions at position 189 (E189F, E189K) or position 190 (D190A, D190F). My modelling suggests that this reflects changes in protein structure meditated by more than just the direct interaction between residues 64 and 189. The rearrangements arising from these novel interactions could lead to changes in the relative orientation of the head domain relative to the neck domain and subsequently affect catalysis.

As both motif A and motif C are contained in the single β-sheet in yeast tRNA-NT and this β-sheet defines the polymerase β superfamily it would be interesting to determine whether or not making substitutions in motif A (at position 64) or in motif C (at position 189 or 190) would alter the character of this β-sheet. Given that this is the only β-sheet in the protein and that tRNA-NT is primarily α-helical (Fig. 1.1) it would be worth using Fourier-transform infrared spectroscopy (FTIR) to see if any of these amino acid substitutions alter this β-sheet or if any of the suppressor mutations result in amino acid changes that restore the β-sheet. Unfortunately, a lack of access to the FTIR facility and personnel at McGill University over the last five months pushed these experiments beyond the scope of this research.

We previously have shown a correlation between turnover number (k_{cat}) and the *ts* phenotypes observed. Reduced activity leads to the *ts* phenotype and partial restoration of the activity suppress the *ts* phenotype. With this in mind, it would be useful to carry out a kinetic characterization of the variants studied here. We would expect the k_{cat} values of the R64 variants to have activity levels such that R64F>R64A>R64P based on the phenotypes that we observed. We also would expect the R64F substitution to raise the k_{cat} of the E189F or E189K variant, but not of the D190A or D190F variant. Although our previously characterized variants showed no major changes in K_m for the binding of any substrate it would be useful to calculate K_m for these variants as well.

Unfortunately, the inability to order radioactive ATP or to use the imaging facility at McGill University over the last five months pushed these experiments beyond the scope of this research.

A solved crystal structure of the yeast tRNA-NT could improve and develop the computational analysis of this enzyme's structure. A direct comparison of the crystal structures of the native and variant enzymes with and without various substrates bound provide a better understanding of the structural changes in different variants that result in changes in enzyme activity.

As my modelling predicted novel interactions between specific amino acids in the variants that I generated, it would be interesting to introduce amino acid substitutions at these new positions (*e.g.*, F180, N182, E187) to see what effects these substitutions would have on the activity of the native or variant enzymes to advance our knowledge of tRNA nucleotidyltransferase structure and function.

6.0 BIBLIOGRAPHY

Aebi, M., Kirchner, G., Chen, J. Y., Vijayraghavan, U., Jacobson, A., Martin, N. C., and Abelson, J. (1990). Isolation of a temperature-sensitive mutant with an altered transfer RNA nucleotidyltransferase and cloning of the gene encoding tRNA nucleotidyltransferase in the yeast *Saccharomyces cerevisiae*. *J Biol Chem, 265*, 16216–16220.

Augustin, M. A., Reichert, A. S., Betat, H., Huber, R., Mörl, M., and Steegborn, C. (2003). Crystal structure of the human CCA-adding enzyme: insights into template-independent polymerization. *J Mol Biol, 328,* 985-994.

Akada, R., Kawahata, M., Nishizawa, Y. (2000). Elevated temperature greatly improves transformation of fresh and frozen competent cells in yeast. *Biotechniques, 28,* 854-856.

Aravind, L., and Koonin, E. V. (1999). DNA Polymerase Beta-like Nucleotidyltransferase Superfamily: Identification of Three New Families, Classification and Evolution History. *Nucl Acids Res, 27,* 1609-1618.

Ausubel, F. M., Brent, R., Kingston, R. E., Moore, D. D., Seidman, J. G., and Struhl, K. (1989). Current Protocols in Molecular Biology. New York: Wiley.co., New York.

Betat, H., Rammelt, C., and Mörl, M. (2010). tRNA nucleotidyltransferases: ancient catalysts with an unusual mechanism of polymerization. *Cell Mol Life Sci, 67*, 1447–1463.

Biasini, M., Bienert, S., Waterhouse, A., Arnold, K., Studer, G., Schmidt, T., Kiefer, F., Cassarino, T.G., Bertoni, M., Bordoli, L., and Schwede, T. (2014). SWISS-MODEL: Modelling Protein Tertiary and Quaternary Structure Using Evolutionary Information. *Nucl Acids Res, 42*, 252–258.

Bradford, M. M. (1976). A rapid and sensitive method for the quantitation of microgram quantities of protein utilizing the principle of protein-dye binding. *Analytical Biochemistry*, *72*, 248–254.

Chakraborty, P. K., Schmitz-Abe, K., Kennedy, E. K., Mamady, H., Naas, T., Durie, D., … Fleming, M. D. (2014). Mutations in TRNT1 cause congenital sideroblastic anemia with immunodeficiency, fevers, and developmental delay (SIFD). *Blood*, *124*, 2867–2871.

Capage, M., and Hill, C. W. (1979). Preferential unequal recombination in the glyS region of the *Escherichia coli* chromosome. *J Mol Biol, 127,* 73-87.

Chen, J. Y., Kirchner, G., Aebi, M., and Martin, N. C. (1990). Purification and properties of yeast ATP (CTP): tRNA nucleotidyltransferase from wild-type and overproducing cells. *J Biol Chem*, *265*, 16221-16224.

Cho, H. D., Verlinde, C. L., and Weiner, A. M. (2007). Reengineering CCA-adding enzymes to function as (U, G)- or dCdCdA-adding enzymes or poly (C, A) and poly(U,G) polymerases. *Proc Natl Acad Sci USA, 104,* 54–59.

Colasurdo, G. (2011). The role of arginine 204 in *Candida glabrata* tRNA nucleotidyltransferase. Concordia University.

Cudny, H., Lupski, J. R., Godson, G. N., and Deutscher, M. P. (1986). Cloning, sequencing, and species relatedness of the *Escherichia coli* cca gene encoding the enzyme tRNA nucleotidyltransferase. *J Biol Chem*, 261(14), 6444–6449.

Deustcher, M. P. (1982). The Enzyme Boyer, P. Ed., Vol. XV, pp. 183-215, Academic Press, New York.

Dohmen, R. J., Strasser, A. W., Höner, C. B., and Hollenberg, C. P. (1991). An efficient transformation procedure enabling long-term storage of competent cells of various yeast genera. *Yeast, 7,* 691-692.

Gea i Mallorquí, E. (2011). Identification of suppressors of the temperature-sensitive mutation E189F in tRNA nucleotidyltransferase in *Saccharomyces cerevisiae*. Honours thesis, Chemistry and Biochemistry, Concordia University.

Goring, M. E., Leibovitch, M., Gea-Mallorqui, E., Karls, S., Richard, F., Hanic-Joyce, P. J., and Joyce, P. B. M. (2013). The ability of arginine to tryptophan substitution in *Saccharomyces cerevisiae* tRNA nucleotidyltransferase to alleviate a temperature-sensitive phenotype suggests a role for motif C in active site organization. *Biochim Biophys Acta - Proteins and Proteomics, 1834,* 2097-2106.

Guthrie, C., and Fink, G. (1991). Guide to Yeast Genetics and Molecular Biology. *Methods in Enzymology*, *194*, Academic Press, San Diego.

Harper, S., and Speicher, D. W. (2011). Purification of proteins fused to glutathione S-transferase. *Methods Mol Biol, 681*, 259–280.

Holm, L., and Sander, C. (1996). Alignment of three-dimensional protein structures: Network server for database searching. *In Methods in Enzymology, 266,* 653–662.

Holzwarth, G., and Doty, P. (1965). The Ultraviolet Circular Dichroism of Polypeptides. *J. Am. Chem. Soc, 87*, 218–228.

Just, A., Butter, F., Trenkmann, M., Heitkam, T., Morl, M., and Betat, H. (2008). A comparative analysis of two conserved motifs in bacterial poly(A) polymerase and CCA-adding enzyme. *Nucl Acids Res, 36,* 5212–5220.

Kuhn, C-D., Wilusz, J. E., Zheng Y, Beal PA, Joshua-Tor, L. (2015). On-enzyme refolding permits small RNA and tRNA surveillance by the CCA-adding enzyme. *Cell, 160,* 644–658.

Leibovitch, M., Bublak, D., Hanic-Joyce, P. J., Tillmann, B., Flinner, N., Amsel, D., and Schleiff, E. (2013). The folding capacity of the mature domain of the dual-targeted plant tRNA nucleotidyltransferase influences organelle selection. *Biochem J, 453,* 401–412.

Li, F., Xiong, Y., Cho, H. D., Tomita, K., Weiner, A. M., Steitz, T. A. (2002). Crystal Structures of the *Bacillus stearothermophilus* CCA-adding Enzyme and Its Complexes with ATP or CTP. *Cell, 111,* 815-824.

Lin, S. (2008). Expression and purification of fusion-tag proteins. Adapted from AEG-0095.3. *AEGERA*.

Neuenfeldt, A., Just, A., Betat, H., and Mörl, M. (2008). Evolution of tRNA nucleotidyltransferases: A small deletion generated CC-adding enzymes. *Proc Natl Acad Sci USA, 105,* 7953-7958.

Peattie, D. A. (1979). Direct chemical method for sequencing RNA. *Proc Natl Acad Sci USA, 76*, 1760–1764.

Peltz, S. W., Donahue, J. L., and Jacobson, A. (1992). A mutation in the tRNA nucleotidyltransferase gene promotes stabilization of mRNAs in *Saccharomyces cerevisiae*. *Mol Cell Biol, 12,* 5778-84.

Richards, F. M. (1974). The interpretation of protein structures: total volume, group volume distributions and packing density. *J Mol Biol, 82,* 1-14.

Rosset, R., and Monier, R. (1965). Inability of the terminal 3′-hydroxy sequence of transfer RNA in microorganisms. I. Turnover of terminal AMP in *Saccharomyces cerevisiae*. *Biochem Biophys Acta, 108,* 376-384.

Sambrook, J., Maniatis, T., and Fritch, E. F. (1989). Molecular Cloning (2nd ed.). Cold Spring Harbor Laboratory Press.

Sandhu, P. S. (2014). Characterization of *Saccharomyces cerevisiae* tRNA nucleotidyltransferase variants. Master's thesis, Chemistry and Biochemistry, Concordia University.

Sasarman, F., Thiffault, I., Weraarpachai, W., Salomon, S., Maftei, C., Gauthier, J., … Shoubridge, E. A. (2015). The 3′ addition of CCA to mitochondrial $tRNA^{Ser(AGY)}$ is specifically impaired in patients with mutations in the tRNA nucleotidyl transferase TRNT1. *Human Molecular Genetics*, *24*, 2841–2847.

Shan, X., Russell, T. A., Paul, S. M., Kushner, D. B., and Joyce, P. B. M. (2008). Characterization of a temperature-sensitive mutation that impairs the function of yeast tRNA nucleotidyltransferase. *Yeast, 25*, 219–233.

Slade, A., Kattini, R., Campbell, C., Holcik, M. (2020). Diseases Associated with Defects in tRNA CCA Addition. *Int. J. Mol. Sci*, *21*, 3780

Sprinzl, M., and Cramer, F. (1979). The -C-C-A end of tRNA and its role in protein biosynthesis. *Prog Nucl Acids Res Mol Biol, 22*, 1-69.

Steitz, T. A. (1998). A mechanism for all polymerases. *Nature, 391*(6664), 231–232.

The PyMOL Molecular Graphics System, Version 2.4.0 Schrödinger, LLC.

Toh, Y., Takeshita, D., Numata, T., Fukai, S., Nureki, O., and Tomita, K. (2009). The mechanism for the definition of elongation and termination by the class II CCA-adding enzyme. *EMBO J, 28,* 3353-3365.

Tomita, K., Fukai, S., Ishitani, R., Ueda, T., Takeuchi, N., Vassylyev, D. G., and Nureki, O. (2004). Structural basis for template-independent RNA polymerization. *Nature, 430*, 700–704.

Tomita, K., Ishitani, R., Fukai S., and Nureki, O. (2006). Complete crystallographic analysis of the dynamics of CCA sequence addition. *Nature, 443,* 956–960.

Tomita, K., and Yamashita, S. (2014). Molecular mechanisms of template-independent RNA polymerization by tRNA nucleotidyltransferases. *Frontiers in Genetics, 5*, 36.

Voet, D., and Voet, J. G. (1995). *Biochemistry, 23,* 104–105 John Wiley & Sons, Inc, New York.

Vörtler, S., and Mörl, M. (2010). tRNA nucleotidyltransferases: Highly unusual RNA polymerases with vital functions. *FEBS Lett, 584,* 297-302.

Wallace, D. M. (1987A) Large-and-small-scale phenol extractions. *Methods in Enzymology, 152*, 41-48.

Wallace, D. M. (1987B) Precipitation of nucleic acids. *Methods in Enzymology, 152*, 41-48.

Walker, J. M. (2002). Protein handbook (2nd ed.), Humana Press.

Wilusz, J. E., Whipple, J. M., Phizicky, E. M., and Sharp, P. A. (2011). tRNAs marked with CCACCA are targeted for degradation. *Science, 334,* 817-821.

Wong, C., Sridhara, S., Bardwell, J. C. A., and Jakob, U. (2000). Heating Greatly Speeds Coomassie Blue Staining and Destaining. *BioTechniques, 28*, 426–432.

Yamashita, S., Takeshita, D., Tomita, K. (2014). Translocation and rotation of tRNA during template-independent RNA polymerization by tRNA nucleotidyltransferase. *Structure, 22,* 315–325.

Yue, D., Maizels, N., and Weiner, A. M. (1996). CCA-adding enzymes and poly(A) polymerases are all members of the same nucleotidyltransferase superfamily: Characterization of the CCA-adding enzyme from the archaeal hyperthermophile *Sulfolobus shibitae*. *RNA, 2*, 895-908.